SLAC-PUB-1529
January 1975

AMPLITUDE STRUCTURE IN TWO- AND QUASI-TWO-BODY PROCESSES*

Michel Davier

Stanford Linear Accelerator Center
Stanford University, Stanford, California 94305

(Extracted from SLAC Summer Institute, SLAC Report 179, Volume I)

*Work supported by the U. S. Atomic Energy Commission.

OUTLINE

II. GENERAL FEATURES OF EXCHANGE PROCESSES

1. Kinematic Dependence
   - (a) s dependence
   - (b) t dependence and helicity structure
2. Quantum Numbers Exchanged
   - (a) allowed exchange
   - (b) exotic exchanges
   - (c) SU(3) symmetry
3. Phases
   - (a) $t = 0$
   - (b) $t \neq 0$

III. EXTRACTING AMPLITUDES FROM INCOMPLETE DATA

1. Projection of one amplitude: exchanges in elastic scattering
   - (a) cross-over effect
   - (b) polarizations
2. Making Use of Analyticity Properties of Amplitudes
   - (a) application of dispersion relations to πN amplitude analyses
   - (b) derivative analyticity relations
   - (c) application of derivative analyticity relations to amplitude analyses

IV. DUALITY AND ABSORPTION

1. Duality
   - (a) two descriptions of 2-body scattering
   - (b) relating low and high energy descriptions: FESR
   - (c) two-component duality
   - (d) application of duality: exchange degeneracy
   - (e) duality and quarks
   - (f) semi-local duality ?
2. Absorption
   - (a) classical absorption
   - (b) absorption zeroes vs signature zeroes
   - (c) dual absorption

V. MODELS AND SPECULATIONS

1. Models for Two-Body Scattering
   - (a) dual absorptive model
   - (b) strong absorption models
2. Speculations on the Pomeron
   - (a) Pomeron from high energy pp data
   - (b) Can we extract Im $P(s,0)$ at lower s?
   - (c) application to $\gamma p \to \phi p$
   - (d) implications for exchange degeneracy

OUTLOOK

INTRODUCTION

In this series of lectures we are concerned with the experimental determination of two-body amplitudes and their phenomenology. Even though two-body and quasi-two-body processes represent only a small fraction of the total interaction, their study is very important in several respects:

(1) They provide the simplest laboratory for studying the exchange forces between hadrons in a rather controllable way: energies, spins, particle identities and quantum numbers can be varied separately.

(2) Two-body processes constitute a testing ground for--as well as inducing--theoretical ideas in hadron dynamics. Concepts like Regge poles, duality, absorption have been brought forward in trying to understand exchange processes. In turn these new ideas have been applied to more complex situations involving multiparticle final states.

(3) Even at super-high energies where the cross sections for known identifiable two-body processes will become very small--except for elastic scattering--we still hope two-body scattering ideas will be relevant. Indeed in a multiparticle event subenergies will still be rather small and two-body exchanges will probably still happen.

In these lectures we would like to focus our interest on the structure of the amplitudes. Rather than discussing two-body scattering data in a general way, we are going to translate and summarize our knowledge in terms of amplitudes. In the first chapters, we shall try to make as little reference as possible to our sometimes preconceived theoretical ideas, but instead try to extract the maximum unbiased information from the data.

I - GENERALITIES AND COMPLETE EXTRACTION OF AMPLITUDES FROM DATA

1. Generalities on Amplitudes (Spinology)

(a) Helicity formalism.[1,2]

Consider the scattering process

$$1 + 2 \rightarrow 3 + 4$$

where each particle is labelled by a set of quantum numbers: λ_i (helicity), J_i (spin), η_i (parity), m_i (mass) and $\vec{p}_i$ (momentum). The naturality ξ is defined by:

$$\xi = (-1)^J \eta = \tau\eta$$

where τ is the signature. The process can be described in either the s or the t channel with helicity amplitudes:

s-channel t-channel

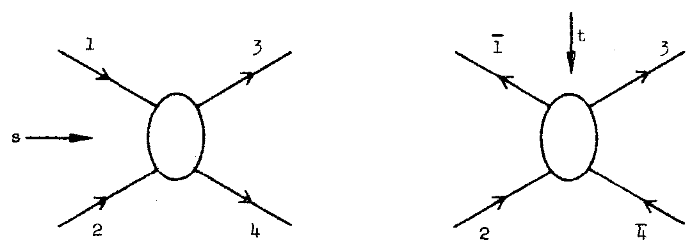

$$F^s_{\lambda_3\lambda_4\lambda_1\lambda_2}(s,t) \qquad\qquad F^t_{\lambda_3\lambda_{\bar{1}}\lambda_{\bar{4}}\lambda_2}(s,t)$$

The amplitudes can be decomposed into amplitudes with well-defined total angular momentum J using the Jacob-Wick expansion:

$$F^s_{\lambda_3\lambda_4\lambda_1\lambda_2}(\theta,\phi) = \sum_J (2J+1)\, F^{s(J)}_{\lambda_3\lambda_4\lambda_1\lambda_2}\, e^{-(\lambda-\mu)\phi}\, d^J_{\lambda\mu}(\theta)$$

with $\lambda = \lambda_1 - \lambda_2$ and $\mu = \lambda_3 - \lambda_4$

At high energy amplitudes are built up by exchanges in the $t(u)$ channel. Usually a given exchange is characterized by a set of quantum numbers: η, τ, $SU(3)$ quantum numbers, etc. ... . Although t-channel helicity amplitudes show simple relations for a well-defined t-channel exchange, s-channel amplitudes are more widely used now: kinematic constraints are easier to take into account in pole models and more importantly they probably have a more physical interpretation.

-exchange of well-defined naturality in the t-channel[3]

Consider an exchange with quantum numbers J, η in the t-channel.

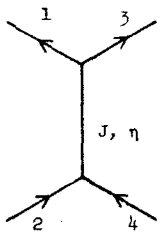

Parity conservation at vertex $2\bar{4}J$ reads:

$$F^{t(J)}_{\lambda_3\lambda_{\bar 1}\lambda_{\bar 4}\lambda_2} = \eta_2\eta_{\bar 4}\eta(-1)^{J+J_4-J_2}\, F^{t(J)}_{\lambda_3\lambda_{\bar 1}-\lambda_{\bar 4}-\lambda_2}$$

$$F^t_{\lambda_3\lambda_{\bar 1}\lambda_{\bar 4}\lambda_2} = (2J+1)\, d^J_{\lambda\mu}(\theta_t)\, F^{t(J)}_{\lambda_3\lambda_{\bar 1}\lambda_{\bar 4}\lambda_2}$$

$$\lambda = \lambda_{\bar 1} - \lambda_3\,, \qquad \mu = \lambda_2 - \lambda_{\bar 4}$$

At high energy (to leading order in s) we have

$$d^J_{-\lambda\mu}(\theta_t) = (-1)^\lambda\, d^J_{\lambda\mu}(\theta_t) + O(\tfrac{1}{s})$$

$$(\cos\theta_t \to 1)$$

leading to:

$$F^t_{\lambda_3\lambda_{\bar 1}\lambda_{\bar 4}\lambda_2} = \eta(-1)^J \eta_{\bar 4}\eta_2 (-1)^{\lambda_{\bar 4}-\lambda_2} (-1)^{J_4-J_2}\, F^t_{\lambda_3\lambda_{\bar 1}-\lambda_{\bar 4}-\lambda_2} + O(\tfrac{1}{s})$$

where $\xi = \eta(-1)^J$ is the exchanged naturality. A similar relation holds for the $\bar{1}3J$ vertex. An important consequence of these formulae is that amplitudes with opposite naturality do not interfere in the unpolarized differential cross section.

To see the effect on the (J,η) exchange on s-channel amplitudes, one must make use of the s-t crossing matrix. After some more non-leading terms in s are dropped, the following relations hold:

$$F^s_{\lambda_3\lambda_4\lambda_1\lambda_2} = \xi\, \eta_2\eta_4(-1)^{J_4-J_2}(-1)^{\lambda_4-\lambda_2}\, F^s_{\lambda_3-\lambda_4-\lambda_1-\lambda_2} + O(\tfrac{1}{s})$$

$$= \xi\, \eta_1\eta_3(-1)^{J_3-J_1}(-1)^{\lambda_3-\lambda_1}\, F^s_{-\lambda_3\lambda_4-\lambda_1\lambda_2} + O(\tfrac{1}{s})$$

As an example, let us consider the processes $\pi N \to \rho N$ or ρN^*. At the $\pi\rho$ vertex, for high energies, one has the relation

$$F^s_{\lambda_\rho\lambda_4\lambda_2} = -\xi\,(-1)^{\lambda_\rho}\, F^s_{-\lambda_\rho\lambda_4\lambda_2}$$

so that $\xi = +1$ exchanges contribute only to helicities $\lambda_\rho = \pm 1$, while $\xi = -1$ exchanges populate all helicities $\lambda_\rho = 0, \pm 1$.

-number of independent helicity amplitudes

Restrictions on helicity amplitudes are imposed by invariance under discrete symmetries: parity, time-reversal, charge conjugation.

parity

$$F_{\lambda_3\lambda_4\lambda_1\lambda_2} = \eta_1\eta_2\eta_3\eta_4(-1)^{J_1+J_2+J_3+J_4}(-1)^{\lambda_1+\lambda_2+\lambda_3+\lambda_4} F_{-\lambda_3-\lambda_4-\lambda_1-\lambda_2}$$

time reversal (restricts the number of amplitudes only for elastic scattering

$$F_{\lambda_3\lambda_4\lambda_1\lambda_2} = F_{\lambda_1\lambda_2\lambda_3\lambda_4}$$

charge conjugation (for charge-conjugate reactions like $\bar{p}p \to \bar{\Lambda}\Lambda$)

$$F_{\lambda_3\lambda_4\lambda_1\lambda_2} = \epsilon_1\epsilon_2\epsilon_3\epsilon_4 F_{\lambda_4\lambda_3\lambda_2\lambda_1}$$

Using these rules enables one to determine the number of independent amplitudes required to describe a given process: a few simple examples are shown in Table 1. A general remark is that except for reactions of the type $0\frac{1}{2} \to 0\frac{1}{2}$ with only 2 amplitudes, the number of amplitudes for processes of interest is large (≥ 4) and consequently the separation of individual amplitudes is a somewhat tedious experimental task.

(b) Invariant amplitudes

Helicity amplitudes refer explicitly to the centre-of-mass frame. When calculating scattering amplitudes from field theory, or when studying analytic properties, it is useful to write down explicitly invariant amplitudes.

If no spins are involved, the only Lorentz scalars are s and t (u) and the scattering amplitude is a scalar

$$T = f(s,t)$$

When some of the particles have spin, Lorentz invariants I_n can be constructed from 4-vectors and spin tensors:

$$T = \sum_n f_n(s,t)\, I_n$$

where the f_n are invariant amplitudes. Invariant amplitudes are related linearly to helicity amplitudes:

$$f_n(s,t) = \sum_{(\lambda)} A_{(\lambda)}(s,t)\, F_{(\lambda)}(s,t)$$

where (λ) represents a set of helicities and the $A_{(\lambda)}$ are known kinematic functions.

-example: $0^- \frac{1}{2}^+ \to 0^- \frac{1}{2}^+$ elastic scattering.

Using the 2 Dirac spinors, it is possible to form 2 invariants and the general form of the amplitudes in terms of the 2 invariant amplitudes A and B is:

$$T = \bar{u}_4 \left[A(s,t) + \frac{1}{2} B(s,t)\, [\not{q}_2 + \not{q}_4] \right] u_2$$

Assuming $m_1 = m_3 << m_2 = m_4 = M$, one can express the s-channel helicity amplitudes in terms of the invariant amplitudes A and B:

$$\begin{cases} F_{++} = \dfrac{M}{4\pi\sqrt{s}} \cos\dfrac{\theta}{2} \left[A + (\nu - \dfrac{t}{4M})B \right] \\[2ex] F_{+-} = \dfrac{M}{4\pi\sqrt{s}} \sin\dfrac{\theta}{2}\, \dfrac{M}{2\sqrt{s}} \left[\dfrac{4M\nu - t + 4M^2}{2M^2} A + \dfrac{4M\nu - t}{2M} B \right] \end{cases}$$

where $\nu = (s-u)/4M$ and the following notation has been used:

$$F_{++} \equiv F_{0\frac{1}{2}0\frac{1}{2}} \qquad F_{+-} \equiv F_{0-\frac{1}{2}0\frac{1}{2}}$$

$$\frac{d\sigma}{dt} = \frac{4\pi}{s} \left[|F_{++}|^2 + |F_{+-}|^2 \right]$$

At high s and for t not too large, we have the simpler expressions:

$$\begin{cases} F_{++} \simeq \frac{M}{4\pi\sqrt{s}} (A + \nu B) = \frac{M}{4\pi\sqrt{s}} A' \\ F_{+-} \simeq \frac{M}{4\pi\sqrt{s}} \frac{\sqrt{-t}}{s} [(\nu + M)A + M\nu B] \xrightarrow[s\to\infty]{} \frac{\sqrt{-t}}{8\pi\sqrt{s}} A \end{cases}$$

so that

$$\left(\frac{d\sigma}{dt}\right)_{s\to\infty} = \frac{M^2}{4\pi s^2}\left[|A'^2| - \frac{t}{4M^2}|A|^2\right]$$

$$= \frac{1}{s^2}\,[|M_{++}|^2 + |M_{+-}|^2]$$

The amplitudes A and B are free of kinematic singularities and possess simple properties under s-u crossing. Defining the amplitudes $A^{(\pm)}$ and $B^{(\pm)}$ for πN scattering:

$$A^{(+)} = \frac{1}{3}\,[A(I_s = \tfrac{1}{2}) + 2A(I_s = \tfrac{3}{2})] = \frac{1}{\sqrt{6}}\,A(I_t = 0)$$

$$A^{(-)} = \frac{1}{2}\,[A(I_s = \tfrac{1}{2}) - A(I_s = \tfrac{3}{2})] = \frac{1}{2}\,A(I_t = 1)$$

(and similar relations for $B^{(\pm)}$), s-u crossing means:

$$A^{(\pm)}(s,t,u) = \pm A^{(\pm)}(u,t,s)$$
$$B^{(\pm)}(s,t,u) = \mp B^{(\pm)}(u,t,s)$$

(c) Density matrices and polarizations

The initial state is described by a density matrix ρ^i with $\mathrm{Tr}\,\rho^i = 1$. If no polarization is observed in the final state, the differential cross section is expressed by

$$\frac{d\sigma}{dt} = \frac{1}{s^2}\,\mathrm{Tr}(M\rho^i M^\dagger) = \frac{1}{s^2} \sum_{\substack{\lambda_3\lambda_4 \\ \lambda_1\lambda_2\lambda_1'\lambda_2'}} M_{\lambda_3\lambda_4\lambda_1\lambda_2}\, \rho^i_{\lambda_1\lambda_2\lambda_1'\lambda_2'}\, M^\dagger_{\lambda_3\lambda_4\lambda_1'\lambda_2'}$$

For unpolarized initial state ρ^i is a diagonal unit matrix multiplied by a normalization constant:

$$\rho^i = \frac{I}{(2J_1+1)(2J_2+1)}$$

The polarization information on the final state is described by a density matrix ρ^f:

$$\left(\frac{d\sigma}{dt}\right)\rho^f = \frac{1}{s^2}\,M\rho^i M^\dagger$$

$$\rho^f = \frac{M\rho^i M^\dagger}{\mathrm{Tr}(M\rho^i M^\dagger)}$$

The expectation value of an observable A referring to the spins of the final state particles is given by:

$$\langle A\rangle = \frac{\mathrm{Tr}(\rho^f A)}{\mathrm{Tr}\,\rho^f}$$

For the construction of density matrices describing polarization states for arbitrary spins, see Ref. 4.

-examples.

$0\,\frac{1}{2} \to 0\,\frac{1}{2}$: the density matrix describing the nucleon polarization has the general form $\rho = \frac{1}{2}\,[I + \vec{P}\cdot\vec{\sigma}\,]$ corresponding to a polarization P_i of the nucleon along the axis i

$$P_i = \frac{1}{2}\,\frac{\mathrm{Tr}(\rho\sigma_i)}{\mathrm{Tr}\,\rho}$$

$\frac{1}{2}\frac{1}{2}\to\frac{1}{2}\frac{1}{2}$: the most general density matrix with correlations will involve the tensor products between I, $\vec{\sigma}_1$ and $\vec{\sigma}_2$:

$$\rho = \frac{1}{4}\left[I + \vec{P}_1\cdot\vec{\sigma} \otimes I + \vec{P}_2\cdot\vec{\sigma} \otimes I + \sum_{i,j=x,y,z} c_{ij}\sigma_i \otimes \sigma_j\right]$$

(d) <u>observables in</u> $0^-\,\frac{1}{2}^+ \to 0^-\,\frac{1}{2}^+$ <u>scattering</u> (such as $\pi N\to\pi N$, $\pi N\to K\Sigma$, $\bar{K}N\to K\Lambda$, etc.)

The amplitude is a 2×2 matrix in helicity space and parity conservation gives the form:

$$\begin{array}{cc} M = \begin{bmatrix} M_{++}e^{i(\phi/2)} & -M_{+-}e^{-i(\phi/2)} \\ M_{+-}e^{i(\phi/2)} & M_{++}e^{-i(\phi/2)} \end{bmatrix} & \longleftarrow \lambda_2 \\ \uparrow \\ \lambda_4 \end{array}$$

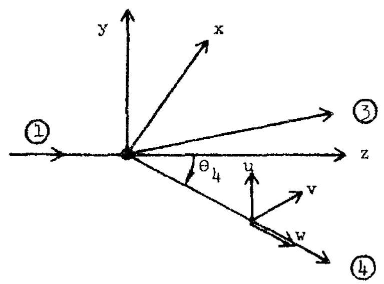

(axes convention; $\Phi = 0$)

$$\cos\Phi = \hat{y}\cdot\hat{n}$$

$$\rho^i = \frac{1}{2}\begin{bmatrix} 1+P_z^i & P_x^i - iP_y^i \\ P_x^i + iP_y^i & 1-P_z^i \end{bmatrix}$$

where $\vec{P}^{\,i}$ is the initial polarization vector of the nucleon. It is straightforward, although tedious, to compute the 3 components of polarization of the final baryon. Defining:

$$\frac{d\sigma}{dt} = \frac{1}{s^2}\left[|M_{++}|^2 + |M_{+-}|^2\right]$$

$$P = -\frac{2\,\mathrm{Im}\,M_{++}M_{+-}^*}{|M_{++}|^2 + |M_{+-}|^2}$$

$$A' = \frac{|M_{++}|^2 - |M_{+-}|^2}{|M_{++}|^2 + |M_{+-}|^2}$$

$$R' = -\frac{2\mathrm{Re}\,M_{++}M_{+-}^*}{|M_{++}|^2 + |M_{+-}|^2}$$

one finds the final polarization components:

$$P_z^f\,\mathrm{Tr}\,\rho^f = A'P_z^i + P_x^i[R'\cos\Phi - P\sin\Phi] + P_y^i\,[R'\sin\Phi + P\cos\Phi]$$

$$P_x^f\,\mathrm{Tr}\,\rho^f = -R'P_z^i + A'P_x^i + A'P_y^i$$

$$P_y^f\,\mathrm{Tr}\,\rho^f = P_y^i + P - P_x^i\sin\Phi$$

with $\mathrm{Tr}\,\rho^f = 1 - PP_x^i\sin\Phi + PP_y^i\cos\Phi$.

For a stable baryon, polarization can be experimentally analyzed in a rescattering experiment: in this case only the transverse component of the polarization is measured and one must consider different orientations of the target polarization in order to separate A' and R'. Usually the rotated A and R parameters (corresponding to the transverse polarization) are measured:

$$\left.\begin{array}{l} A = A'\sin\theta_4^L + R'\cos\theta_4^L \\ R = -A'\cos\theta_4^L + R'\sin\theta_4^L \end{array}\right. \quad \text{(lab angle)}$$

For small t, $\theta_4^L\to\pi/2$ and $A\to A'$, $R\to R'$. P, A and R are not 3 independent observables since $P^2 + R^2 + A^2 = 1$ and in general P and R measurements will suffice, except for the sign of A. Figure 1 shows schematically the experimental configurations in the scattering plane to measure A and R when only transverse polarization is measured for the outgoing baryon.

2. πN Amplitudes at 6 GeV/c

This represents the only case where all observables have been measured, therefore permitting the separation of all helicity amplitudes. It is worth looking with some detail since it represents, in principle, the only unbiased source of information on individual amplitudes.

(a) Data and observables

In addition to helicity subscripts, we will use the isospin exchange in the t-channel I_t to label amplitudes. We have:

$$F(\pi^{\pm} p \to \pi^{\pm} p) = F^0 \mp F^1$$

$$F(\pi^- p \to \pi^0 n) = \sqrt{2}\, F^1$$

In terms of "particle" exchange F^0 corresponds to (Pomeron + f) exchange while F^1 corresponds to ρ exchange. To describe the 3 reactions, one needs 4 independent amplitudes, therefore 8 real numbers for each t value. The observables for each reaction are:

$$\frac{d\sigma}{dt} = |F_{++}|^2 + |F_{+-}|^2$$

$$-P\,\frac{d\sigma}{dt} = 2\,\mathrm{Im}(F_{++}\,F^*_{+-})$$

$$-R\,\frac{d\sigma}{dt} = [|F_{++}|^2 - |F_{+-}|^2]\cos\theta_L + 2\,\mathrm{Re}(F_{++}\,F^*_{+-})\sin\theta_L$$

$$A\,\frac{d\sigma}{dt} = [|F_{++}|^2 - |F_{+-}|^2]\cos\theta_L - 2\,\mathrm{Re}(F_{++}\,F^*_{+-})\cos\theta_L$$

The measured observables around $P_L = 6$ GeV are:[5-12]

$$\frac{d\sigma^+}{dt}, \quad \frac{d\sigma^-}{dt}, \quad \frac{d\sigma^0}{dt}$$

$$P^+, \quad P^-, \quad P^0$$

$$R^+, \quad R^-$$

$$(A^-)$$

(b) Amplitude extraction

For $t \neq 0$ amplitudes can be determined up to an overall phase. Since F^0_{++} is the dominant diffractive amplitude, thus mostly imaginary, all other amplitudes are projected on F^0_{++}. Therefore at each t value there are 7 unknown real numbers to be determined: F^0_{++}, $(F^0_{+-})_{\parallel}$, $(F^0_{+-})_{\perp}$, $(F^1_{++})_{\parallel}$, $(F^1_{++})_{\perp}$, $(F^1_{+-})_{\parallel}$ and $(F^1_{+-})_{\perp}$ (where $\perp$, $\parallel$ denotes component orthogonal, collinear to F^0_{++}). It follows that:

F^0_{++} is mostly determined from $\frac{d\sigma^+}{dt} + \frac{d\sigma^-}{dt}$

$(F^0_{+-})_{\parallel}$ is mostly determined from R^-

$(F^0_{+-})_{\perp}$ is mostly determined from $P^+\frac{d\sigma^+}{dt} + P^-\frac{d\sigma^-}{dt}$

$(F^1_{++})_{\parallel}$ is mostly determined from $\frac{d\sigma^-}{dt} - \frac{d\sigma^+}{dt}$

and $(F^1_{+-})_{\perp}$ is mostly determined from $P^+\frac{d\sigma^+}{dt} - P^-\frac{d\sigma^-}{dt}$

$(F^1_{+-})_{\parallel}$ could be determined from $R^-(d\sigma^-/dt) - R^+(d\sigma^+/dt)$, but data on $R^{\pm}$ is not good enough to proceed in this way: so that, in practice, the remaining two amplitudes $(F^1_{+-})_{\parallel}$ and $(F^1_{+-})_{\perp}$ are determined by two quadratic equations involving $d\sigma^0/dt$ and P^0.

In general two solutions for the F^0 amplitudes are found, whereas 4 solutions emerge for $(F^1_{++})_{\perp}$ and $(F^1_{+-})_{\parallel}$. Continuity from $t = 0$ together with the sign of $R^-(d\sigma^-/dt) - R^+(d\sigma^+/dt)$ seem sufficient to remove the ambiguities. At larger t values ($-t > 0.5$ GeV^2) ambiguities appear again because of insufficient information on R.

(c) Experimental problems

Besides the difficult experiments to measure $R^{\pm}$ (it is significant that only one experimental group has performed that experiment so far), the determination of the πN amplitudes suffer from uncertainties of experimental origin.

--it is hard to measure $\frac{d\sigma^-}{dt} - \frac{d\sigma^+}{dt}$ and hence $F(^1_{++})_\parallel$.

At 6 GeV, $d\sigma^-/dt \sim 40\ e^{7.7t}$ and $d\sigma^+/dt \sim 37\ e^{7.1t}$ (in mb/GeV^2), giving a cross-over zero around $t_c = -0.15$ GeV^2 (approximately the zero of $(F^1_{++})_\parallel$). If normalization uncertainties are 5%, then the error in location of t_c is $\Delta t_c = 0.1$ GeV^2, namely, its accurate position is not known. This situation has been improved by the experiment of Ambats et al. who claimed a normalization uncertainty of $\pm$ 1.5% between π^+p and π^-p, giving a Δt_c error of $\pm$ .025 GeV^2.

--measured values of P^0 are spread over a wide range outside quoted errors. Argonne points[11] are typically lower (~ 0.2) than CERN points[10] (~ 0.4). This particularly affects the determination of $(F^1_{++})_\perp$ as its zero can be moved from $t = -0.25$ to -0.5 GeV^2 according to what P^0 measurements are used.

(d) Results

There have been several analyses,[13-16] all using essentially the same sets of data. We are going to discuss the latest analysis[5] by the Argonne group since it uses their new data on $d\sigma^\pm/dt$.

--$I_t = 0$ exchange $(P + f)$ (Fig. 2).

F^0_{++} is large and is the dominant amplitude; it is roughly exponential in t. F^0_{+-} is small, but predominantly imaginary so that s-channel helicity is approximately conserved. To express the deviation in a quantitative way, it is useful to consider the invariant amplitudes A and A':

$$\left|\frac{A_0}{A'_0}\right| = \frac{2M\ |F^0_{+-}|}{\sqrt{-t}\ |F^0_{++}|} = 0.32 \pm 0.04, \qquad 0.10 < -t < 0.5\ \text{GeV}^2$$

The same ratio computed from t-channel helicity amplitudes yields a value of 1.5.

It is important to note that P and f exchanges cannot be separated since they have the same quantum numbers and consequently they always appear together in the observables. It is only through the energy dependence of the F^0 amplitudes over a large s range that P and f could be disentangled; unfortunately we only have 6 GeV so far.

--$I_t = 1$ exchange (ρ), (Fig. 3).

$(F^1_{++})_\parallel$ has a zero at $-t \sim 0.15$ GeV^2 and is strongly peripheral. A Bessel-Fourier transformation into impact parameter space shows a broad peak centered at about 1 f. $(F^1_{++})_\perp$ also goes through zero in the same t range, although at a larger value than $(F^1_{++})_\parallel$: it occurs at $-t \sim 0.25$ GeV^2 with the Argonne polarization data[11] while it moves out to $-t \sim 0.4$ GeV^2 with the CERN data.[10] The modulus of F^1_{+-} vanishes around $-t \sim 0.6$ GeV^2. Ambiguities preclude from making a precise conclusion above 0.6: in particular (although there is a hint in the data) it is not possible to see if there is a single zero in $(F^1_{+-})_\parallel$ and a double zero in $(F_{+-})_\perp$ as would be expected from a ρ Regge pole amplitude. The behaviour of the phase difference between F^0_{++} and F^1_{+-} is interesting since it is essentially independent of t for $-t < 0.4$ GeV^2: if ρ exchange is Regge-behaved in the helicity-flip amplitude, it therefore means that the phase of F^0_{++} is changing significantly with t. This is important to keep in mind since F^0_{++} is the reference amplitude and consequently the correspondence between $\perp$ and $\parallel$ components and real and imaginary parts is unfortunately not straightforward.

(e) Future of complete amplitude analyses

In πN scattering, R^- measurements already exist at 16 and 40 GeV,[17] but P_0 measurements do not extend beyond 11 GeV. At 16 GeV some information can be obtained on F^0 amplitudes:

$$\frac{2M\,|F^0_{+-}|}{\sqrt{-t}\,|F^0_{++}|} = 0.26 \pm 0.06$$

i.e. not very much smaller than the value at 6 GeV.

In KN and $\overline{K}N$ scattering there are 8 independent amplitudes and therefore 15 unknown quantities (+ overall phase). Eight independent observables have so far been measured around 8 GeV:

$$\frac{d\sigma}{dt}(K^{\pm}p) \qquad \frac{d\sigma}{dt}(K^0_L p \to K^0_S p)$$

$$\frac{d\sigma}{dt}(K^-p \to \overline{K}^0 n) \qquad \frac{d\sigma}{dt}(K^+n \to K^0 p)$$

$$P(K^{\pm}p) \qquad P(K^-p \to \overline{K}^0 n)$$

while a measurement of $P(K^+n \to K^0p)$ is underway at CERN. So at least 6 other experiments are needed to measure:

$$\frac{d\sigma}{dt}(K^{\pm}n) \qquad P(K^{\pm}n)$$

$$P(K^0_L p \to K^0_S p) \qquad R(K^+p)$$

The complete extraction of KN and $\overline{K}N$ amplitudes at high energy will remain a dream still for some time.

3. Hypercharge Exchange Reactions

In hypercharge exchange processes the final baryon is a Λ^0, Σ^+ or a Y^* decaying into Λ or Σ. It is therefore possible to measure all the components of its polarization vector with the observation of the angular distribution of the weak decay (we exclude final states with Σ^0 which decays electromagnetically). Examples of such processes are:

$$\pi^+p \to K^+\Sigma^+$$

$$K^-p \to \pi^0\Lambda^0$$

$$\pi^+p \to K^+Y_1^{*+}$$

$$\hookrightarrow \Sigma^+\pi^0,\ \Lambda^0\pi^+$$

(a) Decay angular distribution of an unstable baryon

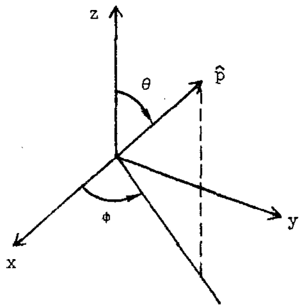

Generally the decay angular distribution is given by:

$$W(\hat{p}) = \sum_{\substack{\lambda\lambda' \\ (\mu)}} \rho^{(\mu\mu)}_{\lambda\lambda'}\, B^{\lambda\lambda'}(\hat{p})$$

where $\rho^{(\mu\mu')}_{\lambda\lambda'}$ is the density matrix for the final state plarization in the reaction (μ refers to the helicity state of the particles accompanying the hyperon in the final state).

For a weak two-body decay ($\Lambda^0 \to p\pi^-$, $\Sigma^+ \to p\pi^0$) where $\hat{p}$ can be taken along the final proton, the elements $B^{\lambda\lambda'}$ take the following form:

$$B^{\frac{1}{2}\,\frac{1}{2}} = \frac{1}{4\pi}(1 + \alpha\cos\theta)$$

$$B^{-\frac{1}{2}\,-\frac{1}{2}} = \frac{1}{4\pi}(1 - \alpha\cos\theta)$$

$$B^{\frac{1}{2}\,-\frac{1}{2}} = \frac{\alpha}{4\pi}\,e^{i\phi}\sin\theta$$

$$B^{-\frac{1}{2}\,\frac{1}{2}} = \frac{\alpha}{4\pi}\,e^{-i\phi}\sin\theta$$

where α is the decay parameter in the parity-violating weak decay, measuring the interference between S and P waves:

$$\alpha = \frac{2\,\mathrm{Re}\,S^*P}{|S|^2 + |P|^2}$$

Using the expression used previously for the density matrix elements of a spin 1/2 particle expressed in terms of the polarization vector, we get

$$W(\hat{p}) = \frac{1}{4\pi}\,(1 + \alpha\,\vec{P}_{Y}.\,\hat{p})$$

where P_Y is the hyperon polarization vector. Experimentally the situation is hopeful:

$$\left.\begin{aligned}\alpha(\Lambda^0 \to p\pi^-) &= 0.65\\ \alpha(\Sigma^+ \to p\pi^0) &= -0.98\end{aligned}\right\}\quad \text{(very good analyzers)}$$

$$\alpha(\Xi^- \to \Lambda\pi^-) = -0.39$$

$$\alpha(\Xi^0 \to \Lambda\pi^0) = -0.44$$

$$\alpha(\Sigma^+ \to n\pi^+) = 0.07 \qquad \text{(useless)}$$

(b) Application to amplitude analysis

For an unpolarized target experiment, the observation of the hyperon decay measures the P parameter as defined in Section 1:

$$W(\theta,\phi) = \frac{1}{4\pi}\,(1 + \alpha\,P \sin\phi \sin\theta)$$

If the target is polarized along the direction $\vec{P}^i$ with components $P^i_x = P^i_\perp \cos\psi$, $P^i_y = P^i_\perp \sin\psi$, P^i_z with respect to the reaction plane (ψ azimuthal angle), then the complete observation of the angular distribution of the decay measures all three polarization parameters P, R', A':

$$\begin{aligned}W(\theta,\phi)\\ &= \frac{1}{4\pi}\,[1 + \alpha P^i_y \sin\phi \sin\theta + P(\alpha \sin\phi \sin\theta + \alpha P^i_y)\\ &\quad + R'(\alpha P^i_y \cos\theta - \alpha P^i_z \cos\phi \sin\theta) + A'(\alpha P^i_x \cos\phi \sin\theta + \alpha P^i_z \cos\theta)]\end{aligned}$$

We note that P can be measured in two ways: observation of the hyperon decay with an unpolarized target[18] or left-right asymmetry with a polarized target.[19] It is comforting that the two experiments agree well.

An experiment designed to measure R' in the process $\pi^- p \to K^0\Lambda^0$ is planned at CERN.[20] Contrary to $R^\pm$ in elastic scattering, it is expected that R can be large in non-diffractive exchange reactions and therefore will be very useful to sort out the underlying amplitudes.

4. Generalization to Several Spins; Resonance Production and Joint-Decay Distributions

When higher-spin particles are produced, or when several particles in the final state have spin, the number of observables increases sharply and can exceed the number of independent real amplitudes. For example, in the process $\pi^- p \to (\text{spin J meson})^0 + \Lambda^0$ where the Λ^0 and meson decays are observed the number of observables with unpolarized target is $2(J+1)(2J+1)$ while there are only $4(2J+1)-1$ independent real amplitudes. There is therefore some degree of redundancy in the measurements and it becomes extremely important to understand the relations between all the observables and to define a set of independent observables to be measured with a minimum use of polarized targets.

Our purpose in this section is not to derive results in detail but rather to present a formalism to describe any two-body process with any spins in order to reconstruct amplitudes from experimental data in the most efficient way.

(a) Transversity amplitudes[21-23]

When several particles with spin are involved it becomes more interesting to use the transversity--rather than helicity--quantization axes.

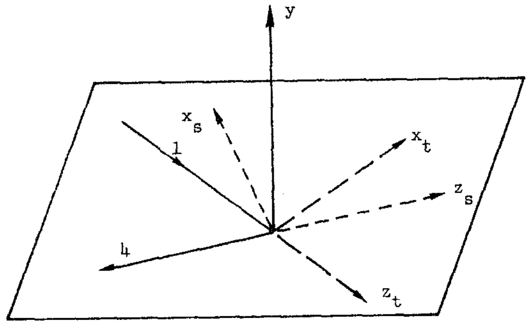

reaction plane and center-of-mass of particle 3

The following reference frames are defined:

(x_s	y	z_s)	s-channel	helicity axes
(x_t	y	z_t)	t-channel	
(z_s	x_s	y)	s-channel	transversity axes
(z_t	x_t	y)	t-channel	

In the s-channel helicity frame the third axis is collinear to the momentum $(\hat{z} \parallel \vec{p}_3)$, while they are orthogonal $(\hat{z} \perp \vec{p}_3)$ in the transversity frame. Going from helicity to transversity frames only involves a rotation with Euler angles $\pi/2$, $\pi/2$ and $-\pi/2$.

As we shall see, transversity amplitudes are very useful because they are much more closely related to the measured observables than helicity amplitudes; in particular the redundancy between several measurements is easier to see and it is simple to define a set of independent measurements, both problems not being very transparent in the helicity quantization.

-parity conservation: $H_{\lambda\ldots}$ helicity amplitudes

$T_{\tau\ldots}$ transversity amplitudes

$$H_{\lambda_3\lambda_4\lambda_1\lambda_2} = \eta(-1)^{\Sigma J-\Sigma\lambda} H_{-\lambda_3-\lambda_4-\lambda_1-\lambda_2}$$

for unpolarized initial state $\rho^{\lambda_3\lambda_3'}_{\lambda_4\lambda_4'} = (-1)^{\lambda_3-\lambda_3'+\lambda_4-\lambda_4'} \rho^{-\lambda_3-\lambda_3'}_{-\lambda_4-\lambda_4'}$

$$T_{\tau_3\tau_4\tau_1\tau_2} = 0 \quad \text{if} \quad \eta(-1)^{\tau_1+\tau_2-\tau_3-\tau_4} = -1$$

for unpolarized initial state $\rho^{\tau_3\tau_3'}_{\tau_4\tau_4'} = 0$ for $\tau_3-\tau_3'+\tau_4-\tau_4'$ odd

-naturality conserving amplitudes

With linear combination of helicity amplitudes, one can define naturality amplitudes to leading order in s as in Section 1 of this chapter.

$$N^{\pm}_{\lambda_3\lambda_4\lambda_1\lambda_2} = \frac{1}{\sqrt{2}} \left[H_{\lambda_3\lambda_4\lambda_1\lambda_2} \pm \epsilon(\lambda_3\lambda_1)\, H_{-\lambda_3\lambda_4-\lambda_1\lambda_2} \right]$$

$$\text{with} \quad \epsilon(\lambda_3\lambda_1) = \eta_1\eta_3 \exp[i\pi(v + J_3 - \lambda_3 + J_1 - \lambda_1)]$$

and $v = 0$ for boson exchange, $v = 1/2$ for baryon exchange.

Let us write down the transformation from helicity to transversity amplitudes:

$$T_{\tau_3\tau_4\tau_1\tau_2} = \sum_{\lambda_1\lambda_2\lambda_3\lambda_4} D^{J_1}_{\lambda_1\tau_1}(R)\, D^{J_2}_{\lambda_2\tau_2}(R)\, D^{J_3}_{\lambda_3\tau_3}(R^*)\, D^{J_4}_{\lambda_4\tau_4}(R^*)\, H_{\lambda_3\lambda_4\lambda_1\lambda_2}$$

where R is the rotation $R(\frac{\pi}{2}, \frac{\pi}{2}, -\frac{\pi}{2})$

$$= \frac{1}{2} \sum_{\lambda_1\lambda_2\lambda_3\lambda_4} D^{J_1} D^{J_2} D_*^{J_3} D_*^{J_4} \Big[H_{\lambda_3\lambda_4\lambda_1\lambda_2} + \xi\eta_1\eta_3 \exp[i\pi(v + J_1-\lambda_1+J_3-\lambda_3)] \times H_{-\lambda_3\lambda_4-\lambda_1\lambda_2} \Big]$$

We therefore have the important result that T amplitudes are naturality-conserving amplitudes with

$$\xi = \eta_1\eta_3 \exp[i\pi(v + \tau_3 - \tau_1)]$$

In conclusion, transversity amplitudes are simpler to work with because of the parity relations (some amplitudes are plainly zero) and they correspond to well-defined naturality in the t channel. These properties make them closer to experimental data. However, helicity amplitudes have a more physical interpretation and one needs to know <u>all</u> of the transversity amplitudes to reconstruct any <u>one</u> of the helicity amplitudes.

(b) <u>Naturality of exchange</u>[23]

Since transversity amplitudes correspond to pure naturality exchange, they constitute the simplest description of a two-body process in terms of t or u channel exchanges. More practically, they tell us what measurements are needed to extract the different naturalities and their interference.

The transversity density matrix elements for particle 3 when the initial state is unpolarized, are:

$$\rho_{\tau_3\tau_3'} = \frac{1}{N} \sum_{\tau_1\tau_2\tau_4} T_{\tau_3\tau_4\tau_1\tau_2} T^*_{\tau_3'\tau_4\tau_1\tau_2}$$

and the only non-zero elements have $\tau_3-\tau_3'$ even.

-With unpolarized initial state and measurement of one final polarization, all observables can be expressed by (superscript = naturality)

$$\sum [T^+_\lambda T^{+*}_\mu + T^-_\lambda T^{-*}_\mu]$$

and are therefore insensitive to the relative phase between opposite naturalities.

-When particle 1 has spin 0, $\rho_{\tau_3\tau_3'}$ is the form

$$\sum T^+_\lambda T^{+*}_\mu \qquad \text{or} \qquad \sum T^-_\lambda T^{-*}_\mu$$

and isolates the exchanged naturality. In the helicity description, one has to combine $\rho_{\lambda_3\lambda_3'}$ elements to project out a given exchanged naturality.

-If both particles 1 and 3 have spins, the naturality separation requires polarization of 1 and analysis of polarization of 3 through its decay or in a rescattering experiment. When particle 3 decays strongly some polarization information is obtained and allows the naturality separation when a meson is produced (1 = meson, 3 = meson) but not when a baryon is produced (1 = meson, 3 = baryon decaying strongly).

-To measure the interference between opposite naturality exchanges requires polarization measurements at opposite vertices; for example, measurement of the double density matrix elements $\rho^{\tau_4\tau_4'}_{\tau_3\tau_3'}$ with $\tau_3-\tau_3'$ and $\tau_4-\tau_4'$ both even.

These results are summarized below in a pictorial way[23] with diagrams representing incoming and outgoing particles; lines can be reversed at the same vertex. All particles have spin (otherwise indicated) and a vertical arrow has the meaning of a polarization measurement (either incoming polarized particle, or measurement of an outgoing particle polarization)

<u>measurements</u> <u>amplitudes measured</u>

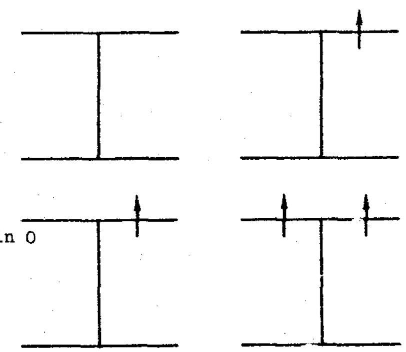

spin 0

incoherent sum of naturalities

$|T^+_\lambda|^2 + |T^-_\lambda|^2$

opposite naturalities separation

$|T^+_\lambda|^2$

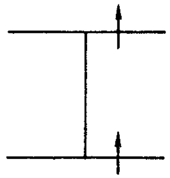

interference between opposite naturalities

$T^{+}_{\lambda} T^{-*}_{\mu}$

(c) Applications

(1)

spin 0 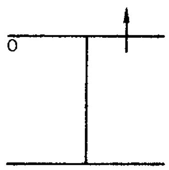 spin 1

Exchanged naturality	Transversity density matrix elements	Helicity density matrix elements
$\xi = \eta_1\eta_3$	ρ^T_{00}	$\rho^H_{11} + \rho^H_{1-1}$
$\xi = -\eta_1\eta_3$	$\rho^T_{11} + \rho^T_{1-1}$	ρ^H_{00}
	Re ρ^T_{1-1}	$\rho^H_{11} - \rho^H_{1-1}$
	Im ρ^T_{1-1}	Re ρ^H_{10}

$\pi N \to \rho N$

$\xi = +1$	$(\rho^H_{11} + \rho^H_{1-1}) \frac{d\sigma}{dt}$	"ω, A_2" exchange (helicity 1)
$\xi = -1$	$\rho^H_{00} \frac{d\sigma}{dt}$	"π" exchange (helicity 0)
	$(\rho^H_{11} - \rho^H_{1-1}) \frac{d\sigma}{dt}$	"π" exchange (helicity 1)

A complication which should be accounted for is due to the presence of an S-wave $\pi\pi$ which interferes with the ρ amplitudes. An example of the 3-amplitude separation is shown in Fig. 4.

$\gamma N \to \pi N$

The naturality separation is particularly clear in this reaction where it is achieved by using linearly polarized photons.

$$\left(\frac{d\sigma}{dt}\right)_{\xi=+1} = \frac{d\sigma_\perp}{dt} \qquad (P_\gamma \text{ perpendicular to the scattering plane})$$

$$\left(\frac{d\sigma}{dt}\right)_{\xi=-1} = \frac{d\sigma_\parallel}{dt}$$

The separation is shown in Fig. 5 for $\gamma p \to \pi^0 p$ at 6 GeV. Extensive measurements of that type have been carried out for $\pi^\pm$ photoproduction ($\gamma N \to \pi N$ and $\gamma N \to \pi\Delta$).[24]

(2)

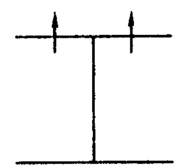

A well-known example is vector meson photoproduction with linearly polarized photons where the meson decay measures the amount of natural and unnatural parity exchange.[25] This is particularly striking in the case of ω production where around 5 GeV both π exchange and diffraction occur in similar magnitude and can be fully separated by this technique.

(3)

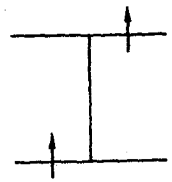

An experiment of this type is in progress at CERN[26] with $\pi^- p\uparrow \to \rho^0 n$. The upper vertex determines the exchanged naturality while correlations between proton polarization and ρ^0 decay distributions relate to the interference between opposite naturalities. Even ignoring the S-wave problem this experiment still does not measure all the helicity amplitudes in this process (see next section) since the ρ decay is parity-conserving.

(d) Joint-decay distributions; statistical tensors

If both particles 3 and 4 decay, the joint-decay distribution takes a simple form when expressed in terms of statistical tensors $t^{LL'}_{MM'}$:

$$W(\theta_3\phi_3\theta_4\phi_4) = \sum_{\substack{L_3L_4\\M_3M_4}} F_3(L_3)\, F_4(L_4)\, t^{L_3L_4}_{M_3M_4}\, Y^{L_3 *}_{M_3}(\theta_3\phi_3)\, Y^{L_4 *}_{M_4}(\theta_4\phi_4)$$

where $F(L)$ are known coefficients depending of the spin on the decaying particle and its decay mode. If parity is conserved in the decay, then $F(L) = 0$ for L odd: an important consequence is that strong decays only measure even polarization tensors (even L_3 and even L_4). Experimentally the elements $t^{L_3L_4}_{M_3M_4}$ are measured by evaluating moments:

$$F_3(L_3)\, F_4(L_4)\, t^{L_3L_4}_{M_3M_4} = \left\langle Y^{L_3}_{M_3}(\theta_3\phi_3)\;\; Y^{L_4}_{M_4}(\theta_4\phi_4)\right\rangle$$

The statistical tensors are related to the double density matrix elements:

$$\rho^{\lambda_3\lambda_3'}_{\lambda_4\lambda_4'} = \sum_{\substack{L_3L_4\\M_3M_4}} (-1)^{J_3+\lambda_3-L_3+J_4+\lambda_4-L_4}\, \langle J_3 - \lambda_3;\, J_3\lambda_3'|L_3M_3\rangle \langle J_4-\lambda_4; J_4\lambda_4'\; L_4M_4\rangle\, t^{L_3L_4}_{M_3M_4}$$

and have the following properties

normalization $\qquad t^{00}_{00} = \dfrac{1}{\sqrt{(2J_3+1)(2J_4+1)}}$

hermicity $\qquad \left(t^{L_3L_4}_{M_3M_4}\right)^* = (-1)^{M_3+M_4}\, t^{L_3L_4}_{-M_3-M_4}$

parity $\begin{cases} \text{helicity frame} & t^{L_3L_4}_{M_3M_4} = (-1)^{L_3+L_4-M_3-M_4}\, t^{L_3L_4}_{-M_3-M_4} \\ \text{transversity frame} & t^{L_3L_4}_{M_3M_4} = 0 \qquad M_3 + M_4 \;\text{odd.} \end{cases}$

Let us see in one example how to use statistical tensors in the transversity frame.

$$\pi^+ p \to K^+ Y^*(1385)$$

$$\tfrac{3}{2}^+$$

$$\hookrightarrow \Lambda^0 \pi^+$$

$$\hookrightarrow p\pi^-$$

Four amplitudes are necessary to describe this reaction and therefore we have seven unknown quantities to solve for at each t value. Here, since Λ decays weakly, both L odd and even components of t^L_M are non-zero; however due to parity conservation in the production all $M = 1$ components vanish in the transversity frame. So there are 6 non-vanishing tensor elements:

$$t_0^0 \quad t_0^1 \quad t_0^2 \quad t_0^3 \qquad \text{(real)}$$

$$t_2^2 \quad t_2^3 \qquad \text{(complex)}$$

To relate the amplitudes let us come back to the density matrix elements in the transversity frame. The following elements

$$\rho_{\frac{3}{2}\frac{3}{2}} = \left|T_{\frac{3}{2}-\frac{1}{2}}\right|^2$$

$$\rho_{\frac{1}{2}\frac{1}{2}} = \left|T_{\frac{1}{2}\frac{1}{2}}\right|^2$$

$$\rho_{-\frac{1}{2}-\frac{1}{2}} = \left|T_{-\frac{1}{2}-\frac{1}{2}}\right|^2$$

$$\rho_{-\frac{3}{2}-\frac{3}{2}} = \left|T_{-\frac{3}{2}\frac{1}{2}}\right|^2$$

are linear combinations of the t_0^L components and yields the magnitude of the 4 amplitudes while the elements

$$\rho_{\frac{3}{2}-\frac{1}{2}} = \rho^*_{-\frac{1}{2}\frac{3}{2}} = T_{\frac{3}{2}-\frac{1}{2}} T^*_{-\frac{1}{2}-\frac{1}{2}}$$

$$\rho_{\frac{1}{2}-\frac{3}{2}} = \rho^*_{-\frac{3}{2}\frac{1}{2}} = T_{\frac{1}{2}\frac{1}{2}} T^*_{-\frac{3}{2}\frac{1}{2}}$$

are linear combinations of the complex t_2^L components and measure two of the three relative phases. Without a polarized target it is thus possible to separate amplitudes up to an overall phase and to the phase between amplitudes with opposite target transversities.

The previous conclusion is quite general: with an unpolarized target one can at best (when all components of polarizations are measured, in a weak decay) measure N-1 real amplitudes with an arbitrary overall phase convention when N numbers are needed to extract all the amplitudes: this last unmeasured phase necessitates the use of a polarized target. When a polarized target is used, many more observables can be measured, providing constraints for the amplitude determination. The situation is summarized in Table 2 for typical reactions.[27] Reactions like $\pi N \to K^*\Lambda$ and $\pi N \to KY^*$ should be very helpful in our understanding of strong amplitudes: analyses of the type described previously will involve high-statistics experiments with large solid-angle systems to observe the decay correlations.

(e) polarized proton beams

Experiments are being done at ANL with a polarized proton beam; in particular elastic scattering in pure spin states has been measured.[28] To understand the meaning of the data in terms of the more familiar helicity amplitudes[29-30] it is necessary to transform spin states $|s_y = \pm\frac{1}{2}\rangle$ into helicity states $|s_z = \pm\frac{1}{2}\rangle$:

$$|{\uparrow \atop \downarrow}\rangle = |s_y = \pm\tfrac{1}{2}\rangle = \frac{1}{\sqrt{2}}\,[\,|s_z = +\tfrac{1}{2}\rangle \pm i\,|s_z = -\tfrac{1}{2}\rangle]$$

Proton-proton elastic scattering is described by 5 helicity amplitudes:

$$\left.\begin{array}{l} H_1 = \langle ++|M|++\rangle \\ H_2 = \langle ++|M|--\rangle \\ H_3 = \langle +-|M|+-\rangle \end{array}\right\} \text{overall no helicity flip}$$

$$H_4 = \langle +-|M|-+\rangle \qquad \text{double helicity flip}$$

$$H_5 = \langle ++|M|+-\rangle \qquad \text{single helicity flip}$$

One can then express the pure spin states cross-sections shown in Fig. 6 in terms of the amplitudes H_i or even better in terms of linear combinations of H_i isolating pure naturality exchange. It is then easy to show that $\frac{d\sigma}{dt}(\uparrow\uparrow \to \uparrow\uparrow)$, $\frac{d\sigma}{dt}(\downarrow\downarrow \to \downarrow\downarrow)$ and $\frac{d\sigma}{dt}(\uparrow\downarrow \to \uparrow\downarrow)$ only involve natural parity exchange, while $\frac{d\sigma}{dt}(\uparrow\uparrow \to \downarrow\downarrow)$ and $\frac{d\sigma}{dt}(\uparrow\downarrow \to \downarrow\uparrow)$ correspond to pure unnatural parity exchange.

The data at 6 GeV and $t = 0.5\ \mathrm{GeV}^2$ shows that these unnatural parity cross sections are small, typically 10% or less of the dominant natural parity cross sections.

TABLE 1

Reaction type	Number of helicity amplitudes				
	no discrete symmetry	using P	using T	using C	using PTC
$\pi N \to \pi N$	4	2	2	-	2
$\pi N \to \pi\Delta$	8	4	-	-	4
$\gamma N \to \gamma N$	16	8	10	-	6
$\pi N \to \rho N$	12	6	-	-	6
$NN \to NN$	16	8	10	-	5
$\bar{N}N \to \bar{Y}Y$	16	8	-	12	6

TABLE 2

Reaction type	Number of amplitudes	Number of real independent observables	measured observables (+ constraints)		
			unpolarized target	polarized target	
				transverse	longitudinal
$\pi N \to \pi N$	2	3	1	2	(+0)
$K\Lambda$	2	3	2	3(+3)	(+2)
ρN	6	11	4	10	(+2)
$K^*\Lambda$	6	11	10(+2)	11(+25)	(+12)
$\pi\Delta$	4	7	4	7(+3)	(+2)
KY^*	4	7	6(+2)	7(+17)	(+8)
$\rho\Delta$	12	23	20	23(+33)	(+16)
K^*Y^*	12	23	22(+26)	23(+121)	(+48)

II - GENERAL FEATURES OF EXCHANGE PROCESSES

We shall discuss almost exclusively non-diffractive two-body processes, although in some cases the diffractive part cannot be easily separated out, such as in elastic scattering for $I_t = 0$ exchange. We are going to summarize properties of data on two-body scattering in order to gather information on the behaviour of the underlying amplitudes. We have seen that our knowledge of single amplitudes is rather limited; on the other hand there is a wealth of data on cross sections and polarizations which can cast some light on our problem.

1. Kinematic Dependence

(a) s dependence

--t = 0

Very useful information on the behaviour at $t = 0$ of the imaginary parts of the amplitudes can be extracted from total cross section measurements. These measurements are rather complete--$\pi^\pm$, $K^\pm$ and $p^\pm$ on protons and neutrons--and cover a wide range of s values from threshold to $\sim 400\ \mathrm{GeV}^2$. It is useful to project each forward amplitude onto t-channel quantum numbers, conveniently labelled by particles' names:

$$\sigma_T(\pi^\pm p) = P_\pi + f_\pi \mp \rho_\pi$$

$$\sigma_T(K^\pm p) = P_K + f_K \mp \omega_K \mp \rho_K + A_K$$

$$\sigma_T(K^\pm n) = P_K + f_K \mp \omega_K \pm \rho_K - A_K$$

$$\sigma_T(p^\pm p) = P_p + f_p \mp \omega_p \mp \rho_p + A_p$$

$$\sigma_T(p^\pm n) = P_p + f_p \mp \omega_p \pm \rho_p - A_p$$

Defining sums and differences

$$\Delta(Ap) = \sigma_T(A^-p) - \sigma_T(A^+p)$$

$$\Sigma(Ap) = \sigma_T(A^-p) + \sigma_T(A^+p)$$

we can express the pure t-channel exchanges in terms of the measured cross sections:

$$\left.\begin{aligned} 2\rho_\pi &= \Delta(\pi p) \\ 4\rho_K &= \Delta(KP) - \Delta(Kn) \\ 4\omega_K &= \Delta(Kp) + \Delta(Kn) \\ 4A_K &= \Sigma(Kp) - \Sigma(Kn) \end{aligned}\right\} \text{ and similar relations for } p^{\pm}N$$

Experimental problems are obvious in these extractions: systematic differences between experiments show up, particularly in different energy regions; also neutron data comes from deuterium experiments where a Glauber correction has to be applied. In regard to the last remark it is interesting that a better determination of the s dependence of ω_K and ω_p comes from $\Delta(Kd)$ and $\Delta(pd)$ directly. We are not going to discuss here f and P exchanges since they cannot be separated simply; we shall come back to this problem in the last chapter.

The s-dependence of the imaginary part of exchange amplitudes at $t = 0$ has some remarkable properties:

(i) from well measured differences, amplitudes are seen to be power-behaved in s (or p_L) after a few oscillations at low energies. Energies around 3-4 GeV are typical lower limits for the simple power behaviour. We parameterize the s dependence in the form

for example $$\rho_\pi = \beta_\pi \, s^{\alpha_\rho^\pi - 1}$$

(ii) all the exponents α_i that can be isolated cluster around 0.5 ($\pm$ 0.1). Accurate values depend sensitively on low s cut-offs, uncertainties in neutron data and resolution of discrepancies between experiments. Values found using the data of Ref. 31-35 are shown in Table 3. A typical example of the power behaviour is displayed in Fig. 7 with $\Delta(Kd)$ and $\Delta(pd)$.

(iii) Same exchanges in different processes show a close similarity in their energy dependence. In particular α_ρ^π is equal to α_ρ^K within errors and is also consistent with the badly determined α_ρ^P. Also the very accurately determined α_ω^K and α_ω^P are the same, as can be seen directly in Fig. 7. One therefore concludes that, within the limited range of processes and exchanges afforded by elastic scattering, the power behaviour of a given t-channel exchange is not affected in a strong way by s-channel effects (like absorption) at $t = 0$.

The s dependence of amplitudes at $t = 0$ can also be obtained from measurements on differential cross sections, $(d\sigma/dt)_{t=0}$. Experimentally this is not always easy: if a recoil particle has to be observed, data will only exist up to some minimum $|t|$ value and extrapolation at $t = 0$ will be necessary with the corresponding uncertainties; if, on the other hand, no recoil is observed $t = 0$ can be easily reached, if not smeared by resolution effects or not affected by Coulomb effects, such as in elastic scattering where Coulomb scattering (γ exchange) has to be subtracted out. When well-defined t-channel quantum numbers can be isolated, information is thus obtained on the s dependence of the modulus of the corresponding amplitude and is therefore complementary to the information contained in total cross-sections.

Experimental determinations of the s dependence of some $(d\sigma/dt)_{t=0} \sim s^{2\alpha-2}$ are shown in Table 4. An immediate conclusion when results in Tables 3 and 4 are compared is that α values obtained from $(d\sigma/dt)_{t=0}$ and σ_T are consistent with one another when the same exchange is involved: this is very important because it means that the phase of the amplitude at $t = 0$ is essentially energy-independent. This, as we shall see in Chapter 3, is a consequence of analyticity in energy and power behaviour.

--$t \neq 0$

Data on differential cross sections have traditionally been parametrized using:

"slope" $\qquad \frac{d\sigma}{dt} = A(s)\ e^{B(s)t}$

"α_{eff}" $\qquad \frac{d\sigma}{dt} = As^{2\alpha_{eff}(t)-2}$

The experience has been that s dependence of slopes is not particularly illuminating for exchange reactions and the α_{eff} approach has been in general more fruitful. However we would like to warn against an abusive use of α_{eff}: if, in non-diffractive reactions, it seems that cross sections are reasonably well power-behaved (see $\pi^- p \to \pi^0 n$ in Fig. 8), it is not the case in elastic scattering and α_{eff} determinations depend on the energy range considered and can be very misleading.

The most reliable α_{eff} determination comes from $\pi^- p \to \pi^0 n$ over a very wide s range (with the new NAL data[39]) and shows a simple linear function $\alpha_{eff}(t)$[36]

$$\alpha_\rho(t) = (.56 \pm .02) + (.97 \pm .04)t$$

out to t values around $-1.5\ \text{GeV}^2$ (Fig. 9).

The situation is not so pretty for the case of A_2 exchange where a crude linear behaviour seems to exist for $0 > t \gtrsim -0.5\ \text{GeV}^2$ but larger $|t|$ data is too imprecise to pin down unambiguously the s dependence. Information on the ω α_{eff} is still very primitive.

(b) t dependence and helicity structure

Exchange amplitudes generally exhibit an exponential fall-off in t, but even some of the crudest characteristics of the t dependence are determined by the relative amount of the different helicity amplitudes present in a given process.

In the forward t region the presence of a peak or a turn-over immediately informs us of the relative importance of overall helicity non-flip amplitudes and flip amplitudes at small t, since flip amplitudes have to vanish kinematically at $t = 0$. We observe:

$\pi^- p \to \pi^0 n$: ρ exchange mostly helicity flip (confirmed by complete amplitude analysis)

$K^- p \to \bar{K}^0 n$: ρ, A_2 mostly helicity flip

$K^+ n \to K^0 p$: (Im ρ_{++} and Im A_{++} given by σ_T data and are small at $t = 0$)

$K_L^0 p \to K_S^P p$: from the peak at $t = 0$, ω mostly helicity no-flip.

Dips for $t \neq 0$ (or absence of dip) provide direct information on helicity amplitudes, although it is hard to translate the facts into statements on real or imaginary parts of the amplitudes:

-from πN amplitudes at 6 GeV, both Re ρ_{+-} and Im ρ_{+-} vanish for $-t \sim 0.6\ \text{GeV}^2$ producing a dip in $d\sigma/dt\ (\pi^- p \to \pi^0 n)$.

- $d\sigma/dt(\pi^- p \to \eta n)$ is dominated by A_{+-} but no dip is seen at 0.6, so that we do not know simply the behaviour of Re A_{+-} and Im A_{+-} there.

-$I_t = 0$ exchange can be isolated in $\pi N \to \rho N$:

$$\left(\frac{d\sigma}{dt}\right)_{I_t=0} = \frac{1}{2}\left[\frac{d\sigma}{dt}(\pi^- p \to \rho^- p) + \frac{d\sigma}{dt}(\pi^+ p \to \rho^+ p) - \frac{d\sigma}{dt}(\pi^- p \to \rho^0 n)\right]$$

and it is seen to be almost completely natural parity exchange as given by $(\rho_{11}^H + \rho_{1-1}^H)(d\sigma/dt)_{I_t=0}$. It strongly resembles $|\rho_{+-}|^2$ (Fig. 10) with a forward turnover and a dip at $0.6\ \text{GeV}^2$. It therefore tells us that, because of the helicity flip at the upper vertex, ω exchange is predominantly non-flip at $N\bar{N}$ vertex--a fact we already knew from $K_L^0 p \to K_S^0 p$ forward peak.

A summary of our qualitative knowledge on dominant helicity couplings to baryon-antibaryon is indicated in Table 5.

One interesting phenomenological exercise is to follow the position of these dips as a function of s. It is remarkable that over a very large s range above a few GeV^2 their position is essentially at fixed t (or u) although the accuracy to detect a change is somewhat limited: for example the dip at $0.6\ \mathrm{GeV}^2$ in $\pi^- p \to \pi^0 n$ is rather well measured but it is difficult to assign a precise value to its location at high energies because of the steep fall-off of $d\sigma/dt$. There are a few cases where a systematic dip displacement has been observed, all of them in the low energy region. One remarkable example is given by the dip at $u \sim -0.2\ \mathrm{GeV}^2$ in $\pi^+ p$ backward scattering[40] (see Fig. 11) which shows, not a fixed u position, but a fixed $u' = u - u_{min}$. More interestingly, the same phenomenon is seen in the crossed channel process $\bar{p}p \to \pi^- \pi^+$ where the dip appears at larger $|u|$ but is well accounted for by a constant u' position. Such an observation is consistent with a geometrical origin of this dip since u' is directly related to the scattering angle, $|u'| \sim p^2\theta^2$.

Measurements of polarization are very useful tools to study the helicity structure of amplitudes. However, besides elastic scattering, data are rather poor and most of the time not very informative regarding t dependence. On the other hand the s dependence has a characteristic feature:

(i) for elastic processes, fixed-t polarization is generally power-behaved in s corresponding to the interference between a dominant $(P + f)_{++}$ amplitude slowly varying in s with a flip amplitude (ρ_{+-}, A_{+-}) falling like a power.

(ii) for inelastic processes, P is rather independent of energy, as expected from the interference between helicity amplitudes falling with s at similar rates.

2. <u>Quantum Numbers Exchanged</u>

It is an experimental fact that exchange amplitudes are connected with the existence of particles with the same quantum numbers; in particular when t or u-channel quantum numbers do not correspond to any known particle the corresponding amplitudes are always small.

(a) <u>Allowed exchange</u>

We have so far mainly talked about $(P + f)$, ρ, ω and A_2 exchanges. Let us complete here a rapid survey of meson exchange.

<u>K^* exchange</u>

A large amount of data exist on hypercharge exchange cross sections and polarizations. Of particular importance, line-reversed reactions such as

$$\pi N \to K\binom{\Sigma}{\Lambda} \qquad\qquad \bar{K}N \to \pi\binom{\Sigma}{\Lambda}$$

have been measured over a wide range of energies. Unfortunately the measurements are not complete yet for an amplitude analysis and only model-dependent studies have been made. An interesting fact is the absence of a forward turn-over, such as in $\pi^- p \to \pi^0 n$ and $\pi^- p \to \eta n$ indicating that these reactions will be in principle very powerful tools to study non-flip amplitude with K_V^* and K_T^* exchange, and compare them with their non-strange SU(3) partners.

<u>π exchange</u>:

Good spectrometer data exist at 6 GeV[41] and 17 GeV.[26] Unnatural parity exchange as given by

$$\sigma_0 = \rho_{00}^H \frac{d\sigma}{dt} \qquad\qquad (\lambda_p = 0)$$

$$\sigma_- = (\rho_{11}^H - \rho_{1-1}^H)\frac{d\sigma}{dt} \qquad\qquad (\lambda_p = \pm 1)$$

is thought to be dominated by π exchange. As seen in Fig. 12, σ_0 shows no shrinkage between 6 and 17 GeV for $0 < -t < 0.5\ \mathrm{GeV}^2$ corresponding to a constant $\alpha_{eff} \simeq 0$.

Natural parity exchange

$$\sigma_+ = (\rho^H_{11} + \rho^H_{1-1}) \frac{d\sigma}{dt} \qquad (\lambda_\rho = \pm 1)$$

also has $\alpha_{eff} \simeq 0$ for $-t < 0.15$ GeV^2 but seems to behave more like expected A_2 exchange at larger $|t|$ although α_{eff} is a bit too large there.

Good data relevant to π exchange exist on $KN \to K^*N$ at 6[41] and 13 GeV,[42] π photoproduction[24] $\gamma\uparrow N \to \pi^\pm N$, and $\pi^\pm\Delta$ (mostly natural parity exchange) and $np \to pn$, $\bar{p}p \to \bar{n}n$.

Reactions with π exchange are rather complex in the fact they generally involve many exchanges,and it is clear that the underlying amplitudes can only be uncovered by complete measurements. There is however good evidence here that the identification of t-channel quantum numbers with "pure" exchanges fails, presumably because of large absorption correction to π exchange, spilling over to $\xi = +1$ amplitudes. Of course the proximity of the π pole from $t = 0$ makes π exchange something unique where some of the Regge character shown by other exchanges may be washed out. For practical purposes it is very important to understand π exchange since it is one of the most productive areas of meson spectroscopy through $\pi\pi$ and $K\pi$ scattering, and improved knowledge of the π exchange amplitudes will consolidate the process of extrapolating to the pion pole.

Baryon exchange

The experimental situation is rather poor since cross sections in the backward direction are small at high energy. For allowed baryon exchange, s dependence vary between $\alpha(0) = 0$ and $\alpha(0) = -0.7$. Looking at the s dependence of the backward peak over a large energy range (for example in Fig. 13), we notice that s channel effects are still present at energies ~ 5 GeV; a consequence of this fact is that data at higher energies are needed in order to see the distinct properties of "smooth" u-channel exchange. It is interesting that before the s dependence of baryon exchange sets in, the fall-off in s is fairly steep, s^{-7} to s^{-11}, averaging over resonances.

The closest we come to u-channel amplitudes is in πN scattering around 6 GeV where $\pi^\pm p \to p\pi^\pm$, $\pi^- p \to n\pi^0$ differential cross sections and $\pi^\pm p \to p\pi^\pm$ polarizations have been measured. In terms of $I_u = \frac{1}{2}\,(N)$ and $I_u = \frac{3}{2}\,(\Delta)$ quantum numbers we have (summing over nucleon helicities)

$$\frac{d\sigma^+}{du} = \frac{d\sigma}{du}\,(\pi^+ p \to p\pi^-) = \frac{1}{9}\,|2N + \Delta|^2$$

$$\frac{d\sigma^0}{du} = \frac{d\sigma}{du}\,(\pi^- p \to n\pi^0) = \frac{2}{9}\,|N - \Delta|^2$$

$$\frac{d\sigma^-}{du} = \frac{d\sigma}{du}\,(\pi^- p \to p\pi^-) = |\Delta|^2$$

and therefore

$$|N|^2 = \frac{1}{2}\left[3\left(\frac{d\sigma^+}{du} + \frac{d\sigma^0}{du}\right) - \frac{d\sigma^-}{du}\right]$$

$$|\Delta|^2 = \frac{d\sigma^-}{du}$$

$$\mathrm{Re}(N^*\Delta) = \frac{3}{4}\left[\frac{d\sigma^+}{du} - 2\,\frac{d\sigma^0}{du} + \frac{1}{3}\,\frac{d\sigma^-}{du}\right]$$

From the data (Fig. 14) we see that $|N|^2$ possesses a dip at $u \sim 0.2$ GeV^2 while $|\Delta|^2$ is structureless. However accurate analyses of the data are not easy since they rely critically on the relative normalizations of the different sets of data.

Important information could be gathered from the line-reversed reactions observed in $\bar{p}p$ two-body annihilations, i.e., $\bar{p}p \to \pi^\pm\pi^\mp$, allowing one to separate the different signatures. Data exist at 4-5 GeV[43] but relative normalization with πN data is difficult and the energy probably not high enough. In any case s dependence of annihilation data is generally compatible with the corresponding backward data.

(b) Exotic exchanges

Two definitions of an exotic exchange can be adopted;

1st kind: when quantum numbers are different from those of the $\underline{1}$ and $\underline{8}$ SU(3) representations for mesons or $\underline{8}$ and $\underline{10}$ for baryons.

2nd kind: where quantum numbers cannot be generated by a simple quark model with $q\bar{q}$ for mesons and qqq for baryons (more restrictive definition)

-experimental evidence

I = 2, I = 3/2 meson exchange

Cross sections for forbidden centre-of-mass hemisphere for the processes:

$\pi^- p \to K^+\Sigma^-$ $\qquad \pi^- p \to K^+ Y^{*-}$

$K^- p \to \pi^+\Sigma^-$ $\qquad K^- p \to \pi^+ Y^{*-}$

$\bar{p}p \to \bar{\Sigma}^+\Sigma^-$

$\pi^- p \to \pi^+\Delta^-$

$K^- p \to K^0\,\Xi^{*0}$

$K^- p \to K^+\,\Xi^{*-}$

all show fast fall-off in s $(\sim s^{-6})$ and are typically of the same order of magnitude (~ 1 μb at 5 GeV), with the notable exception of $\bar{p}n \to \bar{\Delta}^-\Delta^{++}$ (~ 100 μb at 5 GeV). Almost all of these reactions do not show a peak at small momentum transfer, thus failing to show the usual distinctive appearance of crossed-channel exchange: an exception is $\bar{p}p \to \bar{\Sigma}^+\Sigma^-$ at 5.7 GeV/c although the slope is somewhat small (~ 1 GeV^2).

The s dependence of $(d\sigma/dt)_{t\simeq 0}$ shows a more interesting behaviour (Fig. 15), particularly for $\pi^- p \to K^+\Sigma^-$,[44] although only meagre information on t dependence is provided. A significant change in s dependence seems to occur near 4 GeV/c however from looking at the t dependence it is still possible that the flattening could come from fluctuations in the angular distributions (as caused by s channel resonances, for instance). Higher s data are needed before a clear-cut conclusion can be drawn. Concerning the order of magnitude, let us note that at 5 GeV

$$\left[\frac{\frac{d\sigma}{dt}(\pi^- p \to K^+\Sigma^-)}{\frac{d\sigma}{dt}(\pi^+ p \to K^+\Sigma^+)}\right]_{t\simeq 0} \sim 2\ 10^{-4}$$

In view of the smallness of exotic amplitudes, it seems more fruitful to look for them through their interference with allowed amplitudes. For example,

$$A(\pi^- p \to K^0\Sigma^0) = \frac{\sqrt{2}}{3} A_{1/2} + \frac{\sqrt{2}}{3} A_{3/2} \qquad (A_{I_t})$$

$$A(\pi^+ p \to K^+\Sigma^+) = -\frac{2}{3} A_{1/2} + \frac{1}{3} A_{3/2}$$

where $A_{3/2}$ is the exotic amplitude. It follows that:

$$\frac{\mathrm{Re}\, A_{1/2} A^*_{3/2}}{|A_{1/2}|^2} = -\frac{1}{2}\, \frac{\frac{d\sigma}{dt}(\pi^+ p \to K^+\Sigma^+) - 2\frac{d\sigma}{dt}(\pi^- p \to K^0\Sigma^0)}{\frac{d\sigma}{dt}(\pi^+ p \to K^+\Sigma^+) + \frac{d\sigma}{dt}(\pi^- p \to K^0\Sigma^0)}$$

At 3.6 GeV, this ratio is .025 ± .045 with a systematic error of ± .017 and therefore no evidence for $I_t = 3/2$ exchange is found at the 5% level if the two amplitudes are in phase; the limit could obviously be much worse if some large phase difference existed between $A_{1/2}$ and $A_{3/2}$.

Evidence for $I_t = 2$ and $I_t = 3/2$ exchanges comes from photoproduction[45] comparing the reactions:

$$\left.\begin{array}{l}\gamma p \to \pi^- \Delta^{++} \\ \gamma n \to \pi^- \Delta^{+} \\ \gamma p \to \pi^+ \Delta^{0} \\ \gamma n \to \pi^+ \Delta^{-}\end{array}\right\} \qquad \frac{\mathrm{Re}\ A_1 A_2^*}{|A_1|^2} = .10 \pm .015$$

$$\left.\begin{array}{l}\gamma p \to K^+ \Sigma^0 \\ \gamma n \to K^+ \Sigma^-\end{array}\right\} \qquad \frac{\mathrm{Re}\ A_{1/2}\, A_{3/2}^*}{|A_{1/2}|^2} = .05 \pm .01$$

Exotic baryon exchange

Fast s dependence ($\sim s^{-10}$) is seen for exotic baryon exchange (see Fig. 16 for $\bar{p}p \to K^+K^-$ and Fig. 17 for $K^-p \to pK^-$) compared with dependence like s^{-3} - s^{-4} for allowed exchange. It is interesting that exotic channels continue the trend observed in the high-mass resonance region with no evidence of a change in trend observed so far. Nevertheless a backward peak has been observed at 5 GeV[43] in both $K^-p \to pK^-$ and $\bar{p}p \to p\bar{p}$ (Figs. 18 and 19) which is at least a good hint of some kind of exchange. It is unfortunate however that these healthy peaks have almost disappeared in the preliminary data of Ref. 46 at 6.2 GeV/c. So there again it seems that fluctuations (s-channel effects?) are occurring over and above a steeply falling s dependence which still prevail at 6 GeV. The ratio:

$$\left[\frac{\frac{d\sigma}{du}\,(K^-p \to pK^-)}{\frac{d\sigma}{du}\,(K^+p \to pK^+)}\right]_{u \simeq 0}$$

is $\sim 10^{-2}$ at 5 GeV/c, but has already fallen to $\sim 2\,10^{-3}$ at 6.2 GeV/c.

-experimental difficulties

Some difficulties in interpreting an exotic peak have been pointed out when a resonance is produced.[47] As an example let us consider $\pi^-p \to \pi^+\Delta^-$.

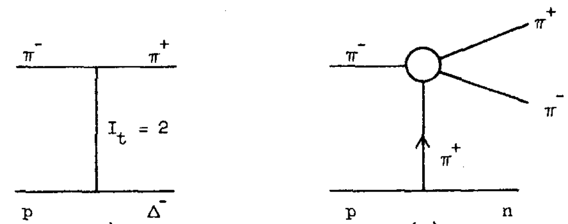

(a) (b)

One would like to describe phenomena with diagram (a); however processes (b) can also contribute and reflect into the $(n\pi^+)$ mass spectrum at low mass simulating a false Δ peak. It is amusing that to achieve this effect $\pi^+\pi^- \to \pi^-\pi^+$ scattering has to occur--also an exotic backward process--but it will do so at a much lower s value and hence the process will still be dominated by $\pi\pi$ resonances. Since these reflections are still badly understood, we think it is safe to use data involving only stable particles, i.e., $\bar{p}p \to \bar{\Sigma}^+\Sigma^-$, $K^-p \to pK^-$ and $\bar{p}p \to p\bar{p}$.

-interpretations.

Real exotic particle exchange is not likely in view of the absence of a persistent peak at small t (u) although the s dependence of $K^-p \to pK^-$ $\alpha_{eff} \simeq -4$ does not rule out a Z^* of mass 2-2.5 GeV for a canonical $\alpha' = 1$ Regge trajectory and a spin of 1/2 or 3/2.

Direct channel effects could be responsible for fluctuations in the angular distribution around a collective steep s dependence. It is then expected that at some energy some exchange will take place in the crossed channel where the most likely candidate is double particle exchange which certainly is the cheapest way to generate exotic quantum numbers. However they have not been seen yet.

-violation of quark selection rules

In the simple quark model the ϕ meson is a $\lambda\bar{\lambda}$ system and therefore couples very weakly to non-strange particles. This is observed for example in backward scattering around 5 GeV where processes like $K^- p \to \Lambda\rho$ and $K^- p \to \Lambda\omega$ occur, but $K^- p \to \Lambda\phi$ has not been detected yet.

Recent results on ϕ forward production in $\pi^- p \to \phi n$ have been obtained recently[48] showing a very fast decrease of the cross section like s^{-8} (Fig. 20) where a corresponding allowed process $\pi^- p \to \omega n$ behaves as $s^{-2.4}$. The differential cross section is flatter for ϕ (slope 1.4 GeV^2 at 5 GeV) than ω (slope $\simeq 3$ GeV^{-2}) production. This reaction is rather interesting because all channels are suppressed by the quark model: s-channel non-strange resonances will not couple to ϕn, u channel exchanges are prohibited by the same properties and t-channel exchanges are suppressed because they cannot couple to both upper and lower vertices. The only reasonable candidate to generate some amplitude seems to be two-particle exchange such as K-K^* which is not prohibited by the quark model. Although such an explanation would not be inconsistent with the ratio $\frac{\sigma(\pi^- p \to \phi n)}{\sigma(\pi^- p \to \omega n)} \sim 3.5\ 10^{-3}$ at 5 GeV, and the shape of $d\sigma/dt$, the steep s dependence is somewhat surprising.

(c) SU(3) symmetry.

We know that SU(3) can only be an approximate symmetry of the strong interactions but it is important to see how useful a tool it can be in understanding two body reactions. Even though it is not exact, it can still be helpful in organizing our systematic understanding of exchanges.

$t = 0$

The difference between $\alpha_\rho(0) = .57 \pm .01$ and $\alpha_\omega(0) = .40 \pm .03$ is not accounted for by the ρ-ω mass difference and linear trajectories of same slope since it yields $\alpha'_\rho = .97 \pm .04$ and $\alpha'_\omega = 1.2 \pm .1$. It therefore seems that ρ and ω exchanges break SU(3) symmetry, while ρ exchange with different external particles is consistent with symmetry $(\alpha^\pi_\rho(0) \simeq \alpha^K_\rho(0))$. On the other hand the residues show a 20% breaking

$$\frac{\rho_\pi}{\rho_K} = 1.6 \pm .1$$

instead of 2 for exact SU(3).

The relationship between the residues of ρ_π and ω_K cannot be tested well because, since $\alpha^\pi_\rho \neq \alpha^K_\omega$ the comparison depends on any scale factor s_0 in $(s/s_0)^\alpha$.

$t \neq 0$

SU(3) can be applied to two-body reactions and yields relations independent of any dynamics producing the reactions. For example, the following equalities between amplitudes are predicted:

$$A(K^- p \to K^0 \Xi^0) = A(K^- p \to \pi^+ \Sigma^-)$$

$$A(K^- p \to K^- p) = A(\pi^- p \to \pi^- p) + A(K^- p \to \pi^- \Sigma^+)$$

$$A(K^+ p \to K^{*+} p) = A(\pi^+ p \to \rho^+ p) + A(\pi^+ p \to K^{*+} \Sigma^+)$$

$$\sqrt{2}\ A(\gamma p \to \pi^+ n) = \sqrt{3}\, A(\gamma p \to K^+ \Lambda^0) - A(\gamma p \to K^+ \Sigma^0)$$

These relations are in general badly violated but they do not teach us a lot about the structure of the breaking. It is more useful to isolate t-channel exchanges in different reactions and relate them using SU(3). Such an exercise awaits some complete amplitude analysis such as in hypercharge reactions to compare K^* exchange to ρ and ω exchanges. Before this is done we can go a few steps in this direction in writing down SU(3) relations when some restrictions are imposed on the t-channel exchanges. In particular, if we assume exotic amplitudes identically vanish, then some new SU(3) relations can be found: for example, take the general SU(3) relation

$$A(K^+p \to K^0\Delta^{++}) + \sqrt{3}\,A(K^-p \to \pi^-\Sigma^+) = \sqrt{3}\,A(K^-n \to K^+\Xi^-) - A(K^-n \to K^0\Xi^-)$$

where the amplitudes on the right-hand side are exotic in the t-channel and can be set to zero; we obtain the simple relation:

$$\frac{d\sigma}{dt}(K^+p \to K^0\Delta^{++}) = 3\,\frac{d\sigma}{dt}(K^-p \to \pi^-\Sigma^+)$$

expressing SU(3) symmetry between (ρ, K_V^*) and (A_2, K_T^*) exchanges. However this kind of relation is expected to be more reliable when there is a dominant helicity amplitude such as for ρ and A_2 exchange:

$$\frac{d\sigma}{dt}(K^-p \to \bar{K}^0 n) + \frac{d\sigma}{dt}(K^+n \to K^0 p) = \frac{d\sigma}{dt}(\pi^-p \to \pi^0 n) + 3\,\frac{d\sigma}{dt}(\pi^-p \to \eta n)$$

Such a prediction is successfully compared to experiment[49] in Fig. 21.

SU(3) symmetry applied to vertices can help us understand the empirical helicity couplings which we have derived from experiment. The coupling of vector and tensor mesons to $B\bar{B}$ is expressed in terms of a symmetric octet coupling (d), an antisymmetric octet coupling (f) and a singlet coupling. Expressing the fact that ϕ and f' completely decouple from $N\bar{N}$ leads to SU(3) couplings depending only on f and d for each helicity amplitude. Table 6 shows the couplings for vector mesons and their numerical values, as compared to $\rho\bar{p}p$ helicity non-flip, obtained with $(f/d)_{++} = -3$ (in order to reproduce $(\rho\bar{p}p/\omega\bar{p}p)_{++}$), $(f/d)_{+-} = 1/3$ (so that $(\omega\bar{p}p)_{+-} = 0$) and $(\rho\bar{p}p)_{+-}/(\rho\bar{p}p)_{++} = 3$ from πN amplitude analysis at 6 GeV. We see that, as is experimentally observed, the K_V^* couplings--also the K_T^* couplings--do not show a dominant helicity transfer.

3. Phases

The phase of an amplitude is in general hard to measure experimentally. At $t = 0$, the optical theorem give one method while, at $t \neq 0$, one need some interference with a known amplitude.

(a) $t = 0$

Coulomb interference

Existing measurements are still very fragmentary. $\pi^{\pm}p$ is the only systematic study from 8 to 20 GeV[50] and the data can be used to measure the phase of $(P + f)$ and ρ exchange at $t = 0$. It shows that the phase is given correctly by dispersion relations, hence checking the analyticity properties of the forward amplitude. The phase of the even-crossing part $(P + f)$ is $\sim 100°$, while for the odd-crossing part no more than the sign is really measured $(\mathrm{Re}\,\rho/\mathrm{Im}\,\rho > 0)$.

At 2 GeV/c in the $\pi^{\pm}p$ system, a new piece of data[51] yields:

$$\begin{cases} \mathrm{Re}(P + f) = -(6.2 \pm .45)\ \mathrm{mb} \\ \mathrm{Im}(P + f) = 32.45\ \mathrm{mb} \end{cases}$$

$$\left.\begin{cases} \mathrm{Re}\,\rho = (2.25 \pm .45)\ \mathrm{mb} \\ \mathrm{Im}\,\rho = 3.35\ \mathrm{mb} \end{cases}\right\} \qquad \phi = (34 \pm 6)°$$

where the ρ Regge phase is 39°.

The situation in $K^{\pm}p$ is still worse, since we have only a few good low energy points[52] and very questionable high energy determinations. Below 3 GeV, $\mathrm{Re}(K^+p)$ is large and negative ($\alpha = \mathrm{Re}/\mathrm{Im} = -0.44$ at 2.6 GeV) while $\mathrm{Re}(K^-p)$ oscillates in the resonance region and then seems to settle to very small values. The corresponding phases are found to be:

$P_{L(GeV/c)}$	$\phi^{(+)}(P + f + A_2)$	$\phi^{(-)}(\rho + \omega)$
1.2	97°	(22 ± 5)°
1.8	98°	(35 ± 2)°
2.6	100°	(38 ± 3)°

where the ω Regge phase (ω dominates over ρ at $t = 0$) is 53° for $\alpha_\omega(0) = 0.41$. Reliable high energy determinations of the forward phases in $K^\pm p$ are particularly wanting.

Special Case of $K_L^0 p \to K_S^0 p$

One can use the CP violating decay $K_L^0 \to \pi^+\pi^-$ to interfer with K_S^0 regenerated from a hydrogen target. Knowing the decay phase ϕ_{+-}, both the regeneration amplitude and its phase are measured at $t = 0$ by observing the interference pattern as a function of the K^0 decay time. The probability distribution of events is:

$$\frac{dN}{d\tau} = |R|^2 \exp(-\Gamma_S \tau) + |\eta_{+-}|^2 \exp(-\Gamma_L \tau) + 2|R\eta_{+-}| \exp[-(\Gamma_S+\Gamma_L)\frac{\tau}{2}] \cos(\delta\tau + \phi - \phi_{+-})$$

where $[A(K_L^0 p \to K_S^0 p)]_{t=0} = Re^{i\phi}$, $\eta_{+-}e^{i\phi_{+-}}$ is the CP violating amplitude, δ the $K_L^0 K_S^0$ mass difference and Γ_S and Γ_L the K_L^0 and K_S^0 inverse lifetimes.

The results show[53] that between 10 and 50 GeV:

-ϕ is roughly independent of s

$$\phi = (-131 \pm 8)° = \pi + (49 \pm 8)°$$

-$\alpha_{eff}(0) = .47 \pm .13$ in agreement with the s dependence of $\sigma_T(K^-n) - \sigma_T(K^+n)$ related by SU(2) invariance to $\sigma_T(\bar{K}^0 p) - \sigma_T(K^0 p)$, the imaginary part of $K_L^0 p \to K_S^0 p$ at $t = 0$.

Using the optical theorem

Measurements at $t = 0$ of $d\sigma/dt$ yields $(\mathrm{Re}\,A)^2 + (\mathrm{Im}\,A)^2$ and using the optical theorem ($\mathrm{Im}\,A \sim \sigma_T$) on can deduce the absolute value of Re A. This approach has not been very successful in elastic scattering because of the smallness of the real parts and problems connected with relative normalization and possible curvature of $d\sigma/dt$ at small t. However the approach has been most fruitful for odd-crossing amplitudes.

$$\mathrm{Im}\,A(\pi^- p \to \pi^0 n) = -\frac{k}{4\sqrt{2}\,\pi}\,[\sigma_T(\pi^- p) - \sigma_T(\pi^+ p)]$$

$$\mathrm{Im}\,A(K_L^0 p \to K_S^0 p) = -\frac{k}{8\pi}\,[\sigma_T(K^- n) - \sigma_T(K^+ n)]$$

Figure 22 shows the ratio $\alpha = \mathrm{Re}\,A/\mathrm{Im}\,A$ for $\pi^- p \to \pi^0 n$, yielding a phase $\phi = \pi + (43.5 \pm 2.5)°$ corresponding to a Regge $\alpha_\rho(0) = .52 \pm .04$ in good agreement with the s dependence of the imaginary part. In $K_L^0 p \to K_S^0 p$ the phase is $\phi + (40 \pm 10)°$ giving $\alpha_\omega(0) = .55 \pm .11$ in accord with direct phase measurements and the s dependence of the corresponding total cross sections.

A more interesting exercise can be carried through for the KN and $\overline{KN}$ change exchange reactions:

$$[\mathrm{Im}(K^- p \to \bar{K}^0 n)]^2 = \frac{1}{16\pi}\,[\sigma_T(K^- n) - \sigma_T(K^- p)]^2$$

$$[\mathrm{Im}(K^+ n \to K^0 p)]^2 = \frac{1}{16\pi}\,[\sigma_T(K^+ p) - \sigma_T(K^+ n)]^2$$

In Fig. 23 we compare the values of $[\mathrm{Im}\,A]^2$ to the differential cross sections at $t = 0$: it strikingly shows that the process $K^- p \to \bar{K}^0 n$ is purely imaginary at $t = 0$, while its counterpart $K^+ n \to K^0 p$ is purely real. This result confirms some of the duality ideas that we are going to discuss in Chapter IV.

(b) $t \neq 0$

A very attractive method which can be used in ρ and ω production is provided by $\rho - \omega$ electromagnetic mixing as observed in the $\pi^+\pi^-$ decay channel, leading to the exciting possibility of measuring the production phase difference between ρ and ω.

Corresponding to the production amplitudes:

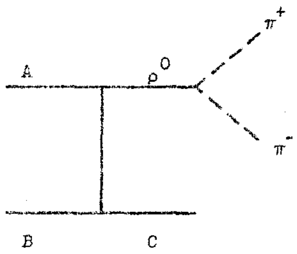

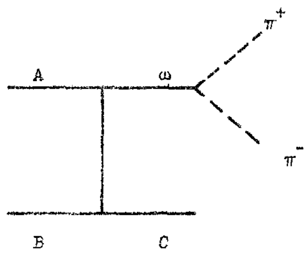

one can observe interferences of the form:

$$\sum_\lambda M_\lambda(\rho)\, M^*_\lambda(\omega) = \xi \sqrt{(\sum_\lambda M_\lambda(\rho)^2)(\sum_\lambda M_\lambda(\omega)^2)} \quad e^{i\phi}$$

where ξ is a coherence factor and ϕ is the phase difference including the phase of $\omega \to \pi^+\pi^-$ (known and checked in e^+e^- production or ρ and ω photoproduction where the hadronic phase difference is small). Ideally if all the amplitudes were sorted out one could measure the phase difference for each helicity state; however experiments have not reached that point yet and several helicity states are still summed over so that a coherence factor has still to be used.

This method has been used recently by an Argonne group in a rather elegant way.[54] They measured the charge-symmetric processes

$$\pi^- p \to \pi^+\pi^- n$$
$$\pi^+ n \to \pi^-\pi^+ p$$

which should have equal cross sections except for SU(2) electromagnetic breaking. The interference pattern is striking in the mass spectrum of Fig. 24, showing a constructive interference for $\pi^- p \to \pi^+\pi^- n$ and a destructive one for $\pi^+ n \to \pi^-\pi^+ p$. The interference term can be projected out:

$$\Delta = \sigma(\pi^- p \to \pi^-\pi^+ n) - \sigma(\pi^+ n \to \pi^+\pi^- p) = 4\ \mathrm{Re}(\rho^*\omega)$$

for different $\lambda_{\pi\pi}$ and naturalities ξ.

Figure 25 shows the t-dependence of the phases and some idea of the s dependence. The phase of the unnatural parity exchange Δ^0 is $(122 \pm 6)°$ where one would expect 90° for π - B exchange degeneracy (π in ρ production and B in ω production). The phase Δ^+, the amplitude with natural parity exchange, is changing with t going from 90° at $t = 0$ to about 0° at $t = -0.3$, there, ρ - A_2 exchange degeneracy would predict - 90° and so, again, we see a strong departure at small t from the expected exchanges, a discrepancy already noticed with the behaviour of $\alpha_{eff}(t)$.

A ρ - ω interference analysis has been carried out by the CERN-Munich group[55] observing only $\pi^- p \to \pi^+\pi^- n$ at 17 GeV/c. Their results for the phase of the natural parity exchange is in agreement with the previous analysis, but they disagree on the phase of the unnatural parity exchange with $\lambda_{\pi\pi} = 0$: with the phase convention of the Argonne group, they find phases below 90°, showing either an unsuspected s dependence or some experimental disagreement.

Similar measurements could be extended to other reactions such as

$$K^- p \to (\rho,\omega)\Lambda$$

where the interference effects could be even more visible due to about equal cross sections for ρ and ω production; in constrast ρ production in πN is larger than ω production and the smallness of the decay rate $\omega \to \pi^+\pi^-$ renders the observations rather difficult.

TABLE 3

Amplitude	P_L range (GeV/c)	β (mb)	α
ρ_π	4-200	3.43 ± 0.07	$.57 \pm .01$
ρ_K	3-200	2.16 ± 0.12	$.57 \pm .03$
ω_K	3-200	13.0 ± 2.6	$.39 \pm .01$
A_K	3-200	1.8 ± 0.2	$.48 \pm .05$
$\Delta(Kd) \sim \omega_K$	6-200		.41
$\Delta(pd) \sim \omega_p$	6-200		.41

TABLE 4

Reaction	exchanges	α (t = 0)	Ref.
$\pi^- p \to \pi^0 n$	ρ	$.58 \pm .03$	36
$\pi^- p \to \eta n$	A_2	$.47 \pm .07$	37
$K^- p \to \bar{K}^0 n$	$\rho + A_2$		
$K^+ n \to K^0 p$	$\rho - A_2$		
$K_L^0 p \to K_S^0 p$	$\rho + \omega$		
$K_L^0 d \to K_S^0 d$	ω	.43	38

TABLE 5

Exchange	Dominant helicity coupling to $B\bar{B}$
P + f	++
ω	++
ρ	+-
A_2	+-
π	+-
$K_V^* K_T^*$	? (++ important)

TABLE 6

$VB\bar{B}$ vertex	SU(3) coupling	helicity non-flip coupling	helicity flip coupling
$\rho p\bar{p}$	$\frac{1}{\sqrt{2}}(f + d)$	1.	3.
$p\bar{p}$	$\frac{1}{\sqrt{2}}(-3f + d)$	-5.	0.
$K^* \Lambda \bar{p}$	$\frac{1}{\sqrt{6}}(3f + d)$	2.3	2.6
$K^* \Sigma^{+-} \bar{p}$	$- f + d$	-2.8	2.1

III - EXTRACTING AMPLITUDES FROM INCOMPLETE DATA

There is so much data in incomplete form and so little information on amplitudes, that it seems worthwhile to try methods where a few amplitudes can be extracted out in an approximate way. On the other hand we have treated real parts and imaginary parts as two independent sets of observables where we know that analyticity relates them: so it seems that analyticity can be used in amplitude analyses in order to reduce the number of measurements to be carried out.

1. Projection of One Amplitude: Exchanges in Elastic Scattering

Amplitude analyses at 6 GeV tell us that the $I_t = 0$, πN amplitude is, to a good approximation, helicity non-flip. This point is also established in ρ^0 photoproduction, a process with very similar amplitudes $(P + f)$. Furthermore, from the energy dependence of elastic scattering we know that the dominant part of this amplitude is contributed for by the Pomeron at energies above a few GeV. We also know that the phase at $t = 0$ is very close to $\pi/2$ and we do not suspect that it will change drastically away from $t = 0$, as long as we stay in the very forward region. (We shall come back later on to this assumption.) With these experimental facts (and one assumption) in mind, it is easy to see that elastic processes will provide very direct and interesting information on exchange amplitudes from their interference with the dominant (imaginary, helicity *non-flip*, $I_t = 0$) *diffractive amplitude.*

(a) Cross-over effect

Consider the elastic scattering of particle A and antiparticle $\bar{A}$ on protons, expressed in terms of even and odd-crossing amplitudes $F^{\pm}$:

$$\frac{d\sigma}{dt}(\bar{A}p) = \sum_{\lambda} |F_{\lambda}^{+} + F_{\lambda}^{-}|^2$$

$$\frac{d\sigma}{dt}(Ap) = \sum_{\lambda} |F_{\lambda}^{+} - F_{\lambda}^{-}|^2$$

$$\frac{d\sigma}{dt}(\bar{A}p) - \frac{d\sigma}{dt}(Ap) = \sum_{\lambda} 4\, \mathrm{Re}(F_{\lambda}^{+} F_{\lambda}^{-*})$$

$$\frac{d\sigma}{dt}(\bar{A}p) + \frac{d\sigma}{dt}(Ap) = \sum_{\lambda} 2[|F_{\lambda}^{+}|^2 + |F_{\lambda}^{-}|^2]$$

At high energy F_{++}^{+} becomes the dominant amplitude and we are going to project all amplitudes onto it. We shall further neglect $|F^{-}|^2$ in front of $|F^{+}|^2$ and F_{+-}^{+} in front of F_{++}^{+}. We have therefore

$$\frac{d\sigma}{dt}(\bar{A}p) - \frac{d\sigma}{dt}(Ap) = 4\, F_{++}^{+}(F_{++}^{-})_{\parallel} + 4(F_{+-}^{+})_{\parallel}\,(F_{+-}^{-})_{\parallel} + 4(F_{+-}^{+})_{\perp}\,(F_{+-}^{-})_{\perp}$$

$$\simeq 4F_{++}^{+}(F_{++}^{-})_{\parallel}$$

$$\frac{d\sigma}{dt}(\bar{A}p) + \frac{d\sigma}{dt}(Ap) = 2(F_{++}^{+})^2 + 2|F_{+-}^{+}|^2 + 2|F_{++}^{-}|^2 + 2|F_{+-}^{-}|^2$$

$$\simeq 2(F_{++}^{+})^2$$

leading to

$$(F_{++}^{-})_{\parallel} = \frac{\frac{d\sigma}{dt}(\bar{A}p) - \frac{d\sigma}{dt}(Ap)}{\sqrt{8[\frac{d\sigma}{dt}(\bar{A}p) + \frac{d\sigma}{dt}(Ap)]}} = \Delta_A$$

Δ_A can be measured in 3 processes isolating the following amplitudes:

$\pi^{\pm}p$	$\mathrm{Im}\,\rho^{\pi}_{++}$
$K^{\pm}p$	$\mathrm{Im}(\rho+\omega)^{K}_{++} \simeq \mathrm{Im}\,\omega^{K}_{++}$
$p^{\pm}p$	$\mathrm{Im}(\rho+\omega)^{p}_{++} \simeq \mathrm{Im}\,\omega^{p}_{++}$

This method was applied first to $K^{\pm}p$ scattering at 5 GeV/c[56] and clearly showed that $\mathrm{Im}\,\omega^{K}_{++}$ had zeroes at $t = -0.2$ and ~ -1.3 GeV^2 (Fig. 26) and could be fitted rather well to an expression

$$\mathrm{Im}\,\omega^{K}_{++} = F(t) = Ae^{Bt}\,J_0(R\sqrt{-t})$$

with $R \simeq 1f$. It is rather illuminating to transform the amplitude into impact parameter space using a Fourier-Bessel transformation:

$$\tilde{F}(b) = \int_0^{\infty} dt\, F(t)\, J_0(b\sqrt{-t})$$

With the parametrization for $\mathrm{Im}\,\omega^{K}_{++}$, we find

$$\widetilde{\mathrm{Im}\,\omega^{K}_{++}} = \frac{A}{B}\exp\left(-\frac{R^2+b^2}{4B}\right) I_0\left(\frac{Rb}{2B}\right)$$

where $I_0(x)$ is a Bessel function of an imaginary argument. $\widetilde{\mathrm{Im}\,\omega^{K}_{++}}$ has a strong peak around $b \sim R$ and most of its strength is given by the impact parameters around this value. Alternatively, it is probably better to use the exact Legendre expansion at lower energies:

$$\mathrm{Im}\,\omega^{K}_{++} = \frac{\sqrt{\pi}}{k^2}\sum_J \left(J+\frac{1}{2}\right) d^J_{\frac{1}{2}\frac{1}{2}}(\theta)\, a_J$$

The partial wave amplitude a_J is then given by

$$a_J = \frac{1}{\sqrt{\pi}\,(2J+1)}\int dt\, \mathrm{Im}\,\omega^{K}_{++}\cos\frac{\theta}{2}\left(P'_{J+\frac{1}{2}} - P'_{J-\frac{1}{2}}\right)$$

Figure 27 shows the a_J amplitudes from the data of Ref. 43: the peripheral nature of $\mathrm{Im}\,\omega^{K}_{++}$ is very dramatic. This is to be contrasted with the impact parameter structure of the Pomeron amplitude which is best approximated by the $K^{+}p$ amplitude itself.[56] Figure 28 shows that the Pomeron amplitude receives contributions from all partial waves up to the most peripheral waves, consistent with an optical picture of diffraction. Notice that $\widetilde{\mathrm{Im}\,\omega^{K}_{++}}$ in Fig. 28 appears as a relatively minor correction to the dominant diffractive term.

More information can be gathered from the systematic data between 3 and 6 GeV obtained by the Argonne group,[5] an example of which can be seen in Fig. 29. All the measured "amplitudes" $\Delta_{\pi,K,p}$ are fitted well with the form $Ae^{Bt}\,J_0(R\sqrt{-t})$ for $0 < -t < 0.8$ GeV^2 (Fig. 30). Of course, Δ_{π} is small and and its t dependence is not well measured and suffers most of all from systematic uncertainties between π^{+} and π^{-} data. Beyond $-t > 0.8$ GeV^2 the data deviate considerably from the low t fit especially at lower energies: we ascribe these failures to helicity-flip amplitudes and real parts and expect the effect to decrease with energy. Already at 6 GeV, the fitted form for Δ works well up to $-t \sim 1.2$ GeV^2, namely, the second cross-over zero. It is hard at these rather low energies to make a quantitative study of the s dependence of $\mathrm{Im}\,\omega^{K}_{++}$ and $\mathrm{Im}\,\omega^{p}_{++}$ since s-dependent effects affect the extraction of the amplitude. Qualitatively we have the following behaviour:

-R is approximately constant at about 1f and does not change too much between the three processes.

-The shrinkage question is not settled (s dependence of B).

-Im ω_{++}^{K} and Im ω_{++}^{p} are becoming more and more similar in shape as the energy increases, up to a constant factor of 3 predicted by the quark model.

It is interesting that the peripherality of the ω exchange amplitude has the consequence that total elastic cross sections for K^+p and K^-p on one hand, and pp and $\bar{p}p$ on the other hand, are nearly equal, although the differential cross sections are very different. Indeed we have:

$$\int dt \left[\frac{d\sigma}{dt}(\bar{A}p) - \frac{d\sigma}{dt}(Ap)\right] = 4AA' \int dt\ e^{(B+B')t}\ J_0(R\sqrt{t})$$

where

$$\frac{1}{2}\left[\frac{d\sigma}{dt}(\bar{A}p) + \frac{d\sigma}{dt}(Ap)\right] \simeq A'\ e^{B't}$$

giving

$$\sigma_{el}(\bar{A}p) - \sigma_{el}(Ap) = \frac{4AA'}{B+B'} \exp\left(-\frac{R^2}{4(B+B')}\right)$$

Numerically at 5 GeV the difference amounts to .3 mb for $K^{\pm}p$ (8%) while it is 3.3 mb for $p^{\pm}p$ (23%).

This method of extracting the imaginary part of the odd-crossing amplitude through elastic scattering has limitations of both theoretical and experimental origins.

-on the theoretical side, limitations occur from 2 opposite directions. On one hand, if Im $F_{++}^{(-)}$ is small (as in $\pi^{\pm}p$), then its extraction becomes sensitive to neglected amplitudes (flip); on the other hand, if Im $F_{++}^{(-)}$ becomes too large, one can no longer safely neglect $|F^{(-)}|^2$ involving the knowledge of Re $F_{++}^{(-)}$ in particular. Therefore we can say that qualitatively the method will work best for $K^{\pm}p$, will improve with energy for $p^{\pm}p$ and could be questionable for $\pi^{\pm}p$. It is fortunate that the worst case of $\pi^{\pm}p$ can be tested against the results of the complete amplitude analysis at 6 GeV: in Fig. 31 we see that Δ_{π} agrees very well with the "exact" amplitude $(F_{++}^{1})_{\|}$ giving us some confidence in the method. For πN however, one does not need even to neglect $|F^{(-)}|^2$ in the sum since it is measured by $d\sigma/dt\ (\pi^- p \to \pi^0 n)$ and can be subtracted out:

$$\frac{d\sigma}{dt}(\pi^- p \to \pi^- p) + \frac{d\sigma}{dt}(\pi^+ p \to \pi^+ p) - \frac{d\sigma}{dt}(\pi^- p \to \pi^0 n) = 2|F^{(+)}|^2$$

-on the experimental side, relative normalization between Ap and $\bar{A}p$ measurements is of crucial importance for measuring the shape of $\Delta(t)$ and in locating the position of the zeroes. The uncertainty in the cross over position t_c is

$$\Delta t_c = \frac{\Delta N/N}{b_{\bar{A}} - b_A}$$

where $\Delta N/N$ is the relative normalization uncertainty and $b_{\bar{A}}$, b_A are the elastic slopes. For example, $\pi^{\pm}p$ at 6 GeV have the following slopes:

$$b_+ = 7.1\ , \qquad b_- = 7.7 \qquad (\text{in GeV}^{-2})$$

yielding an uncertainty $\Delta t_c = .04\ \text{GeV}^2$ for a 2% relative normalization uncertainty.

Detailed studies of elastic scattering will teach us several important features of the peripherality picture we have of Im $F_{++}^{(-)}$. To see that, let us consider the successful parametrization Im $F_{++}^{(-)} = Ae^{Bt}\ J_0(R\sqrt{t})$: the peak position in b space is determined by R and the width of the distribution is controlled by B. Then for a given amplitude, say Im $F_{++}^{(-)}(Kp)$, one would like to know the s dependence of R and B: for example, if B increases with s (shrinkage), does R also increase, thus preserving the peripherality picture? Also the comparison of $\pi^{\pm}$, $K^{\pm}$ and $p^{\pm}$ at an energy higher than 6 GeV would be very interesting since these processes have different interaction volumes, as indicated by the wide range in the total cross section values. The indications, at 6 GeV, are that there does not seem to be any simple relationship between the absorption radius R and the interaction radius as measured by the total elastic slope. New experiments are in progress at SLAC and NAL and it is interesting that, from the preliminary measurements, the method of extracting $\mathrm{Im}\, F_{++}^{(-)}$ will probably work in $K^{\pm}p$ and $p^{\pm}p$ up to rather large energies (~ 100 GeV) since the difference in slopes does not decrease too fast with s (Fig. 32).

(b) Polarizations in elastic scattering

Let us consider polarizations for elastic scattering of particle A and antiparticle $\bar{A}$ on protons and isolate leading terms in the sums and the differences.

$$P \frac{d\sigma}{dt} (\bar{A}p) = -2\, \mathrm{Im}[(F_{++}^{+} + F_{++}^{-})(F_{+-}^{+} + F_{+-}^{-})^{*}]$$

$$P \frac{d\sigma}{dt} (Ap) = -2\, \mathrm{Im}[(F_{++}^{+} - F_{++}^{-})(F_{+-}^{+} - F_{+-}^{-})^{*}]$$

$$\begin{aligned}\Delta P &= P \frac{d\sigma}{dt} (\bar{A}p) - P \frac{d\sigma}{dt} (Ap) \\ &= -4\, \mathrm{Im}[F_{++}^{+} F_{+-}^{-*} + F_{++}^{-} F_{+-}^{+*}] \\ &= -4[F_{++}^{+}(F_{+-}^{-})_{\perp} + (F_{++}^{-})_{\parallel} (F_{+-}^{+})_{\perp} - (F_{++}^{-})_{\perp} (F_{+-}^{+})_{\parallel}] \\ &\simeq -4\, F_{++}^{+}(F_{+-}^{-})_{\perp}\end{aligned}$$

$$\begin{aligned}\Sigma P &= P \frac{d\sigma}{dt} (\bar{A}p) + P \frac{d\sigma}{dt} (Ap) \\ &= -4\, \mathrm{Im}[F_{++}^{+} F_{+-}^{+*} + F_{++}^{-} F_{+-}^{-*}] \\ &= -4[F_{++}^{+}(F_{+-}^{+})_{\perp} + (F_{++}^{-})_{\parallel} (F_{+-}^{-})_{\perp} - (F_{++}^{-})_{\perp} (F_{+-}^{-})_{\parallel}] \\ &\simeq -4F_{++}^{+}(F_{+-}^{+})_{\perp}\end{aligned}$$

In the case of $\pi^{\pm}p$ scattering, one gets the exact relation:

$$P \frac{d\sigma}{dt} (\pi^{-}p) + P \frac{d\sigma}{dt} (\pi^{+}p) - P \frac{d\sigma}{dt} (\pi^{-}p \to \pi^{0}n) = -4F_{++}^{+}(F_{+-}^{+})_{\perp}$$

These relations can be applied to $\pi^{\pm}p$ and $K^{\pm}p$ data and teach us the following properties:

-πN scattering

$(F_{+-}^{-})_{\perp}$ is approximately equal to $\mathrm{Re}\, \rho_{+-}$, in excellent agreement with the complete amplitude analysis, as seen in Figs. 33 and 34. It has a double zero at $-t \sim 0.6$ GeV^2, like a pure Regge pole amplitude

$$\mathrm{Re}\, \rho_{+-} = \tan \frac{\pi\alpha}{2}\, \mathrm{Im}\, \rho_{+-}$$

where both $\mathrm{Im}\, \rho_{+-}$ and $\tan(\pi\alpha/2)$ vanish at $-t = 0.6$ GeV^2. The energy dependence of $(F_{+-}^{-})_{\perp}$ between 3 and 14 GeV shows a slightly faster fall-off than given by the ρ trajectory as measured in charge-exchange scattering. However $(F_{+-}^{-})_{\perp}$ is not quite $\mathrm{Re}\, F_{+-}^{-}$ since the phase of F_{++}^{0} can be changing with t, hence inducing a false t dependence in $(F_{+-}^{-})_{\perp}$.

$(F_{+-}^{+})_{\perp}$ is obtained from the exact relation between polarizations and shows no clear structure (Fig. 35); an f Regge pole would not have structure either since

$$\mathrm{Re}\, f_{+-} = -\cot \frac{\pi\alpha}{2}\, \mathrm{Im}\, f_{+-}$$

Accurate polarization data at 10 and 14 GeV seem to indicate a single zero around $-t = 0.8$ GeV^2. It is not clear whether this is due to the Pomeron, f exchange, or both.

-KN scattering

$(F_{+-}^{-})_{\perp}$ is dominated by ρ exchange since ω is mainly helicity non-flip; it is rather poorly determined from the data, but it is consistent with $\mathrm{Re}\, \rho_{+-}^{\pi}$ data scaled using SU(3) symmetry (Figs. 36 and 37).

Contrary to πN, the amplitude $(F_{+-}^{+})_{\perp}$ is large indicating a large coupling of A_2 exchange to helicity-flip (as we already knew). The data clearly show that $\mathrm{Re}\, A_{+-}$ does not vanish for $0 < -t < 1.2$ GeV^2 unlike $\mathrm{Re}\, \rho_{+-}$ (this is consistent with the Regge phase even if $\mathrm{Im}\, A_{+-} = 0$ at -0.6 GeV^2).

2. Making Use of the Analyticity Properties of Amplitudes

Fixed -t analyticity provides in principle a very powerful constraint on amplitude analyses. This constraint is generally expressed as a dispersion relation satisfied by the invariant amplitudes where the real part at $s = s_0$ is related to an integral over the imaginary part as a function of s. Thus knowing $\mathrm{Im}\, F(s,t)$ over a large range of s values from threshold to s_{max} determines $\mathrm{Re}\, F(s,t)$ for $s \ll s_{max}$, therefore halving the number of independent real amplitudes in that interval.

Dispersion relations have been experimentally tested at $t = 0$ only and in a few cases: $\pi^{\pm}p$ between 8-20 GeV and pp over a larger energy range. We will assume the validity of the analyticity properties of the amplitudes at all t values.

(a) Application of dispersion relations to πN amplitude analyses[57-59]

The main idea is to develop an iterative procedure using the data on $d\sigma/dt$ and the dispersion relations. Starting from the fact that $d\sigma/dt$ is predominantly $(\mathrm{Im}\, A_+')^2$, one can use $\sqrt{d\sigma/dt}$ as a zeroth order input to the dispersion integral, which result is used to correct $d\sigma/dt$ and so on. Schematically,

$$\frac{d\sigma}{dt} \simeq (\mathrm{Im}\, A_+'^{(0)})^2$$

$$\Downarrow$$

$$\mathrm{Im}\, A_+'^{(0)} \xrightarrow{\text{Dispersion relation}} \mathrm{Re}\, A_+'^{(0)}$$

$$\Downarrow$$

$$\cdots \Longleftarrow \mathrm{Im}\, A_+'^{(1)} \simeq \sqrt{\frac{d\sigma}{dt} - \mathrm{Re}[A_+'^{(0)}]^2}$$

For the A_+' even amplitude, the dispersion relation reads:

$$\mathrm{Re}\, A_+'(\nu,t) = \frac{\nu F_B^+(\nu,t)}{1-\frac{t}{4M^2}} + C_+(t) + \frac{2\nu^2}{\pi} P \int_{\nu_0}^{\infty} \frac{d\nu'}{\nu} \frac{\mathrm{Im}\, A_+'(\nu',t)}{\nu'^2 - \nu^2}$$

with

$$\nu_0 = m_\pi + \frac{t}{4M}$$

$$\nu = \frac{s-u}{4M} = E_L + \frac{t}{4M}$$

$$F_B^+(s,t) = \frac{g^2}{M} \frac{\nu}{\nu_B^2 - \nu^2} \qquad \text{(Born term)}$$

$$\nu_B = -\frac{m_\pi^2}{2M} + \frac{t}{4M}$$

and where g is the πNN coupling constant $(g^2/4\pi \sim 14.6)$ and $C_+(t)$ is a subtraction function.

These analyses make use only of $d\sigma/dt\ (\pi^+p)$, $d\sigma/dt\ (\pi^-p)$, $d\sigma/dt\ (\pi^-p \to \pi^0 n)$, $P(\pi^+p)$ and $P(\pi^-p)$. They do not use any data on $P(\pi^-p \to \pi^0 n)$, nor do they rely on A and R measurements. The main conclusions reached by these studies are:

-the t dependence of $\mathrm{Re}\, A_+'$ shows a slow variation with t of the phase: ϕ_{++} increases from 101° to 117° when $-t$ increases from 0 to 0.4 GeV^2 (Fig. 39) corresponding to a flatter t dependence for $\mathrm{Re}\, A_+'$ as compared to $\mathrm{Im}\, A_+'$ (Fig. 38). Uncertainties in $\mathrm{Re}\, A_+'$ arise mainly from the low-energy part of the dispersion integrals.

-the determination of $\mathrm{Re}\, B_+(s,t)$ is not so reliable and does involve some assumptions. However good agreement is found with $R^{\pm}$ data at 6 GeV. It is interesting to note that, in general, only using P and $d\sigma/dt$ data leaves an ambiguity between flip and nonflip amplitudes; this problem is solved here since in the phase shift region the full amplitudes can be reconstructed and propagated to high energy.

-Re A'_- shows a zero much closer to the cross over zero of the imaginary part than indicated by amplitude analysis; this effect could come from the t dependence of ϕ_{++} since conventional analyses assume $\phi_{++} = \pi/2$ independent of t. This shows a much closer similarity between the t dependences of $\mathrm{Re}\, F^1_{++}$ and $\mathrm{Im}\, F^1_{++}$, with both zeroes around $-t = 0.15\ \mathrm{GeV}^2$. Also, since the behaviour of $\mathrm{Re}\, F^1_{++}$ was mostly derived, in the 6 GeV amplitude analyses, from the charge exchange polarization--a weak measurement--we suspect this new result to be more reliable. Actually this analysis can be used to predict P_0 and it is seen in Fig. 40 that it prefers the Argonne results to the CERN results (in agreement with our discussion of amplitudes at 6 GeV).

-Re B_- shows a remarkable Regge phase (Fig. 38) as we already knew from just looking at ΔP.

This method using analyticity appears most interesting in that it provides solid constraints for amplitude analyses and does not use the weaker and most controversial sets of data. However the use of dispersion relations is cumbersome, really dependent on low energy data, suffering from inconsistencies between different sets of data over these large energy ranges and finally not very transparent.

(b) Derivative analyticity relations

We will show that at high energy the nonlocal connection between real and imaginary parts can be replaced by a quasilocal relation between the real part and the derivatives of the imaginary part at the same energy.

-derivation[60]

Consider an even-crossing amplitude $F_+(s,t)$ normalized to

$$\mathrm{Im}\, F_+(s,0) = s\sigma_T^+$$

It satisfies a subtracted dispersion relation where the subtraction constant $C_+(t)$ and Born terms have been omitted for simplicity:

$$\mathrm{Re}\, F_+(s,t) = \frac{2s^2}{\pi} P \int_{s_0}^{\infty} \frac{ds'}{s'} \frac{\mathrm{Im}\, F_+(s',t)}{s'^2 - s^2}$$

$$= \frac{2s^2}{\pi} \lim_{\substack{\epsilon \to 0 \\ (\epsilon > 0)}} \left[\int_{s_0}^{s-\epsilon} \frac{ds'}{s'} \frac{\mathrm{Im}\, F_+(s',t)}{s'^2 - s^2} + \int_{s+\epsilon}^{\infty} \frac{ds'}{s'} \frac{\mathrm{Im}\, F_+(s',t)}{s'^2 - s^2} \right]$$

Integrating by parts, we get

$$\int_{s_0}^{s-\epsilon} \frac{ds'}{s'} \frac{\mathrm{Im}\, F_+(s',t)}{s'^2 - s^2}$$

$$= -\frac{1}{2s} \left[\ln\left(\frac{s+s'}{|s-s'|}\right) \frac{\mathrm{Im}\, F_+(s',t)}{s'} \right]_{s_0}^{s-\epsilon}$$

$$+ \frac{1}{2s} \int_{s_0}^{s-\epsilon} \frac{ds'}{s'} \ln\left(\frac{s+s'}{|s-s'|}\right) \left[-\frac{1}{s'} + \frac{d}{ds'} \right] \mathrm{Im}\, F_+(s',t)$$

where the first term disappears when taking the principal value except for a term

$$\frac{1}{2s} \ln\left(\frac{s+s_0}{s-s_0}\right) \frac{\mathrm{Im}\, F(s_0)}{s_0}$$

which is negligible for $s \gg s_0$. The dispersion integral then reads:

$$\mathrm{Re}\, F_+(s,t) = \frac{s}{\pi} P \int_{s_0}^{\infty} \frac{ds'}{s'} \ln\left(\frac{s+s'}{|s+s'|}\right) \left[\frac{d}{ds'} - \frac{1}{s'} \right] \mathrm{Im}\, F_+(s',t)$$

Introduce the rapidity variable $e^y = s$

$$\mathrm{Re}\, F_+(y,t) = \frac{e^y}{\pi} P \int_{y_0}^{\infty} dy'\, e^{-y'} \ln\left(\coth \frac{|y-y'|}{2}\right) \left[\frac{d}{dy'} - 1 \right] \mathrm{Im}\, F_+(y',t)$$

More generally we can rewrite this last equation as:

$$\mathrm{Re}\, F_+(y,t) = \frac{e^y}{\pi} P \int_{y_0}^{\infty} dy'\, e^{(\alpha-1)y'} \ln\left(\coth \frac{|y-y'|}{2}\right) \left[\alpha - 1 + \frac{d}{dy'} \right] (\mathrm{Im}\, F_+(y',t) e^{-\alpha y'})$$

which is very useful since it allows us to use $\mathrm{Im}\, F(s,t)\, s^{-\alpha}$ as our working function and we can choose α in order to minimize its s dependence

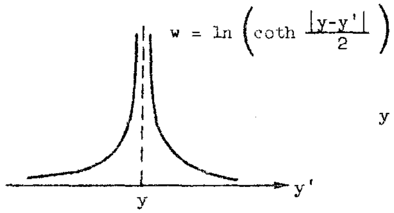

$$y' \to \infty, \qquad w \sim 2e^{-|y-y'|}$$

The rest of the derivation is tedious, but straightforward. We expand $\mathrm{Im}\, F_+(y',t)$ in power series of $(y'-y)$ and we extend the lower limit of the integral to $-\infty$ (for y large enough). We finally get

$$\mathrm{Re}\, F_+(y,t) = e^{\alpha y} \tan\left[\frac{\pi}{2}\left(\alpha - 1 + \frac{d}{dy}\right)\right] \left(e^{-\alpha y}\, \mathrm{Im}\, F_+(y,t)\right)$$

$$= \tan\left[\frac{\pi}{2}(\alpha-1)\right] \mathrm{Im}\, F_+(y,t) + \frac{\pi}{2} \frac{e^{\alpha y}}{\cos^2\left[\frac{\pi}{2}(\alpha-1)\right]} \frac{d}{dy}\left(\mathrm{Im}\, F_+(y,t) e^{-\alpha y}\right) + \cdots$$

For an odd-crossing amplitude we would have instead:

$$\mathrm{Re}\, F_-(y,t) = e^{\alpha y} \tan\left[\frac{\pi}{2}\left(\alpha + \frac{d}{dy}\right)\right] \left(e^{-\alpha y}\, \mathrm{Im}\, F_-(y,t)\right)$$

$$= \tan\left(\frac{\pi\alpha}{2}\right) \mathrm{Im}\, F_-(y,t) + \frac{\pi}{2} \frac{e^{\alpha y}}{\cos^2(\pi\alpha/2)} \frac{d}{dy}\left(\mathrm{Im}\, F_-(y,t)\, e^{-\alpha y}\right) + \cdots$$

These relations should not apply at too low an energy since the lower limit of integration y_0 was moved to $-\infty$ and threshold terms have been dropped. On the other hand, pole terms can be added to the final answer. We can choose the parameter α to minimize the s dependence of the function to be differentiated. Conveniently we take

even amplitude $\quad \alpha = 1 \quad \mathrm{Re}\, F_+ = s \tan\left(\frac{\pi}{2}\frac{d}{dy}\right) \frac{\mathrm{Im}\, F_+}{s}$

odd amplitude $\quad \alpha = 0 \quad \mathrm{Re}\, F_- = \tan\left(\frac{\pi}{2}\frac{d}{dy}\right) \mathrm{Im}\, F_-$

Whereas an integral dispersion relation is a sum over the imaginary part involving a large range of energies, these new relations necessitate the knowledge of the derivatives of the imaginary part taken locally. In practice, however, one will need some range of energies to measure the derivatives. It is obvious that this approach will only be fruitful if only a small number of terms can approximate the true answer--a result to be investigated on the data.

Before going further, let us present a more intuitive way of deriving these derivative relations. Analyticity in energy allows one to write the amplitude in terms of a Mellin transform in the complex J plane (t-channel analyticity)[61]:

$$M^{\pm}(s,t) = \int dJ [s^J \pm (-s)^J]\, T(J,t)$$

with $\mathrm{Im}\, M = s\sigma_T$

$$s^J \pm (-s)^J = s^J \pm (se^{-i\pi})^J = 2e^{-i(\pi/2)J} s^J \begin{Bmatrix} \cos \frac{\pi}{2} J \\ i \sin \frac{\pi}{2} J \end{Bmatrix}$$

Any real constant can be incorporated into the real function $T(J,t)$:

$$M^{\pm}(s,t) = \begin{Bmatrix} 1 \\ i \end{Bmatrix} \int dJ\, s^J e^{-i(\pi/2)J}\, T^{\pm}(J,t)$$

<u>For an even amplitude</u>:

$$\frac{M^+(s,t)}{s} = \int dJ\, s^{J-1} e^{-i(\pi/2)J}\, T^+(J,t)$$

$$= -i \int dJ\, e^{(J-1)y}\, T'^+(J,t) \left[1 - i \tan\left[\frac{\pi}{2}(J-1)\right]\right]$$

$$\frac{\text{Re } M^{+}(s,t)}{s} = -\int dJ\, e^{(J-1)y}\, T'^{+}(J,t)\, \tan[\frac{\pi}{2}(J-1)]$$

$$= -\tan(\frac{\pi}{2}\frac{d}{dy})\int dJ\, e^{(J-1)y}\, T'^{+}(J,t)$$

leading to

$$\frac{\text{Re } M^{+}}{s} = \tan(\frac{\pi}{2}\frac{d}{dy})\,(\frac{\text{Im } M^{+}}{2})$$

For an odd amplitude:

$$M^{-}(s,t) = i\int dJ\, s^{J}\, T^{-}(J,t)\,[1 - i\tan(\frac{\pi}{2}J)]$$

$$\text{Re } M^{-}(s,t) = \int dJ\, s^{J}\, T^{-}(J,t)\, \tan(\frac{\pi}{2}J)$$

$$= \tan(\frac{\pi}{2}\frac{d}{dy})\int dJ\, s^{J}\, T^{-}(J,t)$$

giving

$$\text{Re } M^{-} = \tan(\frac{\pi}{2}\frac{d}{dy})\, \text{Im } M^{-}$$

-application to total cross sections.[60]

Separating into symmetric and antisymmetric parts we have:

$$\text{Re } F^{+} = s\tan(\frac{\pi}{2}\frac{d}{d\ln s})\,\sigma_T^{+}(s)$$

$$\text{Re } F^{-} = \tan(\frac{\pi}{2}\frac{d}{d\ln s})\, s\sigma_T^{-}(s)$$

Above the resonance region $\sigma_T^{+}(s)$ is a smooth function and retaining only the first derivative is a good approximation (Fig. 41). Good agreement is found with calculations using dispersion relations.

We have seen in Chapter II that in general $\sigma_T^{-}(s)$ was power-behaved, $\sigma_T^{-}(s) \sim s^{\alpha-1}$ and consequently:

$$\frac{\text{Re } F^{-}}{\text{Im } F^{-}} = \tan(\frac{\pi\alpha}{2})$$

a result generally labelled "Regge" but in fact following directly from power behaviour and analyticity.

If asymptotically $\sigma_T^{+} \sim (\ln s)^{\beta}$ $(\beta \leq 2)$ it follows that:

$$\frac{\text{Re } F^{+}}{\text{Im } F^{+}} \sim \frac{\pi\beta}{2\ln s}$$

showing that (i) if σ_T rises asymptotically, then the real part becomes positive (as observed in pp scattering above 300 GeV) and (ii) the real part increases with $\ln s$ one power down compared to the total cross section.

(c) Applications of derivative analyticity relations to amplitude analysis[62]

With quasi-local analyticity relations, we are now in a position to incorporate the analyticity constraints in a convenient form, most suited to amplitude analyses.

-formalism

Let us consider for simplicity a process with one even amplitude:

$$s^{2}\frac{d\sigma}{dt} = (\text{Re } F_{+})^{2} + (\text{Im } F_{+})^{2}$$

$$\frac{\text{Re } F_{+}}{s} = \tan(\frac{\pi}{2}\frac{d}{d\ln s})\,\frac{\text{Im } F_{+}}{s}$$

The iterative method outlined in paragraph (a) on dispersion relations can be implemented now in its most convenient form. For our purposes it is somewhat more practical to use a phase-magnitude relation. Writing the amplitude explicitly with modulus and phase:

$$F_{+}(s,t) = R_{+}(s,t)\, e^{i\Phi_{+}(s,t)}$$

the relation between R and Φ reads:

$$\phi_+(s,t) = -\frac{\pi}{2}\frac{d}{d\ln s}(\ln R_+)$$

or

$$\phi_+ = -\frac{\pi\alpha}{2} - \frac{\pi}{2}\frac{d}{dy}[\ln(R_+ s^{-\alpha})]$$

similarly for an odd amplitude:

$$\phi_-(s,t) = \frac{\pi}{2} - \frac{\pi}{2}\frac{d}{d\ln s}(\ln R_-)$$

or

$$\phi_- = \frac{\pi}{2}(1+\alpha) - \frac{\pi}{2}\frac{d}{dy}[\ln(R_- s^{-\alpha})]$$

For amplitudes with pure power-behaviour we find the "Regge" phases:

$$R \sim s^{\alpha} \Longrightarrow \phi_+ = -\frac{\pi}{2}\alpha$$

$$\phi_- = \frac{\pi}{2}(1-\alpha)$$

corresponding to Regge amplitudes $(e^{-i\pi\alpha} \pm 1)$.

In the single amplitude case we have, for positive signature:

$$s\sqrt{\frac{d\sigma}{dt}} = R_+(s,t)$$

$$\phi_+(s,t) = -\frac{\pi}{2} - \frac{\pi}{2}\frac{d}{dy}(\ln\frac{R_+}{s})$$

These simple equations have the following important physical consequence for elastic scattering at sufficiently high energy where Pomeron exchange (even amplitude) dominates. One expects the differential cross sections to increase in the forward direction and the t-slope to increase also. This means that there is a finite value of t at which the function (R_+/s) is essentially constant. This "cross over" in the same amplitude at different energies tells us that the real part has a zero at this t value (see Chapter V).

Let us now turn to a case with two helicity amplitudes, where both the differential cross section and polarization are measured. It is always possible to combine the different measured quantities in order to project out amplitudes with well-defined signature. Therefore consider two even-signatured amplitudes F_{++} and F_{+-} with modulii R_{++}, R_{+-} and phases ϕ_{++}, ϕ_{+-}. We have the two equations:

$$A^2 = R_{++}^2 + R_{+-}^2 = s^2\frac{d\sigma}{dt}$$

$$A^2 P = 2R_{++}R_{+-}\sin(\phi_{++} - \phi_{+-})$$

Using the derivative relations, R_{+-} can be eliminated and a differential equation is obtained for R_{++}:

$$\frac{d}{dy}\left(\ln\frac{R_{++}}{A}\right) = -\frac{2}{\pi}\frac{(A^2 - R_{++}^2)}{A^2}\sin^{-1}\left(\frac{A^2 P}{2R_{++}\sqrt{A^2 - R_{++}^2}}\right)$$

Given data as a function of s, $A(s)$ and $P(s)$, this equation can be solved numerically at each t value and F_{++} and F_{+-} can be reconstructed. There is an arbitrary integration constant which depends only on t and must be determined at one energy value from A and R measurements. An even more attractive approach is to extend the analysis down to energies where complete phase-shift solutions exist and amplitudes can be fully reconstructed.

It is well known that the arbitrary constant is related to an arbitrary rotation in the flip no-flip plane which arises as a consequence of using only $d\sigma/dt$ and P as input. To see that explicitly, let us define

$$R_{++} = A\cos\theta \qquad (\theta = \text{flip no-flip rotation angle})$$

$$R_{+-} = A\cos\theta$$

and solve for θ

$$\pi\frac{d\theta}{dy} = -\sin 2\theta \sin^{-1}\left(\frac{P}{\sin 2\theta}\right)$$

If the polarization is small (one amplitude is small or they both have the same s dependence) then one has the approximate solution

$$\theta(y,t) = \theta_0(t) - \frac{1}{\pi}\int_{y_0}^{y} dy' \, P(y')$$

where $\theta_0(t)$ is the s-independent integration constant which corresponds physically to a rotation in the helicity plane and must be determined at $y = y_0$.

-<u>mathematical examples</u>

Before using this method on real data, it is very instructive to test it on a few examples in order to learn about possible pitfalls.

(i) difference of two Regge poles

$$M_+ = \beta_1 s^{\alpha_1} e^{-i(\pi/2)\alpha_1} - \beta_2 s^{\alpha_2} e^{-i(\pi/2)\alpha_2}$$

A numerical comparison of the exact phase with the approximate one is shown in Fig. 42 for the values $\beta_1 = 1$, $\beta_2 = 0.5$, $\alpha_1 = 0.9 + t$ and $\alpha_2 = 0.5 + 0.6t$. The zeroes of the amplitude are at

$$\ln s = \frac{\ln(\beta_2/\beta_1)}{\alpha_1 - \alpha_2} + i\,\frac{\pi}{2}$$

One sees that the approximately reconstructed amplitudes follow quite well the input functions except when the latter have dips which have been completely smeared out. Away from the zeroes, the procedure is quite accurate.

(ii) absorbed Regge pole (Pomeron)

$$M_+ = s e^{-i(\pi/2)} \left[e^{Bt} - \frac{A}{A+B} \, e^{(ABt/A+B)} \right]$$

with $B = 0.5(\ln s - i\,\frac{\pi}{2})$ and $A = 4$. This amplitude is predominantly imaginary and the differential cross section resulting from it somewhat realistic. The simple phase method gives good results except where M_+ has zeroes (Fig. 43). Since $\mathrm{Re}\, M_+$ is quite small, it is sensitive to details of the procedure and is reconstructed quite well except for the point where $\mathrm{Im}\, M_+$ and the differential cross section have a dip and vary rapidly.

The above two examples are of value to show that the method is workable and particularly to help develop an intuition about how to proceed with real data.

-<u>applications to data</u>

(i) $K_L^0 p \to K_S^0 p$.

The amplitude for this process has odd signature only and therefore it is straightforward to use our method. In general the amplitude will have helicity flip and non-flip parts, respectively dominated by ρ and ω exchange and, since no polarization data are available one cannot perform a general amplitude analysis. However the helicity-flip contribution vanishes at $t = 0$ and presumably $t \simeq -0.5$ GeV^2 and therefore we can hope to measure the phase of the helicity non-flip amplitude at these t values.

At $t = 0$ there are actually two independent ways of measuring the phase: (1) from the s dependence of $(d\sigma/dt)_{t=0}$

$$\phi_{++}^{(-)} = -\frac{\pi}{4}\frac{d}{dy}\left[\ln\left(\frac{d\sigma}{dt}\right)_{t=0}\right]$$

or (2) from the s dependence of the imaginary part of the amplitude as given by the optical theorem

$$\frac{8\pi}{k}\,\mathrm{Im}\, F_{++}^{(-)} = \sigma_T(K^+n) - \sigma_T(K^-n) < 0$$

It is remarkable that experimentally both $(d\sigma/dt)_{t=0}$ and $\mathrm{Im}\, F_{++}^{(-)}$ are power-behaved from a few GeV/c to 60 GeV/c (see Chapter II) and therefore the phase can be obtained most easily. The results for methods (1) and (2) are shown in Fig. 44 and are in good agreement with independent measurements using $K_L^0 - K_S^0$ interference or optical point extrapolations.

At $t = -0.5$ GeV^2 we have[63]

$$\phi^{(-)}_{++} = -\frac{\pi}{4}\frac{d}{dy}\left(\ln\frac{d\sigma}{dt}\right) = \frac{\pi}{2}(1.02 \pm .22)$$

indicating a very small real part in qualitative agreement with Re ρ_{+-} in πN scattering.

(ii) $\gamma p \to \gamma p$.

Compton scattering is a nice example with an even-signatured amplitude. The helicity non-flip amplitude is large and dominated by P and f exchange, while the flip amplitude is much smaller. In the forward direction, $I_t = 1$ exchange (mostly A_2, flip) has been measured to be small by comparing γp and γd Compton scattering. There is no direct experimental information on the helicity structure of $I_t = 0$ exchange, however, we know from πN scattering and $\gamma p \to \rho^0 p$ that it is helicity non-flip to a good approximation and we expect γp to exhibit the same character. We therefore neglect helicity-flip contributions and assume the phase we obtain from $d\sigma/dt$ is that of the dominant helicity non-flip amplitude. Using the data of Ref. 64-66, the real part is obtained at mean momenta of 4 and 10 GeV (Fig. 45). The comparison between the two momenta shows a marked energy dependence, indicating that probably f exchange dominates the real part at these energies, as one would expect a priori. Comparing Im F_{++} and Re F_{++} at 10 GeV (Fig. 46) reminds us very strongly of the πN, $I_t = 0$ amplitudes at the same energy (Fig. 38). Between $t = 0$ and $-t = 0.8$ GeV^2 the phase ϕ_{++} changes from 102° to 110°, in good agreement with πN scattering.

(iii) <u>further applications in progress</u>

The πN system is currently being investigated using only $(d\sigma/dt)\,(\pi^\pm p)$, $(d\sigma/dt)\,(\pi^- p \to \pi^0 n)$ and $P(\pi^\pm p)$. The flip no-flip ambiguity $(\theta_0(t))$ can be fixed at 6 GeV using the known amplitudes or at lower energies using phase shifts.

Hypercharge exchange reactions constitute an interesting area for applications since signature can be dealt with using the appropriate line-reversed pairs of reactions. Denoting even-signatured amplitudes by T_λ (mostly K^*_T exchange) and odd-signatured amplitudes by V_λ (mostly K^*_V exchange) we have

$$\frac{d\sigma}{dt}(\pi N \to KY) = \sum_\lambda |T_\lambda + V_\lambda|^2$$

$$\frac{d\sigma}{dt}(\bar{K}N \to \pi Y) = \sum_\lambda |T_\lambda - V_\lambda|^2$$

leading to the four equations:

$$\frac{1}{2}\Sigma = |T_{++}|^2 + |T_{+-}|^2 + |V_{++}|^2 + |V_{+-}|^2$$

$$\frac{1}{2}\Delta = \mathrm{Re}(T_{++}V^*_{++} + T_{+-}V^*_{+-})$$

$$\frac{1}{4}(\Sigma P) = \mathrm{Im}(T_{++}T^*_{+-} + V_{++}V^*_{+-})$$

$$\frac{1}{4}(\Delta P) = \mathrm{Im}(T_{++}V^*_{+-} + V_{++}T^*_{+-})$$

When the phase-magnitude relations are taken into account, one obtains a system of 4 differential equations which can be solved numerically at each t value, giving back the amplitudes with some ambiguities.

We have tried to show how analyticity can, in a powerful and very practical way, improve our tools to extract amplitudes from incomplete data.

IV - DUALITY AND ABSORPTION

In this chapter we are going to briefly review some of the most important ideas and concepts in the phenomenology of two-body scattering, as they relate in a relevant way to the experimental facts we have gathered through the course of the preceding sections.

1. Duality

(a) Two descriptions of two-body scattering

At low energy ($\sqrt{s} \lesssim 2$ GeV), our knowledge of two-body scattering is embodied in s-channel phase-shifts describing the data with resonant and non-resonant (background) waves. As s increases this description ceases to be practical because of too many waves.

At high energy we have seen that amplitudes are clearly related to t-channel exchanges and that, in general, only a few exchanges are required to describe the experimental situation.

If at low energy there is little uncertainty in the analytical description of s-channel resonances, the situation is less clear at high energy: we know most amplitudes manifest some kind of Regge behaviour, with the phase-energy relation and trajectories approximately related to the particle spectrum. Hence, as a starting point, it is not too unreasonable to assume that t-channel exchanges are mediated by Regge poles. Later, considering some of the difficulties encountered, we shall come back on this assumption.

(b) Relating low and high energy descriptions: FESR[67]

There must be some relation between low s and high s regions since the scattering amplitude is analytic in energy. Using analyticity and Regge behaviour for high energy one can derive a finite energy sum rule (FESR).

Consider a scattering amplitude $F(\nu)$ which is supposed to be a real analytic function of the variable ν every where in the ν plane except for inelastic cuts from $-\infty$ to $-\nu_0$ and from ν_0 to ∞ and some isolated poles on the real axis. We assume a Regge behaviour at high energy:

$$F(\nu) = \sum_k \beta_k \frac{1 + \tau_k e^{-i\pi\alpha_k}}{\sin \pi\alpha_k} \nu^{\alpha_k}$$

$$|\nu| > N, \quad \beta_k, \ \alpha_k \ \text{functions of} \ t.$$

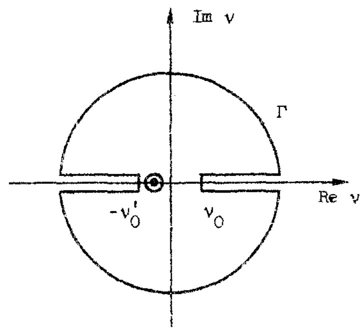

Now if we apply Cauchy's theorem to the closed contour Γ:

$$\oint_\Gamma F(\nu)\, \nu^n \, d\nu = 0$$

$$\int_{-N}^{-\nu'_0} \mathrm{Im}\, F(\nu)\, \nu^n \, d\nu + \int_{\nu_0}^{N} \mathrm{Im}\, F(\nu)\, \nu^n \, d\nu + \sum_k \beta_k \frac{N^{\alpha_k+n+1}}{\alpha_k+n+1} \left[\tau_k - (-1)^n\right] = 0$$

where pole terms are formally included in the dispersion integrals. The expression becomes simpler if $F(\nu)$ has a well-defined signature; if $F(\nu)$ is odd

$$F(\nu) = -F(-\nu) \qquad \text{and} \qquad \tau_k = -1$$

then the FESR reads

$$\int_{\nu_0}^{N} \mathrm{Im}\, F(\nu)\, \nu^n \, d\nu = \sum_k \beta_k \frac{N^{\alpha_k+n+1}}{\alpha_k+n+1} \qquad (n \ \text{even})$$

Thus if we know (from phase-shifts) the behaviour of $\mathrm{Im}\, F(\nu)$ below $\nu = N$, we have a way to use analyticity in order to get some information on high energy parameters, provided (i) the asymptotic form chosen was correct and (ii) the cut-off N is taken high enough for this asymptotic form to be valid. This procedure has indeed been applied with some success.

The limitation that phase-shifts data exist only for low s, well below the "asymptotic" Regge region has been actually a rather favourable situation since it led to the concept of duality. Dolen, Horn and Schmid[68] investigated the πN charge exchange amplitudes taking $N = 1.1$ GeV as their cut-off: they were able to reproduce the main features of t-channel ρ exchange (dominance of B, ρ trajectory, zeroes) even though N was low and resonance behaviour was still seen at higher energies at $t = 0$ (Fig. 47): the high energy amplitude is behaving like the average of the s-channel resonances. An important aspect of the result is that s-channel resonances actually dominate the left-hand side of the FESR with no noticeable background, leading to the powerful idea that, s-channel resonances or t-channel poles are alternate descriptions of the same process with the smooth high s, t-channel pole amplitudes averaging out the s-channel resonant structures.

A powerful use of FESR is realized when both s and t channel descriptions make use of the same singularities; in this case it provides a way of bootstrapping these singularities. Consider, for example, the process $\pi^+\pi^0 \to \pi^0\pi^+$ where ρ exchange occurs in both s and t channel: requiring the first zero of both amplitudes to coincide leads to $1/\alpha' \simeq \frac{3}{2} m_\rho^2$ or $\alpha' \simeq 1.1\ \mathrm{GeV}^2$, a value rather close to the experimental number.

Many applications of FESR have followed for πN, KN, photoproduction etc. .... It would be very interesting to have reliable FESR analyses to learn about those amplitudes not easily accessible at high energy in the t channel. For example we know very little about even crossing amplitudes (in particular, f exchange in πN elastic scattering, f and A_2 exchanges in KN, $\bar{K}N$ elastic scattering). In principle we can learn about A_2 exchange using FESR and low energy KN and $\bar{K}N$ data: however, in practice, this is somewhat unreliable since K^+n low energy data are not yet very complete, nor very accurate and consequently the phase shifts with proper quantum numbers cannot be completely trusted.

For example a recent FESR analysis[69] of KN and $\bar{K}N$ scattering with a cutoff $p_L = 1.5$ GeV/c shows the expected features for the dominant amplitudes like $\mathrm{Im}\,\omega_{++}$ and $\mathrm{Im}\,\rho_{+-}$ while $\mathrm{Im}\,A_{++}$ and $\mathrm{Im}\,A_{+-}$ seem to behave differently from $\mathrm{Im}\,\omega_{++}$ and $\mathrm{Im}\,\rho_{+-}$ respectively. One must keep in mind however that the cutoff is rather low, the phase shifts solutions not always reliable and some of the amplitudes are quite small in magnitude and subject to uncertainties. Such methods will be nevertheless very useful, as the quality of the KN phase shifts improves, to study specific exchanges in the intermediate energy region.

Let us emphasize at this point the dominance of the FESR integral by resonances is expected to make sense only for the imaginary part of the amplitude, while real parts of resonances can contribute to very distant energies, even outside the physical domain.

(c) Two-component duality

The generalization of the duality concept to elastic scattering has been made.[70-71] While s-channel resonances are dual to t-channel exchanges, the background under the resonances builds up the diffractive amplitude--the exchange of the Pomeron.

s-channel resonances $\Longleftrightarrow$ t-channel exchanges

s-channel background $\Longleftrightarrow$ Pomeron exchange

The consequences of this principle are well known:

--<u>if the s-channel has exotic quantum numbers</u>, no resonances will contribute and high energy exchanges will only involve Pomeron exchange, at least in the imaginary part

$$\mathrm{Im}\, F_{s\ \mathrm{large}} \simeq \mathrm{Im}\, P$$

In order to achieve that, allowed t-channel exchanges have to cancel each other (exchange degeneracy). For example K^+p scattering is exotic in the s-channel and we expect that, at high energy,

$$\mathrm{Im}\, f^K = \mathrm{Im}\, \omega^K$$

$$\mathrm{Im}\, \rho^K = \mathrm{Im}\, A^K$$

so that

$$\mathrm{Im}\, A(K^+p) \simeq P$$

$$\mathrm{Im}\, A(K^-p) \simeq P + 2\ \mathrm{Im}\, \omega^K + 2\ \mathrm{Im}\, \rho^K$$

This result is only expected to hold for the imaginary part since the real part of K^+p scattering can receive contribution from the distant Y^* resonances of the s-u crossed channel and is seen experimentally to be large. It is amusing to see that for Regge exchanges with some $\alpha(t)$ we have

$$\mathrm{Re}\, A_R(K^+p) = 2(\beta_\omega^K + \beta_\rho^K)\ s^\alpha$$

$$\mathrm{Im}\, A_R(K^+p) = 0$$

$$\mathrm{Re}\, A_R(K^-p) = 2(\beta_\omega^K + \beta_\rho^K)\cos\pi\alpha\ s^\alpha \qquad (\simeq 0 \text{ at } t = 0)$$

$$\mathrm{Im}\, A_R(K^-p) = -2(\beta_\omega^K + \beta_\rho^K)\sin\pi\alpha\ s^\alpha$$

In Fig. 48 it is shown that indeed the low energy part of $\mathrm{Im}(\rho + A)^K$ is large and dominated by resonances while $\mathrm{Im}(\rho - A)^K$ is much smaller and structureless.

--<u>if the s-channel is exotic and no Pomeron exchange is allowed</u>, we expect the scattering amplitude to be essentially real. This is the case in K^+N charge exchange scattering: we have seen in Chapter II that the phase of the forward amplitude for $K^+n \to K^0p$ was very close to zero. We expect similar results for $K^+p \to K^0\Delta^{++}$, $pn \to np$ and $pp \to n\Delta^{++}$. At the same time the corresponding non-exotic channels are expected to be mostly imaginary, as observed in $K^-p \to \bar{K}^0n$.

--<u>imaginary parts of amplitudes for non-diffractive scattering</u> should be dominated by resonances. This is observed in πN scattering[72] where clean Argand loops show up in $I_t = 1$ amplitudes (no Pomeron) (Fig. 49); the aspect of $I_t = 0$ diagrams is different with a large imaginary background (Pomeron) superimposed to resonance patterns.

(d) <u>application of duality: exchange degeneracy (EXD)</u>

The following set of assumptions (duality) leads to very strong consequences for t-channel exchanges:

(1) analyticity } FESR
(2) asymptotic Regge behaviour }
(3) absence of exotic amplitudes (for imaginary parts only in non-diffractive channels)

--<u>trajectories</u>

Consider exotic $\pi^+\pi^+$, K^+K^+, K^+K^0 scattering. Exchange degeneracy tells us that the ρ and f trajectories should be the same and the same result should hold for (f,ω) and (ρ,A_2) leading to a unique trajectory for ρ, ω, f and A_2 exchange. A look at the Chew-Frautschi plot shows that it is rather well satisfied by the particle spectrum (Fig. 50). From the mass spectrum alone we would deduce a linear trajectory:

$$\alpha(t) = 0.46 + 0.9t$$

when compared to experimental trajectories $\alpha(t) = \alpha(0) + \alpha' t$ measured in the space-like region

	$\alpha(0)$	α'	
ρ	.56	.97	$-t < 1.5\ \mathrm{GeV}^2$
A_2	.48	.9	$-t < 0.4\ \mathrm{GeV}^2$
ω	.40	?	
f	?	?	

we see that the agreement is not overwhelming. In Fig. 51 we directly compare $\alpha_\rho(t)$ and $\alpha_A(t)$ from $\pi^- p \to \pi^0 n$ and $\pi^- p \to \eta n$.

--<u>residues</u>

Duality imposes equality between residues in exotic channels.

--<u>line-reversed reactions</u>

Consider the pair of s-u crossed reactions:

$$a + b \to c + d \qquad (1)$$

$$\bar{c} + b \to \bar{a} + d \qquad (2)$$

asymptotically the two amplitudes have to be equal, but EXD makes some very strong requirements at any s (sufficiently large). Let us separate out odd and even amplitudes:

$$A_+ = \beta_+(1 + e^{-i\pi\alpha})s^\alpha = 2\beta_+ e^{-i\pi(\alpha/2)} \cos \frac{\pi\alpha}{2} s^\alpha$$

$$A_- = \beta_-(1 - e^{-i\pi\alpha})s^\alpha = 2i\beta_- e^{-i\pi(\alpha/2)} \sin \frac{\pi\alpha}{2} s^\alpha$$

A_+ and A_- are $\pi/2$ out of phase and consequently

$$\left(\frac{d\sigma}{dt}\right)_1 = \left(\frac{d\sigma}{dt}\right)_2$$

with

$$\left(\frac{d\sigma}{dt}\right)_{1,2} = \frac{1}{s^2} |A_+ \pm A_-|^2 = 4s^{2\alpha-2}(\beta_+^2 + \beta_-^2)$$

This result follows uniquely from the identity between the two trajectories α_+ and α_-.

Let us now explicitly show helicity amplitudes:

$$A_\pm^{\substack{++\\+-}} = 2e^{-i\pi(\alpha/2)} s^\alpha \left[\beta_+^{\substack{++\\+-}} \cos \frac{\pi\alpha}{2} + i\beta_-^{\substack{++\\+-}} \sin \frac{\pi\alpha}{2}\right]$$

leading to a polarization:

$$P \frac{d\sigma}{dt} = 4s^{2\alpha-2} \sin \pi\alpha[\beta_+^{+-}\beta_-^{++} - \beta_-^{+-}\beta_+^{++}]$$

The equality of residues, $\beta_+^{\substack{++\\+-}} = \beta_-^{\substack{++\\+-}}$, imposed by duality, leads to no polarization in both processes.

It is interesting to compare processes involving the same EXD exchanges and one expects:

$$\frac{\frac{d\sigma}{dt}(ab \to cd)}{\frac{d\sigma}{dt}(\bar{c}b \to \bar{a}d)} = \frac{\frac{d\sigma}{dt}(a'b' \to c'd')}{\frac{d\sigma}{dt}(\bar{c}'b' \to \bar{a}'d')}$$

--<u>experimental tests of line-reversal</u>

We have experimental information on:

$$\frac{d\sigma}{dt}(K^- p \to \bar{K}^0 n,\ K^+ n \to K^0 p) \qquad \text{(Fig. 52)}$$

$$\frac{d\sigma}{dt}(\pi N \to KY,\ \bar{K}N \to \pi Y)$$

$$P(K^- p \to \bar{K}^0 n)$$

$P(\pi N \to KY,\ \bar{K}N \to \pi Y)$

$$\frac{\frac{d\sigma}{dt}(K^-p \to \bar{K}^0 n,\ K^-n \to K^0\Delta^-)}{\frac{d\sigma}{dt}(K^+n \to K^0 p,\ K^+p \to K^0\Delta^{++})} \qquad \text{(Fig. 53)}$$

Agreement with EXD is not good in general. However one does not have to blame duality as a whole since some other assumptions were used in particular the assumed Regge pole behaviour with its factorization properties. Since we have numerous examples where the simple Regge-pole description breaks down, mostly through factorization, one may still hope to retain basic dual properties once the structure of the singularities is better understood. Along this direction it is instructive to compare the non-zero polarizations in $K^-p \to \bar{K}^0 n$ (duality + Regge pole behaviour predicts zero polarization) and in $\pi^-p \to \pi^0 n$ (Regge pole assumption leads to zero polarization).

--dip mechanisms

In a Regge amplitude

$$A_+ = \beta_+ \frac{1 + e^{-i\pi\alpha}}{\sin \pi\alpha} s^\alpha$$

the residue function $\beta_+(t)$ must have zeroes to cancel the possible poles of $\sin \pi\alpha$.

$$\alpha = 0 \qquad \sin \pi\alpha = 0 \qquad \Longrightarrow \beta_+(\alpha = 0) = 0$$

Then exchange degeneracy forces the same zero on the corresponding exchange

$$\beta_-(\alpha = 0) = 0$$

where the pole is already cancelled and therefore the amplitude has a zero.

For example, at $\alpha_\rho = \alpha_{A_2} = 0$ we have

$$\text{Im } \rho_{+-} = 0$$

$$\text{Re } \rho_{+-} = 0$$

but $\text{Re } A_{+-} \neq 0$.

These results are in good agreement with experiment for the flip amplitudes. The following processes are dominantly helicity-flip and should be related by EXD and SU(3):

$$\frac{d\sigma}{dt}(\pi^-p \to \pi^0 n) \sim \beta_\pi^2 \sin^2 \frac{\pi\alpha}{2} \sim 2 \sin^2 \frac{\pi\alpha}{2}$$

$$\frac{d\sigma}{dt}(\pi^-p \to \eta n) \sim \beta_\eta^2 \cos^2 \frac{\pi\alpha}{2} \sim \frac{2}{3} \cos^2 \frac{\pi\alpha}{2}$$

$$\frac{d\sigma}{dt}(K^-p \to \bar{K}^0 n) \sim 2\beta_K^2 \qquad \sim 1$$

In Fig. 54 these relations are compared to experimental data: we see that there is good agreement between the shapes (a statement about duality and Regge behaviour for flip amplitudes) and even in magnitude (SU(3) symmetry). The same qualitative agreement is found in vector meson production[73]

$$KN \to K^* N, \quad \bar{K}N \to \bar{K}^* N, \quad \pi N \to \rho N$$

where $I_t = 0$ exchange (f, ω) can be isolated.

This nice systematics obviously will not work for helicity non-flip amplitudes with their zeroes completely uncorrelated with wrong-signature points.

(e) duality and quarks

Duality and the absence of exotic states leads to properties usually attributed to the quark model:

--in meson-meson scattering with SU(3) symmetry, duality leads to nonet structure for t-channel exchanges.

--considering K^+K^+ and K^+K^0 scattering, we find the canonical quark-model mixing angle between $\omega - \Phi$ and $f - f'$

$$\cos^2\lambda = \frac{1}{3}$$

This intriguing correction has been exploited in the duality diagrams,[74-75] but will not be developed here.

(f) semi-local duality?

It is interesting to see how resonances can average and build up the smooth Regge behaviour: in particular let us find experimentally what is a typical momentum range for cancellations to occur. For example, consider backward $K^-p \to \bar{K}^0 n$ scattering[76] which has exotic quantum numbers: Fig. 55 shows the energy dependence of the imaginary part of the amplitudes showing resonance-produced oscillations around the zero value predicted by duality. A typical range $\Delta P_L \sim 1$ GeV/c corresponds to the short-range cancellation between resonances.

This semi-local duality can be exploited as a method to learn about t-channel amplitudes. Having a complete description in terms of phase-shifts over some (low) energy domain, we can reconstruct s-channel helicity amplitudes with well-defined t-channel quantum numbers in a local sense. Then, by observing the s-dependence of these amplitudes over some range of momenta (~ 1 GeV/c) we can hope to learn about them.

--example: $\bar{K}N$ scattering[77]

This type of study is particularly interesting and important for $\bar{K}N$ scattering where phase-shifts exist and are usually parametrized in terms of resonances superimposed to a background: each partial wave is taken as the sum of background and resonant parts

$$f_{\ell\pm} = f^R_{\ell\pm} + f^B_{\ell\pm}$$

The amplitudes reconstructed from the background shows dominance of the helicity non-flip, $I_t = 0$, imaginary part in accordance with Pomeron exchange properties (Fig. 56). It is remarkable that the background only contributes a negligible amplitude to $I_t = 1$ exchange in strong support of the Harari-Freund proposal.

Helicity amplitudes reconstructed from the resonant parts of the $\bar{K}N$ partial wave amplitudes are shown in Fig. 57. Even at momenta 1-1.3 GeV/c the features of high energy t channel exchange are well established with a zero at $t \sim -0.2$ GeV^2 for Im F_{++} (both $I_t = 0$ and $I_t = 1$) and a zero at $t \sim -0.5$ for Im F_{+-} ($I_t = 0, 1$).

As a final remark, let us note that a linear separation between background and resonances

$$\text{Im } F = \text{Im } P + \text{Im } R$$

does not obey unitarity. Indeed for a given partial wave P, we have the S-matrix:

$$S^\ell = \underset{\text{background}}{S^\ell_B}\ \underset{\text{resonance}}{S^\ell_R}$$

and consequently

$$T^\ell = T^\ell_B + T^\ell_R(1 + 2iT^\ell_B)$$

$$\text{Im } T^\ell = \text{Im } T^\ell_B + \text{Im } T^\ell_R + 2\ \text{Re}(T^\ell_R T^\ell_B)$$

The last term is generally ignored in most analyses.

2. Absorption

(a) classical absorption

In a scattering process, both the incident and outgoing waves can be absorbed out and it is convenient to describe the overall scattering amplitude in the impact parameter space:

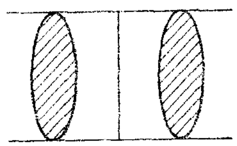

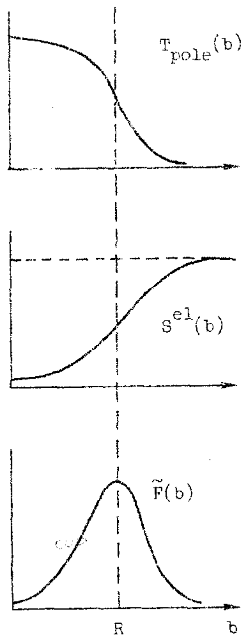

$F_{\Delta\lambda}(s,t)$

$$= \int b\, db\, T^{\Delta\lambda}_{pole}(b,s)\, S^{el}(b,s)\, J_{\Delta\lambda}(b\sqrt{-t})$$

where $S^{el}(b,s)$ is the transmission at the impact parameter b, and $\Delta\lambda$ the overall helicity change.

$$S^{el}(b,s) = 1 + iT^{el}(b,s)$$

$$\simeq 1 - |T^{el}(b,s)|$$

Therefore the dominant effect of absorption is the removal of low partial waves leading to peripherality of the absorbed amplitude in b space.

For a purely imaginary elastic amplitude with $\Delta\lambda = 0$

$$F_{el} = \frac{i\sigma_T}{4\sqrt{\pi}}\, e^{(B/2)t}$$

we have

$T_{el}(b)$

$$= \frac{1}{\sqrt{\pi}} \int_0^\infty \sqrt{-t}\; d\sqrt{-t}\; F_{el}(t)\; J_0(b\sqrt{-t})$$

$$= \frac{i\sigma_T}{4\pi B}\, e^{-b^2/2B}$$

and therefore total absorption of low partial waves if

$$\frac{\sigma_T}{4\pi B} = 1$$

Typically $\sigma_T = 25$ mb, $B = 7\ \mathrm{GeV}^{-1}$ leading to $\sigma_T/4\pi B \sim 0.7$; so that in order to absorb completely the central waves one needs some additional absorption. For example it has been suggested[78] that all the inelastic diffractive states should be included as intermediate states leading to an increase in absorption.

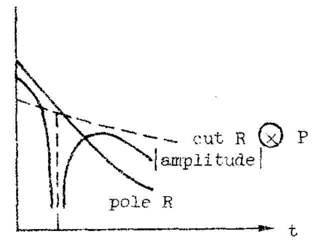

For strong enough an absorption the t-distribution can present dips due to the interference between the bare pole amplitude and the cut resulting from the convolution integral. The cut is destructive at $t = 0$ since T_{el} is imaginary.

Absorption has a qualitatively different effect on different helicity amplitudes due to the kinematic zero at $t = 0$ for flip amplitudes. Schematically we have:

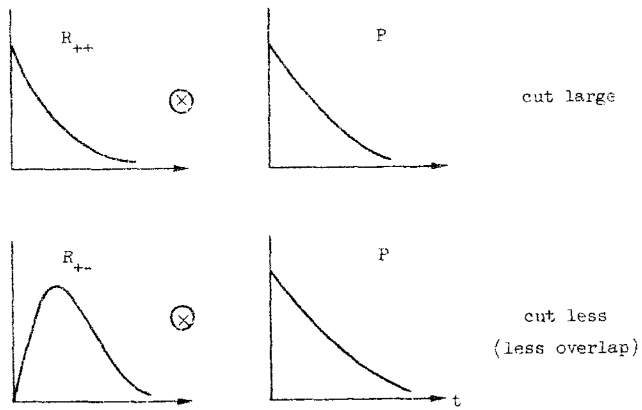

This can also be seen by transforming the pole input into impact parameter space: one then finds that helicity flip amplitudes are in general already peripheral and therefore absorption of low waves is of little effect.

--general form for an absorbed amplitude

$$F_{\Delta\lambda}(t) = \int b\, db\, T(b)\, J_{\Delta\lambda}(b\sqrt{-t})$$

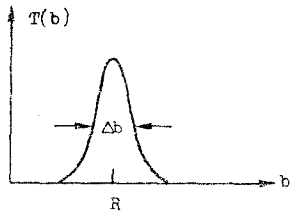

if $T(b) = \delta(b-R)$

$$F_{\Delta\lambda}(t) \sim J_{\Delta\lambda}(R\sqrt{-t})$$

if $T(b)$ peaks at $b \sim R$ with some width Δb, then $F_{\Delta\lambda}(t)$ retains the zeroes of $J_{\Delta\lambda}(R\sqrt{-t})$ for Δb not too large

$$\sqrt{-t} \ll \frac{\pi}{\Delta b}$$

A realistic form is $F_{\Delta\lambda}(t) = Ae^{Bt} J_{\Delta\lambda}(R\sqrt{-t})$ where R is the peak value and B is related to Δb.

$$\Delta b \sim 2\sqrt{B}$$

(b) absorption zeroes versus signature zeroes

Wrong signature occur typically for $t \sim -0.6$ GeV^2 where $\alpha(t)$ passes through zero. Experimentally helcity-flip amplitudes have zeroes around 0.6 GeV^2; however absorption can also produce similar effects: $J_1(R\sqrt{-t})$ vanishes at the same place for $R = 1f$, a very realistic value. Therefore we have the following dilemma in trying to explain these dips:

$$\Delta\lambda = 1 \begin{cases} \text{Regge pole amplitude with signature zeroes} \\ \text{structureless pole} \otimes \text{absorption} \sim J_1(R\sqrt{-t}) \end{cases}$$

For $\Delta\lambda = 0$, there is no question: we have to invoke strong absorption to obtain a zero at -0.2 GeV^2 and there is no trace of Regge zeroes.

A possible way to distinguish between absorption and wrong-signature zeroes arises if R shows some variation with s: in that case the J_1 zero will move with energy while the Regge zero, being a t-channel effect, should stay fixed.

(c) "dual" absorption

We know that s-channel resonances will produce dips in angular distributions due to their well-defined angular momentum. Since duality relates these resonances to the t-channel exchanges, we are interested in the relationship between these dips and the high energy t-channel dips (with or without absorption).

First of all let us see how resonances can produce dips at fixed t values. This will occur if there is a definite relationship between the mass and the spin of the dominant resonances. As an example, consider $\pi\pi$ scattering with no Pomeron ($\pi^+\pi^- \to \pi^0\pi^0$):

$$R(s,t) = \sum_J A_J P_J(\cos\theta)$$

For $J \gg 1$ and $\epsilon < \theta < \pi-\epsilon$

$$P_J(\cos\theta) \sim 2(2\pi J\sin\theta)^{-1/2}\cos\left[(J+\tfrac{1}{2})\theta - \tfrac{\pi}{4}\right]$$

and the first zero of the angular distribution is at:

$$(J+\tfrac{1}{2})\theta = \frac{3\pi}{4}$$

$$\theta \simeq \frac{3\pi}{4J}$$

Since $t = 2q^2(1-\cos\theta)$, a fixed t dip will occur if

$$s \sim \frac{1}{1-\cos\theta} \sim \frac{1}{\theta^2} \sim J^2$$

Thus the looked-for relationship is:

$$J \sim \sqrt{s}$$

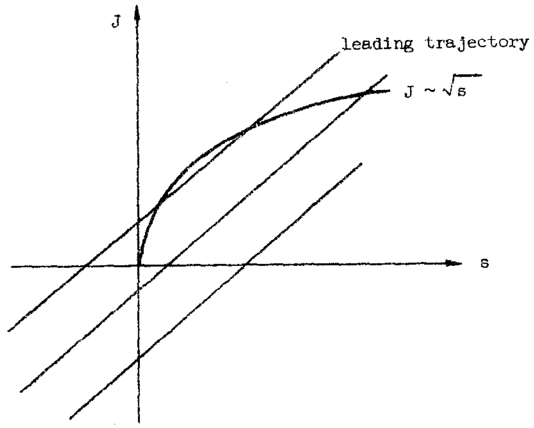

Above the curve $J \sim \sqrt{s}$ we expect angular momentum barrier effects, while below the amplitude is suppressed by absorption of low partial waves leading to the overall peripheral picture.

This behaviour can be checked against the observed N^* and Y^* baryon spectrum in Figs. 58 and 59. It seems satisfied although the deviation from the leading trajectory is still not clearly perceived. There is nevertheless a noticeable lack of low spin resonances at large mass: it seems that one should look experimentally a little harder into this question of low-lying "daughter" resonances, in order to pin down the idea of peripherality. In Fig. 60 we plot the location of the first zero of the $\Delta\lambda = 0$ and $\Delta\lambda = 1$ helicity amplitude from the prominent Y^* resonances: fixed t structures occur already in the lower mass states.

We have seen therefore that the dominance of "peripheral" resonances leads to a peripheral Im R while no insight is gained on the real part. On the other hand, classical absorption has for consequence that <u>both</u> real and imaginary parts are peripheral.

--<u>discussion</u>

It is an experimental fact that known resonances (log J) contribute a zero at 0.2 GeV^2 in Im R_{++} and that Im R_{++} at high energy also possesses such a zero (at least for the observed vector exchanges) as a result of absorption. The most logical connection between these two facts is to assume that <u>resonances are dual to Regge poles + absorption cuts</u>.[79]

Alternatively one could still have resonances dual to poles alone. If central resonances continue to be excited, dips can occur at larger t (~ 0.6 GeV^2) corresponding to the signature zeroes of Regge poles. Also at high energy absorption moves zero down to 0.2 GeV^2 thereby breaking duality. This alternative seems much less natural, but cannot be completely excluded at the present time.

This situation has an immediate consequence for exchange degeneracy: in the first case EXD will be satisfied at the same level than duality itself while in the second case there will be strong violations of duality due to absorption corrections.

Even though we are not yet seeing overwhelming evidence for peripheral high-mass resonances (in the $J \sim \sqrt{s}$ sense), the low mass resonances do exhibit striking peripheral properties in b space:[80] see, for example Fig. 61 where the $\bar{K}N$ resonant partial wave amplitudes are used to reconstruct Im R_{++}. The peripheral resonance contributions peak around 1f in a clear way almost outside the diffractive impact parameter distribution (Fig. 62). This feature is not unique to $\bar{K}N$ scattering and is also observed in πN phase shifts: Fig. 63 shows the full amplitude Im R_{++} + Im P where the resonance contribution is clearly visible on the edge of the diffractive background distribution of central character. From the same $\bar{K}N$ analysis it is interesting to follow the zero positions at 0.2 and 0.5 GeV^2 of the resonant amplitudes Im $R_{++}^{(I_t=0)}$ and Im $R_{+-}^{(I_t=1)}$ which are essentially constant within the accuracy of the different phase-shift analyses (Fig. 64).

V - MODELS AND SPECULATIONS

1. Models for Two-Body Scattering

From what we have seen in the preceding chapters it is clear that any model for high energy scattering should incorporate or possess the following properties:

- some Regge features, in particular in $\Delta\lambda = 1$ amplitudes
- strong absorption of the bare exchanges by Pomeron cuts
- duality for the imaginary parts
- approximate SU(3) symmetry for residues

Different models will have their emphasis on a few properties and will generally try to "explain" the remaining properties. Pure pole models are not reliable, except for flip amplitudes, and cannot yield a complete description of two-body processes. Strong absorption appears to be an important ingredient which has to be included in any realistic model.

We are not going to review all potentially successful models but rather select two of them in order to illustrate different assumptions and problems: on one hand, the dual absorptive model where duality and absorption are strongly linked together; on the other hand the strong absorption model where the accent is put on calculating strong-absorption cuts with no relationship to duality.

(a) Dual absorptive model (Harari[81])

--rules

The imaginary part of a non-diffractive t-channel exchange is built up by peripheral resonances. The $J \sim \sqrt{s}$ peripheral resonances are dual to the sum of poles and their absorption cuts:

$$\text{Resonances} \Longleftrightarrow R + R \otimes P$$

For a change $\Delta\lambda$ of helicity the imaginary part of an amplitude has a zero structure approximately given by $J_{\Delta\lambda}(R\sqrt{-t})$ where R is around 1 f

$$\text{Im } F_{\Delta\lambda} \sim J_{\Delta\lambda}(R\sqrt{-t})$$

For $\Delta\lambda = 0$ the cut correction is large while it is much smaller for $\Delta\lambda =$

The structure of the real parts is not given by duality requirements but one can invoke analyticity: if $\text{Im } F \sim s^{\alpha}$ then

$$\frac{\text{Re } F}{\text{Im } F} \sim \begin{cases} -\cot \frac{\pi\alpha}{2} & \text{(even exchange)} \\ \tan \frac{\pi\alpha}{2} & \text{(odd exchange)} \end{cases}$$

These crossing relations are claimed to work only for $\Delta\lambda = 1$ amplitudes where the s^{α} dependence is not perturbed too much by cuts; in $\Delta\lambda = 0$ amplitudes strong cuts can introduce log factors in the amplitude and the crossing relation could fail.

The Pomeron amplitude is assumed to be structureless in t, central in impact parameter space, mostly imaginary and helicity no-flip.

--comparison with experiment

(i) dips in inelastic processes ($\Delta\lambda = 1$ amplitudes)

Imaginary parts behave like $J_1(R\sqrt{-t})$ while real parts are

$$\tan\left(\frac{\pi\alpha}{2}\right) J_1(R\sqrt{-t}) \qquad \text{or} \qquad -\cot\left(\frac{\pi\alpha}{2}\right) J_1(R\sqrt{-t})$$

according to the signature:

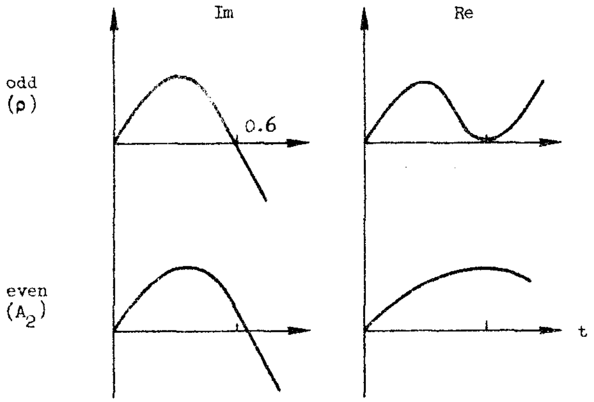

$$\frac{d\sigma}{dt} \sim \frac{J_1^2}{\cos^2 \frac{\pi\alpha}{2}}$$

$$\frac{d\sigma}{dt} \sim \frac{J_1^2}{\sin^2 \frac{\pi\alpha}{2}}$$

The most simple way to produce dips at $-t \sim 0.6\ \mathrm{GeV}^2$ in differential cross sections is when $\Delta\lambda = 1$ amplitudes with zero dominate. If other helicity amplitudes are important they are likely to wash out any indication of a dip: for example $[J_0(R\sqrt{-t})]^2$ has a bump in this t region. In order to see if a given process will have a dip or not, it is sufficient to apply the helicity coupling rules derived empirically in Chapter II and find out if $\Delta\lambda = 1$ dominates. If this latter condition is true, a dip will be observed if the exchange is odd under crossing since $d\sigma/dt$ has the zero of $[J_1(R\sqrt{-t})]^2$.

The dip is predicted and observed for the processes:

$$\pi^- p \to \pi^0 n, \qquad \pi N \to \pi\Delta, \qquad \gamma p \to \pi^0 p, \qquad (\pi N \to \rho N)_{I_t=0} \;.$$

For reaction dominated by $\Delta\lambda = 1$ even exchanges, no such dip is observed: $\pi^- p \to \eta n$, $\pi N \to \eta\Delta$. This is also true when both even and odd exchanges occur such as in $K^- p \to \bar{K}^0 n$, $K^+ n \to K^0 p$, $KN \to K\Delta$ and $\bar{K}N \to \bar{K}\Delta$.

When $\Delta\lambda = 1$ does not dominate, no dip is expected as in $\gamma p \to \eta p$, $\pi N \to \omega N$, despite a strong ρ exchange.

The behaviour of elastic polarizations is also in good agreement with the dual absorptive model, as a test of $\mathrm{Re}\, R_{\Delta\lambda=1}$.

(ii) elastic scattering ($\Delta\lambda = 0$ amplitudes)

The (dominant) imaginary part of an elastic scattering amplitude receives contributions from resonances (or t channel poles) and the Pomeron. For exotic channels, only the Pomeron term survives, as in K^+N and NN scattering:

$$F \sim P \sim \mathrm{Im}\, P$$

while for non-exotic processes, such as K^-N and $\bar{N}N$ scattering, we have the complete form

$$\mathrm{Im}\, F = \mathrm{Im}\, P + \mathrm{Im}\, R$$

For s high enough, the $\Delta\lambda = 0$, imaginary Pomeron amplitude dominates so that the leading terms in the differential cross section are:

$$\frac{d\sigma}{dt}\,(\text{exotic}) \simeq P^2$$

$$\frac{d\sigma}{dt}\,(\text{nonexotic}) \simeq P^2 + 2P\, \mathrm{Im}\, R_{\Delta\lambda=0}$$

where $\mathrm{Im}\, R_{\Delta\lambda=0}$ behaves like a $J_0(R\sqrt{-t})$ function. We therefore expect the following pattern:

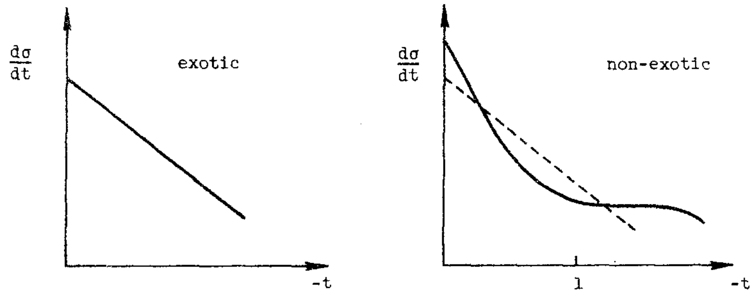

This behaviour is clearly seen in the data in the intermediate energy region for $\pi^\pm p$ (both non-exotic), $K^\pm p$ and up to ~ 10 GeV for $p^\pm p$ where the resonance contribution is larger. Obviously as the contribution from the resonances slowly decreases as the energy goes up, we expect the two patterns to become more and more similar and the "dip" in the non-exotic channel to fade away. We can translate this effect in terms of the exponential slope of the forward differential cross section which energy dependence comes from the proper s dependence of the Pomeron slope (which shrinks according to K^+p and pp data) and the disappearance of the Regge term (producing an apparent anti-shrinkage). The following trends are therefore expected in the dual absorptive model:

$$\frac{d\sigma}{dt} \sim e^{Bt}$$

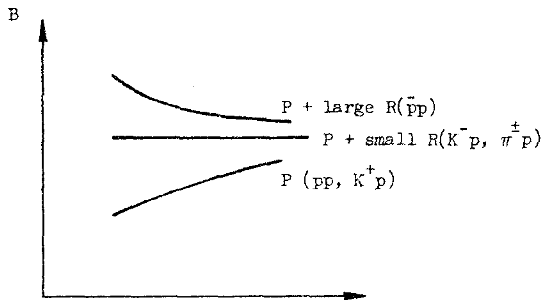

and are in good agreement with experimental data.

--questions and problems

Dips at $t \sim -0.6\ \text{GeV}^2$ in $\Delta\lambda = 1$ amplitudes are explained by zeroes of $J_1(R\sqrt{-t})$; at the same time the complete systematics of the dips requires some connection with wrong signature zeroes ($\alpha = 0$): in particular for even exchanges there is a delicate cancellation between J_1 and $\sin(\pi\alpha/2)$ where the J_1 zero is completely determined by the absorption radius R. In order for this effect to happen at every energy, α and R should have the same s dependence. Now experimentally α is pretty independent of s at least for ρ exchange for $-t < 1\ \text{GeV}^2$ and other exchanges at $t = 0$. It then follows that R should be more or less constant with s and it is hard to correlate this fact with the expanding radius of the shrinking Pomeron.

The peripherality picture receives also a warning from the new NAL data[39] on $\pi^-p \to \pi^0 n$, still showing a dip at approximately the same value $-t \sim 0.6\ \text{GeV}^2$. A flip amplitude

$$\text{Im}\ F_1(t) = Ae^{Bt}\ J_1(R\sqrt{-t})$$

corresponds in b space to:

$$\text{Im}\ \tilde{F}_1(b) = \frac{A}{2B}\exp\left(-\frac{(R^2+b^2)}{4B}\right) I_1\left(\frac{Rb}{2B}\right)$$

$$\simeq \frac{A}{2B}\sqrt{\frac{B}{\pi Rb}}\quad \exp\left(-\frac{(b-R)^2}{4B}\right)$$

for $b \gg 2B/R$.

If B shows shrinkage as in the $\pi^-p \to \pi^0 n$ data, the impact parameter distribution becomes wider and the peripheral character slowly disappears. In Fig. 65(a), Im $\tilde{\rho}_{+-}(b)$ is plotted from the exact formula and

$$B(s) = B_0 + \alpha' \ln s \qquad\qquad \alpha' \simeq 1\ \text{GeV}^{-2}$$

Since for a flip amplitude $\mathrm{Im}\,\tilde{F}_1(0)$ vanishes kinematically at $b = 0$, peripherality is maintained in an artificial way. If the same shrinkage occurs for a $\Delta\lambda = 0$ amplitude where no kinematic suppression operates at small b, peripherality is lost rather quickly (see Fig. 65(b)). It will be of crucial interest to check whether $\Delta\lambda = 0$ amplitudes show shrinkage properties.

Another possible problem is connected with even exchanges (f, A_2, K_T^*) which are predicted to be peripheral. There is no model-independent analyses of these amplitudes for $\Delta\lambda = 0$ and therefore it is very difficult to make any sensible statement; however there exist now some evidence from FESR analyses in KN and hypercharge exchange reactions indicating that tensor exchanges may be less peripheral than vector exchanges. It would be very important to confirm this experimentally by a direct test: this could be done for A_2 exchange by studying the differences

$$\Delta_A^K = \frac{d\sigma}{dt}(K^+p) + \frac{d\sigma}{dt}(K^-p) - \frac{d\sigma}{dt}(K^+n) - \frac{d\sigma}{dt}(K^-n)$$

$$\Delta_A^\gamma = \frac{d\sigma}{dt}(\gamma p \to \omega p) - \frac{d\sigma}{dt}(\gamma n \to \omega n)$$

It is remarkable that $I_t = 0$ exchange in πN scattering can be explained[82] by a peripheral f

$$\mathrm{Im}\, f_{++} = A_f\, e^{B_f t}\, J_0(R\sqrt{-t})$$

if the Pomeron amplitude shrinks. There is then a nice consistency between $\pi^\pm p$ and $K^\pm p$ elastic scattering, all being described with peripheral exchanges and a shrinking Pomeron at energies 3-20 GeV (Fig. 66). This harmonious situation is unfortunately shaken by data[83,84] on ϕ photoproduction where Pomeron exchange is expected to dominate in the t channel since non-strange exchanges do not couple strongly to ϕ: the data shows essentially no s dependence for $d\sigma/dt\,(\gamma p \to \phi p)$ at $-t = 0.6$ GeV^2. Even including some s dependence for $(d\sigma/dt)_{t=0}$ leaves little shrinkage

$$\alpha_P' \simeq 0.1 - 0.2 \text{ GeV}^{-2}$$

in the range 2 to 19 GeV. This is to be contrasted with Fig. 66 where in the same energy range $\alpha_P' \simeq 0.6$ GeV^{-2}. Regardless of the ϕ data, it is also possible that a slope $\alpha_P' \simeq 0.6$ GeV^{-2} leads to some inconsistencies in the dual absorptive model analyses since it corresponds to a sizeable real part of the Pomeron amplitude at larger t values-- ~ 50% of the imaginary part at $-t \sim 0.5$ GeV^2.

(b) Strong absorption models (Kane et al.[84]) --calculating $R \otimes P$ cuts

In these models the cut is calculated explicitly as a convolution integral over the pole amplitude and the Pomeron amplitude:

$$R_{abs}(s,t) = R_{pole}(s,t) + i\int dt'\,dt''\,K(t,t',t'')\,R_{pole}(s,t')\,P(s,t'')$$

where $R_{pole}(s,t)$ is a structureless amplitude, having no relationship to exchange degeneracy or duality and $K(t,t',t'')$ is a real positive function. All dips seen in differential cross sections are explained as absorption zeroes coming from the destructive interference between pole and cut.

In its early forms the model suffered from not representing correctly real parts. If P is an imaginary amplitude, both the real and imaginary parts of the pole term are equally strongly absorbed giving a $\sim J_1(R\sqrt{-t})$ behavior for both:

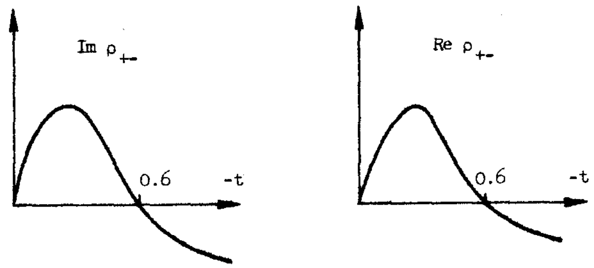

Such a form for Re ρ_{+-} is ruled out by polarization data on $\pi^{\pm}p$ so that a new version of the model was developed.

--<u>a new model</u>

Since the trouble seemed to come from the assumption of a purely imaginary Pomeron (believing the procedure to compute cuts) an easy cure is to allow for a Pomeron real part. This was originally motivated by the steepening forward differential cross section observed in pp scattering at the ISR: parametrizing the imaginary Pomeron amplitude with a dominant central part and a peripheral part with expanding radius

$$\text{Im } P = Ae^{Bt} + Ce^{Dt} J_0(R\sqrt{-t})$$

$$R \sim R_0 \sqrt{\ln s} = R_0 \sqrt{y}$$

one obtains via analyticity a real part proportional to the derivative of J_0

$$\text{Re } P \sim \frac{d}{dy} J_0(R\sqrt{-t}) \sim J_1(R\sqrt{-t})$$

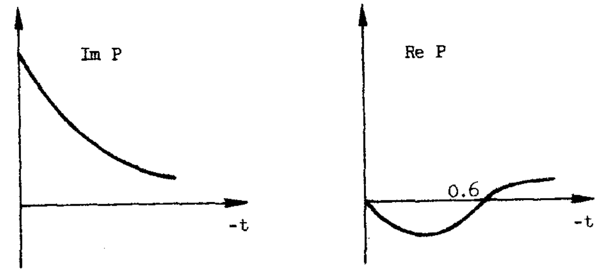

It is easy to understand how the real part of P changes the conclusions about real and imaginary absorbed amplitudes:

$$\text{Re } R_{abs} = \text{Re } P_{pole} - \text{Re } P_{pole} \otimes |\text{Im } P| + \text{Im } R_{pole} \otimes |\text{Re } P|$$

$$\text{Im } R_{abs} = \text{Im } R_{pole} - \text{Re } P_{pole} \otimes |\text{Re } P| - \text{Im } R_{pole} \otimes |\text{Im } P|$$

The result of absorption will now depend on the relative sign of Re P_{pole} and Im P_{pole}, leading to a qualitatively different conclusion for odd and even exchanges:

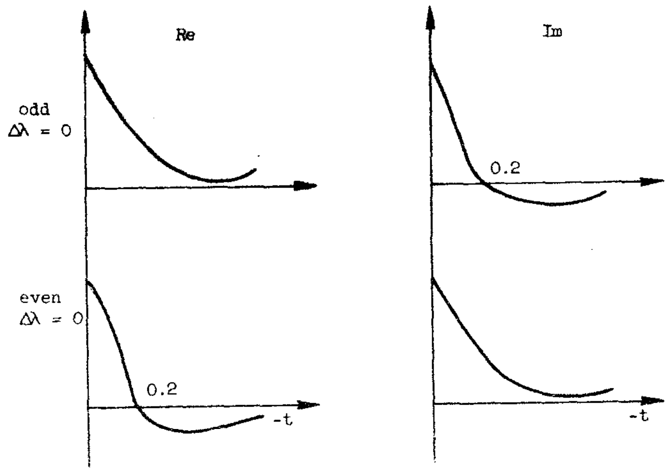

Therefore real parts of even exchanges and imaginary parts of odd exchanges are peripheral (first zero around 0.2 GeV^2) while imaginary parts of even exchanges and real parts of odd exchanges are rather central (with a broad minimum around 0.4 GeV^2).

Using these prescriptions, a zeroth order fit to the available data can be obtained with a few parameters, SU(3) symmetry and some assumptions of simplicity.

--problems

First of all duality is never satisfied at any level and would sadly appear as a mere accident. At the end the absorbed amplitudes have some kind of resemblance to exchange-degenerate amplitudes, but it is only approximate, at any rate worse than the data actually shows: for example $d\sigma/dt$ for $K^{\pm}p$ are not too different with K^+p showing a sizeable curvature which is not supported by the data.

The rise in K^+p total cross section (also pp) is explained by different energy dependences of f and ω amplitudes. Since Im ω is more peripheral than Im f, the model predicts that

$$\alpha^{\omega}_{eff}(0) > \alpha^{f}_{eff}(0)$$

The data from NAL and ISR indicate that P is a rising term as well and there seems to be little evidence for a large effect from f-ω energy dependence.

Since absorption has a larger effect in non-flip amplitudes, one expects in this model

$$\alpha^{eff}_{\Delta\lambda=0} > \alpha^{eff}_{\Delta\lambda=1}$$

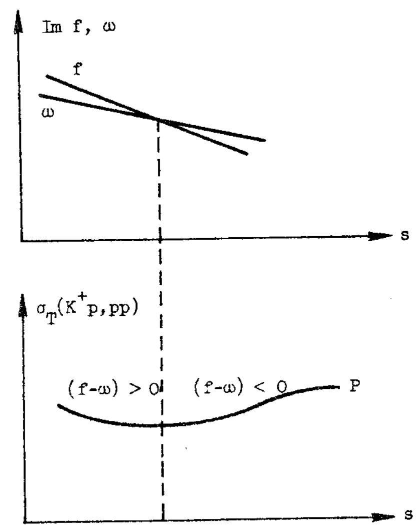

since

$$R_{abs} \sim R_{pole} - R_{cut}$$

$$\sim s^{\alpha}\left[1 - \frac{\lambda}{\ln s}\right]$$

$$\sim s^{\alpha+\epsilon}$$

$$(\epsilon > 0)$$

for a limited s range

where data on $\pi^- p \to \pi^0 n$ and $\Delta(\pi^{\pm}p)$ do not seem to indicate a significant effect. It is interesting to see that the cut term has a strong effect on the phase of the amplitude at $t = 0$: if

$$\mathrm{Im}\, R^- = As^{\alpha}\left[1 - \frac{\lambda}{\ln s}\right] = Ae^{\alpha y}\left[1 - \frac{\lambda}{y}\right]$$

$$\Longrightarrow \mathrm{Re}\, R^- \simeq Ae^{\alpha y}\tan\left(\frac{\pi\alpha}{2}\right)\left[1 - \frac{\lambda}{y} + \frac{\lambda}{\alpha y^2}\right]$$

$$\frac{\mathrm{Re}\, R^-}{\mathrm{Im}\, R^-} \simeq \tan\left(\frac{\pi\alpha}{2}\right)\left[1 + \frac{\lambda}{y(y-\lambda)\alpha}\right]$$

So that one expects a larger real part at low s from the pole term alone: while the data show a small effect in this direction (see Fig. 22) it seems too small considering the large size of the absorptive cut. It is instructive to notice that the phase of an amplitude, being related to derivatives of the modulus with respect to s, is a rather sensitive indicator of any change in the s dependence.

At a more fundamental level, the magnitude of Re P required to fit the data may be too large. In Chapter III we have seen that the real parts of $I_{t=0}$ $\pi^{\pm}p$ and γp elastic scattering were strongly s-dependent and probably related more to f exchange rather than Pomeron exchange. It does mean of course that f exchange should be not ignored in calculating cut diagrams but the whole problem has to be investigated separately--whether and how to compute $R \otimes R'$ cuts. We have seen that for exotic quantum numbers these amplitudes are rather small and this should be understood before engaging in a systematic program to include pole-pole cuts in two-body processes. The half-success of the strong absorption models seems to indicate the need for real part effects in rescattering and $R \otimes R'$ cuts are likely to play a role in them.

2. Speculations on the Pomeron

We have seen in many occasions that it is crucial to learn more about the Pomeron amplitudes at lower energies since it relates to the problems of understanding of elastic amplitudes, separation of f exchange, exchange degeneracy and absorption. Since experimentally the Pomeron is most accesible at very high energies, we shall try to start there and gather the relevant properties of Pomeron exchange.

(a) Pomeron from high-energy pp data (ISR)

We take the following points as clear experimental facts:[85]

- Im P(s, t = 0) is rising with s
- Re P(s, t = 0) is small, crossing zero and becoming positive
- Im P(s,t) is dominantly central, but has a distinct peripheral piece ($\sim J_0$ may be a good parameterization)
- Im $P_{central}(s,t)$ changes very slowly with s (α' small)
- Im $P_{peripheral}(s,t)$ is growing

The stronger shrinkage seen at small t can be induced by any of 3 effects or a mixture of them:

- the growth at $t = 0$
- the shrinkage of the peripheral part
- an expanding radius R in $J_0(R\sqrt{-t})$

Since the first effect we mention is already clearly observed in the data, it is interesting to see if, by itself, one can achieve a good description of pp elastic scattering with other parameters only slowly varying. In this simple model we write

$$\text{Im } P(s,t) = Ae^{Bt} + C(s)\, e^{Dt}\, J_0(R\sqrt{-t})$$

with A, B, D and R are slowly changing with s and the main s dependence comes from $C(s)$, growing with s.

Analyticity requires that

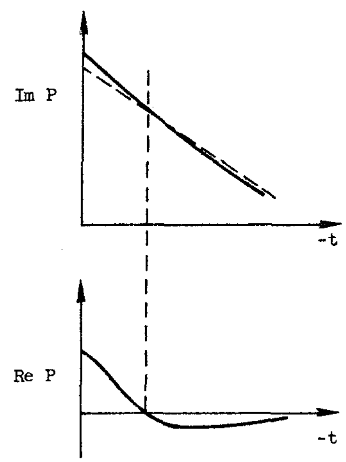

$$\text{Re } P = \tan\left(\frac{\pi}{2}\frac{d}{dy}\right) \text{Im } P$$

$$\simeq \frac{dC}{dy}\, e^{Dt}\, J_0(R\sqrt{-t})$$

with $dC/dy > 0$.

If $C = C_0 y$, then Re P is essentially s-independent while Im P grows like ln s.

An excellent fit to the available ISR data yields

$$B = 4.4\ \mathrm{GeV}^{-2}$$
$$D = 4.7\ \mathrm{GeV}^{-2}$$
$$R = 4.7\ \mathrm{GeV}^{-2} \sim 1\ f$$

showing a rather broad peripheral distribution in b space. Let us note at this point that our picture is quite orthogonal to Kane's[84] where the main s dependence comes from the s dependence of R in the J_0 argument.

At lower energies we expect real parts from Regge exchange to contribute since, although Im R is not very large, Re P can be quite substantial--as seen in Chapter IV.

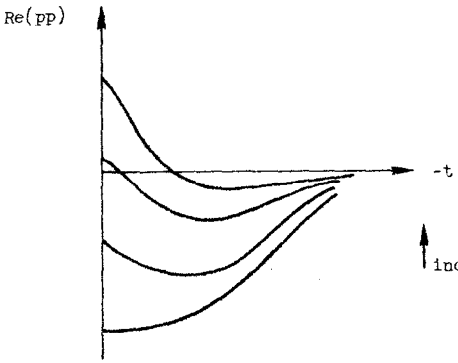

We expect the same qualitative behaviour for meson scattering with R scaled geometrically with $\sim\sqrt{\sigma_T}$ and the peripheral piece will lead to some curvature in $d\sigma/dt$ at high energy.

(b) Can we extract Im P(s,0) at lower s?

We can isolate the combination (P + f) in πN, KN and NN elastic scattering. How to eliminate f exchange? Let us recall the following properties of exchange amplitudes:

-ρ, ω and A_2 exchange is power-behaved at $t = 0$ and probably the same will hold for f exchange.

-within the experimental uncertainty it appears that $\alpha(0)$ for a given exchange is independent of the process; for example, $\alpha_\rho^\pi(0) \sim \alpha_\rho^K(0) \sim \alpha_\rho^P(0)$.

-SU(3) symmetry is approximately true for residues at the 20% level (ρ_π/ρ_K for example).

Guided by these facts we shall assume that the f amplitude has similar properties at $t = 0$:

- $\mathrm{Im}\ f = f s^{\alpha_f - 1}$
- $\alpha_\pi^f = \alpha_f^K\ (= \alpha_f^N)$
- $2f_K = f_\pi$ as given by SU(3).

It is then possible to use cross sections data on $\pi^\pm p$, $K^\pm p$ and $K^\pm n$ to eliminate the f amplitude and obtain a "Pomeron" amplitude. The relation is

$$\frac{1}{2}\,[\Sigma(Kp) + \Sigma(Kn) - \Sigma(\pi p)] = 2P_K - P_\pi$$

and is evaluated using total cross section data in Fig. 67. Since we do not a priori expect a marked difference between the s dependence of P_K and P_π, it is fair to assume that we are seeing in Fig. 67 the s dependence of either P_K or P_π: data shows a rising Pomeron contribution from a momentum of 3 GeV up. Thus the asymptotic behaviour seen at the ISR for pp scattering and also for K^+p scattering at lower energies ($\gtrsim$ 20 GeV) seems to persist to quite low energies, once Regge terms have been removed.

Before going further we must check the stability of our result against the most crucial assumption of an SU(3)-symmetric f coupling to pseudoscalar mesons. From the branching ratio

$$\frac{\Gamma(f \to K\bar{K})}{\Gamma(f \to \pi\pi)} = .025 \pm .01$$

obtained from an analysis[86] including a proper treatment of f-A_2 interference in the $K\bar{K}$ channel, we obtain

$$\frac{2f_K}{f_\pi} = .94 \pm .2$$

in good agreement with SU(3). Since this last result is only accurate to $\pm$ 20%, it is important to see the effect of such variations on the s dependence of the Pomeron amplitude. This is studied in Fig. 68 where the quantity

$$\frac{1}{2}\left[\Sigma(Kp) + \Sigma(Kn) - \left(\frac{2f_K}{f_\pi}\right)\Sigma(\pi p)\right]$$

is evaluated for different values of $2f_K/f_\pi = 1 \pm .2$. Within this range of values, our result stands that the Pomeron amplitude is rising with s, the rise being more linear in $\ln s$ for the values of the ratio closest to symmetry.

More quantitatively there is internal consistency between a linear $\ln s$ growth of the Pomeron term and the ratio f_K/f_π given by SU(3). Parametrizing cross sections as

$$\frac{1}{2}\Sigma(\pi p) = P^0_\pi + P'_\pi y + f_\pi e^{(\alpha_f - 1)y}$$

$$\frac{1}{2}\Sigma(KN) = P^0_K + P'_K y + f_K e^{(\alpha_f - 1)y}$$

yields reasonable values for the parameters:

$$P_\pi = (14.2 \pm 2.5) + (1.4 \pm .3)y$$

$$P_K = (11.5 \pm 1.4) + (1.34 \pm .2)y$$

$$\left.\begin{array}{l} f_\pi = 39.4 \pm 1.1 \\ f_K = 21.6 \pm 7 \end{array}\right\} \quad \frac{2f_K}{f_\pi} = 1.10 \pm .05$$

$$\alpha_f = .44 \pm .07$$

to be compared to

$$\omega_K = 13.0 \pm 2.6$$

$$\alpha_\omega \sim 0.41$$

The fact that $P_\pi \neq P_K$ indicate that Pomeron exchange is not a pure SU(3) singlet[87] in agreement with vector meson photoproduction:

$$\left[\frac{\frac{d\sigma}{dt}(\gamma p \to \phi p)}{\frac{d\sigma}{dt}(\gamma p \to \rho^0 p)}\right]_{t=0} \sim \frac{f^2_{\gamma\phi}}{f^2_{\gamma\rho}}\left(\frac{\sigma_T(\phi p)}{\sigma_T(\rho p)}\right)^2 \sim \frac{1}{60}$$

leading to $\sigma_T(\phi p) \sim 10$ mb around 10 GeV. Experimentally $\sigma_T(\phi N)$ has been directly measured by nuclear absorption to be 12 mb at 6 GeV[88] showing a large reduction compared to $\sigma_T(\rho N) \simeq \sigma_T(\pi N)$. Assuming the SU(3) breaking occurs through octet exchange

$$P = P_1 \cos\alpha + P_8 \sin\alpha$$

measured by a mixing angle α, we can evaluate the Pomeron contribution to forward elastic amplitudes:

$$\left.\begin{array}{l} P_\pi = \left(\cos\alpha + \frac{1}{\sqrt{2}}\sin\alpha\right)P_0 \\ P_K = \left(\cos\alpha - \frac{1}{2\sqrt{2}}\sin\alpha\right)P_0 \end{array}\right\} \quad \text{pseudoscalar nonet}$$

$$\left.\begin{array}{l} P_\rho = P_\omega = \left(\cos\alpha + \frac{1}{\sqrt{2}}\sin\alpha\right)P_1 \\ P_\phi = (\cos\alpha - \sqrt{2}\sin\alpha)P_1 \end{array}\right\} \quad \text{vector nonet}$$

where we have used the canonical ω-ϕ mixing angle. Since $\sigma_T(\rho N) \sim \sigma_T(\pi N)$ we know that $P_0 \sim P_1$ and consequently

$$\sigma_T(\phi N) \sim \frac{1}{2}[\Sigma(Kp) + \Sigma(Kn) - \Sigma(\pi p)]$$
$$\sim 2P_K - P_\pi$$

This serves as an independent check of the f_K/f_π ratio since values for $\sigma_T(\phi N)$ in agreement with data occur for the SU(3) ratio (Fig. 68). We therefore expect $\sigma_T(\phi N)$ to show a linear rise with $\ln s$ from as low a momentum as 3 GeV and up: this can be experimentally checked by studying the s dependence of $(d\sigma/dt)_{t=0}$ $(\gamma p \to \phi p)$ and would be clear-cut confirmation of the Pomeron behaviour at low energies.

(c) Application to $\gamma p \to \phi p$

ϕ photoproduction is dominated by Pomeron exchange and the study of the t distribution of this process should have some similarities with pp elastic scattering as seen at the ISR. Let us parametrize the ϕ photoproduction amplitude in the same way

$$F \sim \text{Im } P = Ae^{Bt} + C(s)\, e^{Dt}\, J_0(R\sqrt{-t})$$

where

-- B, R and D are scaled geometrically from pp scattering leading to $R \sim 3.5$ GeV^{-1} (less peripheral than pp)

-- $C(s)$ is given by $2\sigma_T(KN) - \sigma_T(\pi p)$

In Fig. 69, the above parameter-free description (except for overall s independent scale approximately given by vector dominance and $f^2_{\gamma\phi}$ from e^+e^- colliding beam data) is compared favorably with the data on $\gamma p \to \phi p$ from 2 to 12 GeV. There is shrinkage at small $-t \lesssim 0.3$ GeV^{-2} while the large t cross section is dominated by the central part and is quite independent of s (Fig. 70) in agreement with experiment. In Fig. 71 we show the different amplitudes making up the full Pomeron contribution at 12 GeV.

It is clear that the effects are not very large and that we need new accurate experiments measuring forward ϕ photoproduction down to $t = 0$ and concentrating on the careful study of s dependence. At an easier level it should be verified that the integrated cross section is a growing function of s.

(d) Implications for exchange degeneracy

--$t = 0$

A Pomeron s dependence of the form $A + B \ln s$ implies a breaking of exchange degeneracy since $\sigma_T(K^+p)$ and $\sigma_T(pp)$ show some extra contributions at lower energies. At $s \sim 10$ GeV^2 we have approximately

$$\text{Im } R(K^-p) \simeq \text{Im}(f + \omega) \sim 10 \text{ mb}$$

$$\text{Im } R(K^+p) \simeq \text{Im}(f - \omega) - 1 - 2 \text{ mb}$$

indicating a small violation $\lesssim 20\%$ of exchange degeneracy. If the breaking comes from absorption effects, then the f cut is weaker than the ω cut, as expected from the new strong absorption model (see Section 1(b) of this chapter); but breaking could also come from the pole terms, since the respective values for $\alpha(0)$ are not too different where a strong absorption difference would have an important effect.

--$t \neq 0$

If exchange degeneracy is broken in K^+p and pp elastic scattering, $\text{Im}(f - \omega)$ is going to contribute to the shape of $d\sigma/dt$ since it interferes with the dominant Pomeron amplitude;

-if $\text{Im } f_{++}$ and $\text{Im } \omega_{++}$ have zeroes at the same t value (~ -0.2 GeV^2), then $d\sigma/dt$ (K^+p) will be of the form $P^2 + 2P.$"J_0" with a "J_0" term about 5 times smaller than in K^-p. Since the P term is essentially non-shrinking for $-t > 0.2$-0.3 GeV^2 the effect of the "J_0"

produces a slight anti-shrinking, at variance with the trend of experimental data showing a pronounced shrinkage.

-if $\mathrm{Im}\, f_{++}$ and $\mathrm{Im}\, \omega_{++}$ have different zeroes the shape of $\mathrm{Im}(f-\omega)_{++}$ will depend on the separation between their zeroes.

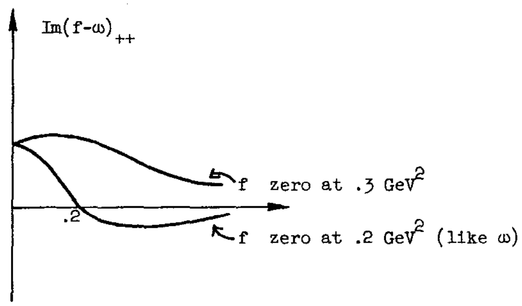

Even for slightly displaced zeroes (0.2 and 0.3 GeV^2), $\mathrm{Im}(f-\omega)_{++}$ can be very different from a J_0 shape, leading to a much flatter amplitude. This results in an apparent shrinking of the K^+p differential cross section since this rather flat amplitude is decreasing with energy:

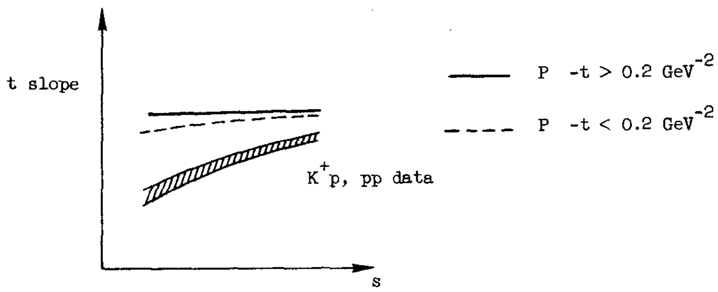

It is interesting to notice that such a small change in the first zero has important consequences for the peripherality of the amplitude: if $\mathrm{Im}\, f_{++} = 0$ at $-t \sim 0.3\ \mathrm{GeV}^2$ it means that $\langle R \rangle \sim 0.5$ f rather than $\langle R \rangle \sim 1$ f for $\mathrm{Im}\, \omega_{++}$ and that $\mathrm{Im}\, f_{++}$ is qualitatively central in agreement with strong absorption with important real parts, a convincing mechanism for which being still lacking.

It thus seems that our picture of a mostly central Pomeron with very slow energy dependence with a growing peripheral (but wide) part leads to a consistent description of elastic processes and vector meson photoproduction. Small breaking of exchange degeneracy follows and has significant effects on the slopes of the differential cross sections; the breaking of exchange degeneracy is strong enough to allow the imaginary part f exchange to become significantly central. To verify these conclusions it is important to carry out accurate measurements of $\gamma p \to \phi p$, and also have some model-independent look at the even exchanges such as in hypercharge exchange reactions and may be $\gamma p \to \omega p$ and $\gamma n \to \omega n$.

OUTLOOK

There has been a qualitative change in understanding two-body reactions when experiments have been geared to extract individual amplitudes instead of just bi-linear products such as cross sections. Information gathered so far is very limited and new experiments should expand our knowledge considerably. Major areas are:

1) energy dependence of πN amplitudes
2) getting closer to KN, $\bar{K}N$ complete amplitude separation
3) measuring even-crossing amplitudes through $K^{\pm}d$, $\gamma N \to \omega N$ and hypercharge exchange reactions
4) production of resonances observing their correlated decays; mostly for lower spins
5) accurate elastic scattering and polarization measurements at high energy (up to ~ 100 GeV) to determine the energy dependence of a few important amplitudes
6) improving experimental knowledge of the Pomeron amplitude at lower energies, mostly through detailed measurements of $\gamma p \to \phi p$
7) determine the importance of non-exotic Regge $\otimes$ Regge cuts through accurate comparison of processes sensitive to interferences.

We also need to develop methods to incorporate the constraints of analyticity into amplitude analyses: while the derivative analyticity relations look promising, one has to understand their limitations more fully. It is possible that a clever use of analyticity will relieve some of the burden of carrying out complete experiments--a task out of sight in most cases.

When unambiguous experimental measurements of even amplitudes are done it will become essential to understand absorption effects, the structure of Pomeron amplitudes and the importance of Regge cuts.

The present picture of a high energy amplitude is aesthetically not particularly pleasing; for example SU(3) symmetry and concepts like exchange degeneracy are only appproximately verified by experiment to about 20%. However we feel that much will be learnt when the breaking mechanisms are understood and then, may be, a simpler picture will emerge.

Bibliography

1. M. Jacob and G. Wick, Annals of Phys. 7, 404 (1959).
2. G. Cohen-Tannoudji et al., Nuovo Cimento 48A, 1077 (1967).
3. G. Cohen-Tannoudji et al., Nuovo Cimento 55A, 412 (1968).
4. J. Werle, Relativistic Theory of Reactions, North Holland (1966), p. 264.
5. I. Ambats et al., ANL/HEP 7329 (1973).
6. A. Stirling et al., Phys. Rev. Lett. 14, 763 (1965).
7. P. Sonderegger et al., Phys. Lett. 20, 75 (1966).
8. M. Whalig and I. Mannelli, Phys. Rev. 168, 1515 (1968).
9. M. Borghini et al., Phys. Lett. 31B, 405 (1970).
10. P. Bonamy et al., Nucl. Phys. B52, 392 (1973).
11. D. Hill et al., Phys. Rev. Lett. 30, 239 (1973).
12. A. DeLesquen et al., Phys. Lett. 40B, 277 (1972).
13. F. Halzen and C. Michael, Phys. Lett. 36B, 367 (1971).
14. R. Kelly, Phys. Lett. 39B, 635 (1972).
15. G. Cozzika et al., Phys. Lett. 40B, 281 (1972).
16. P. Johnson et al., Phys. Rev. Lett. 30, 242 (1973).
17. L. Van Rossum, Proceedings of the 1973 KEK Summer School, KEK 73-10.
18. D. Yovanovitch et al., contribution to the XVI International Conference on High Energy Physics, Chicago (1972).
19. W. Beusch et al., CERN preprint (1974).
20. CERN-ETH-Helsinki-London collaboration (5 GeV/c).
21. A. Kotanski, Proceedings of the 1970 Herceg-Novi School.
22. A.D. Martin, Proceedings of the 1972 Rencontre de Moriond.
23. J.P. Ader et al., CERN preprint TH 1768 (1973).
24. See for example, D.J. Sherden et al., Phys. Rev. Lett. 30, 1230 (1973).
25. J. Ballam et al., Phys. Rev. Lett. 24, 960 (1970).
26. CERN-Munich group; R. Cashmore, private communication.
27. M.G. Doncel et al., CERN/D.Ph.II/Phys 74-7 (1974).
28. R.C. Fernow et al., University of Michigan preprint UMHE 74-21 (1974).
29. F. Halzen and G.H. Thomas, ANL/HEP 7402 (1974).
30. G.L. Kane and U.P. Sukhatme, UMHE 73-30 (1974).
31. W. Galbraith et al., Phys. Rev. 138B, 913 (1965).
32. K. Foley et al., Phys. Rev. Lett. 19, 330 (1967).
33. S. Denisov et al., Phys. Lett. 36B, 415 and 528 (1971).
34. S. Denisov et al., Nucl. Phys. B65, 1 (1973).
35. A.S. Carroll et al., Phys. Rev. Lett. 33, 932 (1974).
36. V.N. Bolotov et al., IHEP 73-52 (1973).
37. V.N. Bolotov et al., IHEP 73-57 (1973).
38. U. Amaldi, Rapporteur's talk, Proceedings of the International Conference on Elementary Particles, Aix-en-Provence (1973).
39. R. Walker, these proceedings.
40. V. Barger et al., preprint (1973).
41. R. Diebold, Proceedings of the International Conference on Elementary Particles, Aix-en-Provence (1973).
42. R.C. Carnegie, these proceedings.
43. A. Eide et al., Nucl. Phys. B60, 173 (1973).
44. C. Akerlof et al., Phys. Rev. Lett. 33, 119 (1974).
45. A. Boyarski et al., Phys. Rev. Lett. 25, 695 (1970).
46. C. Baglin et al., to be published; F. Richard, private communication.
47. C. Berger, Phys. Rev. Lett. 23, 1139 (1969).
48. D. Ayres et al., Phys. Rev. Lett. 32, 1463 (1974).
49. I. Ambats et al., ANL/HEP 7367 (1973).
50. K. Foley et al., Phys. Rev. Lett. 19, 193 and 622 (1967).
51. P. Baillon et al., Phys. Lett. 50B, 387 (1974).
52. P. Baillon et al., Phys. Lett. 50B, 377 (1974).
53. V.K. Birulev et al., Phys. Lett. 38B, 452 (1972).
54. S. Kramer et al., Phys. Rev. Lett. 33, 505 (1974).

55. P. Estabrooks et al., CERN preprint (June 1974).

56. M. Davier and H. Harari, Phys. Lett. 35B, 239 (1971).

57. E. Pietarinen, Nucl. Phys., B49, 315 (1972).

58. H. Hecht et al., CERN preprint TH-1722 (1973).

59. G. Höhler and H. Jakob, Karlsruhe preprint TKP 13/73 (1973).

60. J. Bronzan et al., Phys. Lett. 49B, 272 (1974).

61. F. Zachariasen, Physics Reports, 1 (1971).

62. U. Sukhatme et al., to be published.

63. A.D. Brody et al., Phys. Rev. Lett. 26, 1050 (1971).

64. G. Buschorn, et al., Phys. Lett. 37B, 207 (1971).

65. R.L. Anderson et al., Phys. Rev. Lett. 25, 1218 (1970).

66. A. Boyarski et al., Phys. Rev. Lett. 26, 1600 (1971).

67. K. Igi and S. Matsuda, Phys. Rev. Lett. 18, 625 (1967).
A. Logunov et al., Phys. Lett. 24, 181 (1967).

68. R. Dolen et al., Phys. Rev. 166, 1768 (1968).

69. F. Elvekjaer and B. Martin, CERN preprint TH 1806 (1974).

70. H. Harari, Phys. Rev. Lett. 20, 1395 (1968).

71. P. Freund, Phys. Rev. Lett. 20, 235 (1968).

72. H. Harari and Y. Zarmi, Phys. Rev. 187, 2230 (1969).

73. C. Michael, CERN preprint TH-1627 (1973).

74. H. Harari, Phys. Rev. Lett. 22, 562 (1969).

75. J. Rosner, Phys. Rev. Lett. 22, 689 (1969).

76. C. Bricman et al., CERN preprint (1970).

77. M. Fukugita and T. Inami, Nucl. Phys. B44, 490 (1972).

78. M. Ross et al., Nucl. Phys. B23, 269 (1970).

79. M. Harari, Annals of Physics 63, 432 (1971).

80. M. Fukugita et al., Rutherford preprint RPP/T/32 (1972).

81. H. Harari, Phys. Rev. Lett. 26, 1400 (1971) and Ref. 79.

82. M. Davier, Phys. Lett. 40B, 369 (1972).

83. R.L. Anderson et al., Phys. Rev. Lett. 30, 149 (1973).

84. G. Kane, Phys. Lett. 40B, 363 (1972).

85. D. Leith, these proceedings.

86. A. Irving and C. Michael, CERN preprint TH-1825 (1974).

87. M. Davier, Phys. Rev. Lett. 20, 952 (1968).

88. H. Alvensleben et al., Phys. Rev. Lett. 27, 444 (1971) and references therein.

89. G. Grayer et al., Proceedings of the 3rd International Conference on Experimental Meson Spectroscopy, Philadelphia (1972) and CERN preprint (1973).

90. R.L. Anderson et al., SLAC-Pub 925 (1971).

91. Abrams et al., BNL 14046 preprint (1969).

92. W. Michael and G. Gidal, LBL-744 preprint (1972).

93. B. Haber et al., Contribution to the 1973 APS Meeting, Berkeley

94. D. Crennel et al., Phys. Rev. Lett. 27, 1674 (1971).

95. W.T. Kaune et al., SLAC-Pub 1079 (1972).

96. R. Carnegie, et al., to be published.

97. Y. Antipov et al., IFVE 74-99 (1974).

98. C. Akerlof et al., UMHE 74-20 (1974).

99. W.T. Meyer et al., Contribution to the 1973 APS Meeting, Berkeley.

100. R. Diebold et al., Phys. Rev. Lett. 32, 904 (1974).

101. G. Ferro Fontan, CERN preprint TH 1490 (1972).

Table Captions

Table 1. Number of independent helicity amplitudes for typical processes.

Table 2. Observables and measured quantities for reaction types with and without a polarized target.

Table 3. Energy dependence of forward t-channel amplitudes from total cross section data with a parametrization $\beta s^{1-\alpha}$.

Table 4. Energy dependence of forward differential cross sections parametrized with $s^{2\alpha-2}$.

Table 5. Dominant helicity couplings of mesons to baryon-antibaryon as deduced from experimental data.

Table 6. SU(3) symmetry for $VB\bar{B}$ vertices and helicity couplings.

Figure Captions

Figure 1. Recoil baryon polarization in $0^- \frac{1}{2}^+ \to 0^- \frac{1}{2}^+$ scattering with a polarized target.

Figure 2. $I_t = 0$ πN amplitudes at 6 GeV/c from Ref. 5.

Figure 3. $I_t = 0$ πN amplitudes at 6 GeV/c from Ref. 5.

Figure 4. Naturality amplitudes in $\pi N \to \rho N$ at 17.2 GeV/c from Ref. 86, using data from Ref. 89.

Figure 5. Separation of naturality in $\gamma p \to \pi^0 p$ using linearly polarized photons (Ref. 90).

Figure 6. pp elastic scattering at 6 GeV with measurements of 2 or 3 spins (Ref. 28).

Figure 7. Differences of total cross sections between $K^\pm d$ and $p^\pm d$ using data from Refs. 31, 33, 34, 35 and 91.

Figure 8. s dependence of $\frac{d\sigma}{dt}(\pi^- p \to \pi^0 n)$ at fixed t values (Ref. 36).

Figure 9. ρ Regge trajectory from data on $\frac{d\sigma}{dt}(\pi^- p \to \pi^0 n)$ (Ref. 36).

Figure 10. Separation of $I_t = 0$ exchange in $\pi N \to \rho N$; data from Refs. 92, 93, 94 and 94.

Figure 11. Location of dip for nucleon exchange in $\pi^+ p \to p \pi^+$ and $\bar{p}p \to \pi^- \pi^-$ from Ref. 40.

Figure 12. Differential cross sections for $\pi^- p \to \rho^0 n$ with well-defined naturality in the t channel at 6 and 17.2 GeV/c (Ref. 41).

Figure 13. s dependence of the differential cross-sections for $\bar{p}p \to \pi\pi$ at fixed t (u); data from Ref. 43.

Figure 14. Differential cross sections for backward πN scattering around 6 GeV/c (from Ref. 101).

Figure 15. Cross sections for exotic quantum number exchange in $\pi^- p \to K^+\Sigma^-$ and $K^- p \to \pi^+\Sigma^-$ (Ref. 44).

Figure 16. s dependence of the differential cross section for $\bar{p}p \to K^- K^+$ at fixed t (u); data from Ref. 43.

Figure 17. s dependence of backward $K^\pm p$ differential cross sections (u = 0) from Ref. 43.

Figure 18. Complete angular distribution for $K^\pm p$ elastic scattering at 5 GeV (Ref. 43) and "exotic" $K^- p$ backward peak.

Figure 19. Complete angular distribution for $\bar{p}p$ elastic scattering at 5 GeV (Ref. 43) and "exotic" backward peak.

Figure 20. Energy dependence of the cross section for $\pi^- p \to \phi n$ (Ref. 48).

Figure 21. Test of SU(3) symmetry for amplitudes dominantly helicity flip (from Ref. 49).

Figure 22. Ratio of real to imaginary parts in $\pi^- p \to \pi^0 n$ at $t = 0$ as a function of beam momentum (Ref. 36).

Figure 23. Differential cross sections at $t = 0$ for $K^+ p \to K^0 n$ and $K^- p \to \bar{K}^0 n$ and contributions of the imaginary parts obtained from total cross section data.

Figure 24. ρ - ω interference in the $\pi^+\pi^-$ mass spectrum for $\pi^- p \to \pi^+\pi^- n$ (σ^-) and $\pi^+ n \to \pi^-\pi^+ p$ (σ^+); data from Ref. 54.

Figure 25. Phase differences between ρ and ω production amplitudes in $\pi N \to (\rho,\omega)N$, for different t-channel exchanges (Ref. 54).

Figure 26. Odd-crossing helicity non-flip amplitude parallel to Pomeron exchange ($\sim \mathrm{Im}\,\omega^K_{++}$) in $K^\pm p$ elastic scattering at 5 GeV (Ref. 56).

Figure 27. Impact parameter distribution of amplitude shown in Fig. 26.

Figure 28. Impact parameter profiles in $K^\pm p$ elastic scattering at 5 GeV (Ref. 56).

Figure 29. Differential cross-sections for particle and antiparticle elastic scattering at 5 GeV/c from Ref. 5.

Figure 30. Difference $\Delta(s,t)$ as defined in the text for $\pi^\pm p$, $K^\pm p$ and $p^\pm p$ elastic scattering at 3, 3.65, 5 and 6 GeV/c (Ref. 5).

Figure 31. $(F^1_{++})_\parallel$ amplitude obtained from cross-over data only and compared to result of complete amplitude analysis; data from $\pi^\pm p$ at 6 GeV (Ref. 5).

Figure 32. Difference between exponential slopes in $K^\pm p$ elastic scattering as a function of beam momentum; data from Refs. 5, 96, 97 and 98.

Figure 33. Difference of $\pi^\pm p$ polarizations at 10 GeV as a function of t (Ref. 9).

Figure 34. $(F^1_{+-})_\perp$ and $(F^0_{+-})_\perp$ obtained from polarization and cross section data only and comparison to results of full amplitude analysis.

Figure 35. Sum of $\pi^\pm p$ polarizations at 10 GeV (Ref. 9).

Figure 36. Sum and difference of $K^\pm p$ polarizations at 10 GeV (Ref. 9).

Figure 37. Sum and difference of $K^\pm p$ polarizations at 14 GeV (Ref. 9).

Figure 38. Even-crossing non-flip amplitudes in πN elastic scattering at 10 GeV; real and imaginary parts are separated using analyticity through dispersion relations (from Ref. 58).

Figure 39. Phases of F^0_{++} and F^1_{+-} in πN elastic scattering at 6 GeV (from Ref. 58).

Figure 40. Predicted πN charge-exchange polarization from Ref. 58.

Figure 41. Real and imaginary parts of elastic processes at $t = 0$ using derivative analyticity relations (Ref. 60).

Figure 42. Derivative analyticity relations: difference of 2 Regge poles reconstructed with first derivative only. The solid curve is the input amplitude while the dashed curve represents the reconstructed amplitude. (a) real part (b) imaginary part as a function of s (Ref. 62).

Figure 43. Same as Figure 42 for an absorbed amplitude, as a function of t.

Figure 44. Phase of $K^0_L p \to K^0_S p$ at $t = 0$. Hatched area is the result of derivative relations; data from Refs. 63 and 53.

Figure 45. Real parts of helicity non-flip amplitude in $\gamma p \to \gamma p$ scattering at 4 and 10 GeV using derivative analyticity relations and data from Refs. 64 and 65.

Figure 46. Real and imaginary parts of helcity in non-flip amplitude in $\gamma p \to \gamma p$ at 10 GeV.

Figure 47. Im A' for πN charge exchange at $t = 0$ from Ref. 68.

Figure 48. $\mathrm{Im}(\rho \pm A_2)_{++}$ from $\sigma_T(K^{\pm}N)$ data (Ref. 91).

Figure 49. πN phase shifts projected on t-channel $I_t = 0, 1$ exchanges (Ref. 72).

Figure 50. Meson spectrum and exchange degeneracy of Regge trajectories.

Figure 51. ρ and A_2 trajectories in the scattering region (Refs. 36 and 37).

Figure 52. Test of exchange degeneracy in $K^- p \to \bar{K}^0 n$ and $K^+ n \to K^0 p$ (Ref. 100).

Figure 53. Test of exchange degeneracy in $K^+ p \to K^0 \Delta^{++}$ and $K^- n \to \bar{K}^0 \Delta^-$ (Ref. 99).

Figure 54. Test of exchange degeneracy (dips) and SU(3) for processes dominated by helicity flip amplitudes.

Figure 55. Test of local duality in backward $K^- p \to \bar{K}^0 n$ scattering (Ref. 76).

Figure 56. Helicity amplitudes reconstructed from the background in $\bar{K}N$ phase shifts (Ref. 77).

Figure 57. Helicity amplitudes reconstructed from resonances in $\bar{K}N$ low energy scattering (Ref. 77).

Figure 58. Chew-Frautschi plot for N^* resonances; the number inside the circles is equal to 10 times the elasticity of each resonance.

Figure 59. Chew-Frautschi plot for Y^* resonances and peripheral curve (Ref. 80).

Figure 60. First zeroes in the decay angular distribution of Y^* resonances as contributed to helicity flip and non-flip amplitudes.

Figure 61. Impact parameter profile for the imaginary part of the helicity non-flip amplitude reconstructed from the background in $\bar{K}N$ low energy phase-shifts; the 3 plots correspond to analyses in different energy regions (Ref. 80).

Figure 62. Same as Fig. 61 for the resonant part of $\bar{K}N$ scattering.

Figure 63. Same as Fig. 61 for the sum of background and resonances in πN scattering at low energy.

Figure 64. Zeroes of helicity amplitudes in $\bar{K}N$ low energy scattering (Ref. 77).

Figure 65. (a) Impact parameter profile of $\text{Im}\,F_{+-}$ from $\pi^- p \to \pi^0 n$ using experimental shrinkage; (b) same distribution for $\text{Im}\,F_{++}$ assuming similar shrinkage and constant zero location.

Figure 66. Slope of Pomeron amplitude from a dual absorptive model analysis of πN elastic scattering (Ref. 82); the hatched region corresponds to the slope of $K^+ p$ elastic scattering.

Figure 67. Total cross sections and s dependence of Pomeron amplitude.

Figure 68. Dependence of Pomeron amplitude on the ratio $2f_K/f_\pi$.

Figure 69. Differential cross section for $\gamma p \to \phi p$ between 2 and 12 GeV.

Figure 70. s dependence of $\frac{d\sigma}{dt}(\gamma p \to \phi p)$ at fixed t.

Figure 71. Central and peripheral Pomeron amplitudes in $\gamma p \to \phi p$ at 12 GeV.

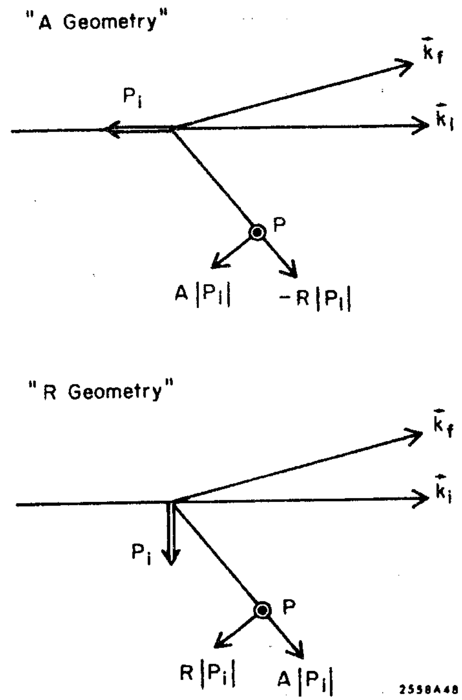

Figure 1

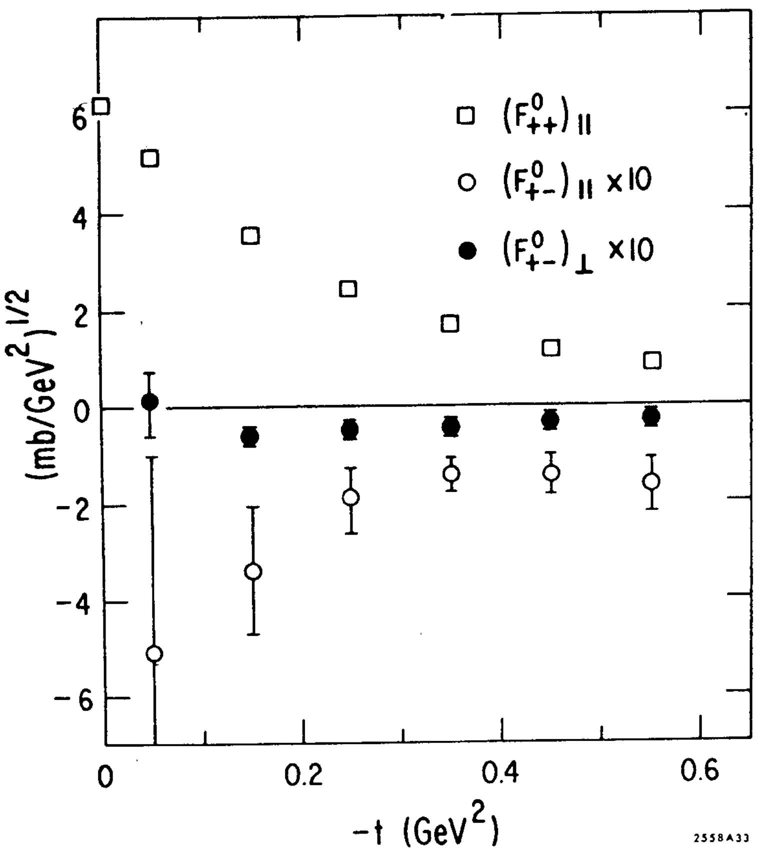

Figure 2

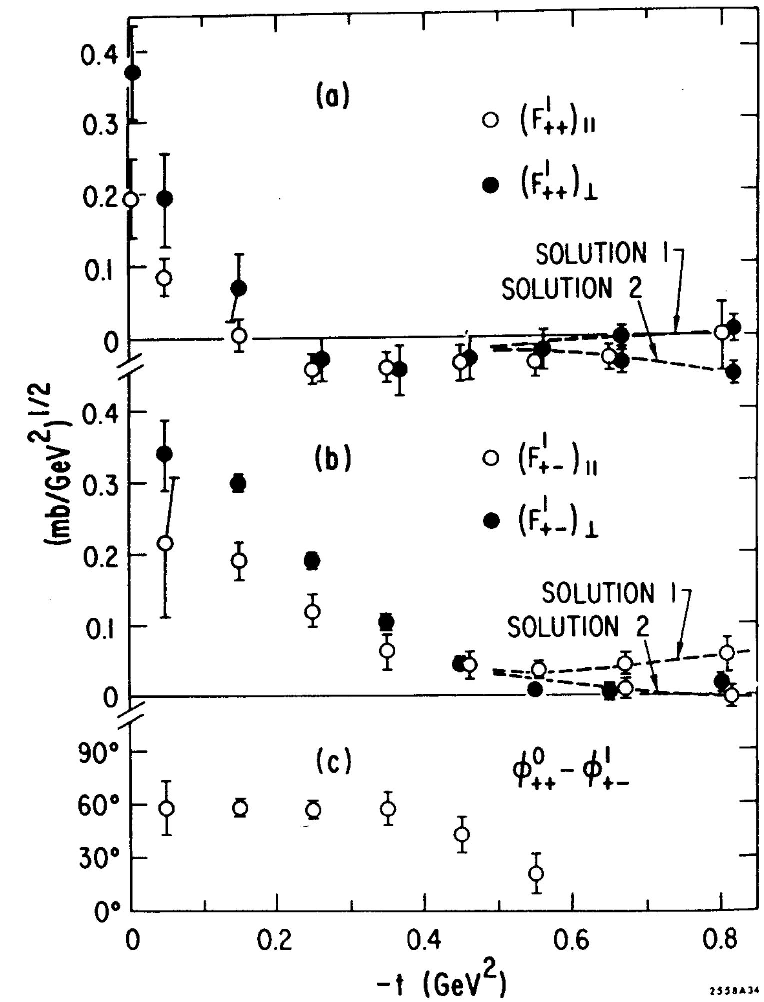

Figure 3

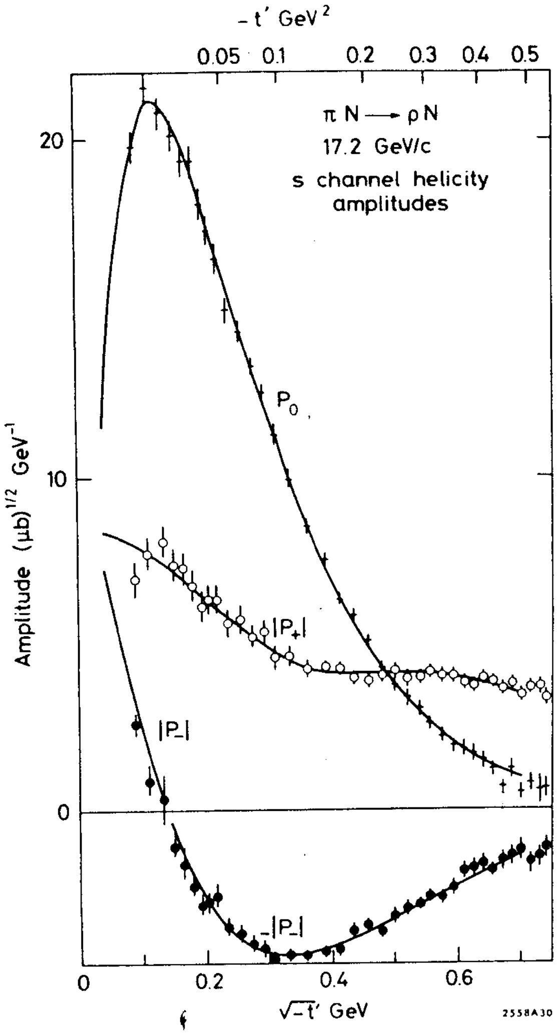

Figure 4

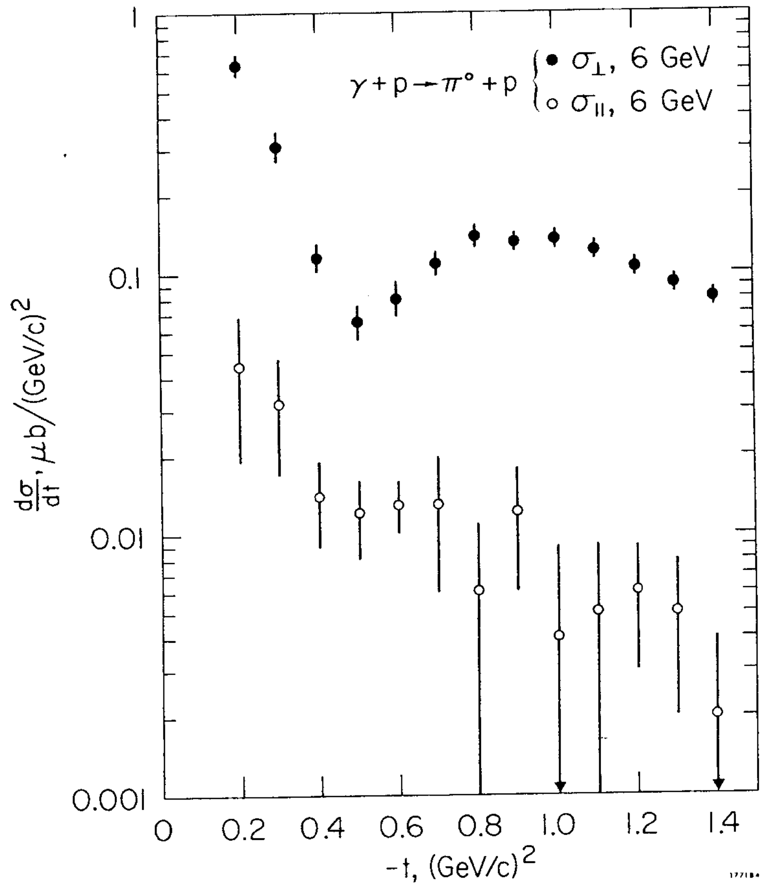

Figure 5

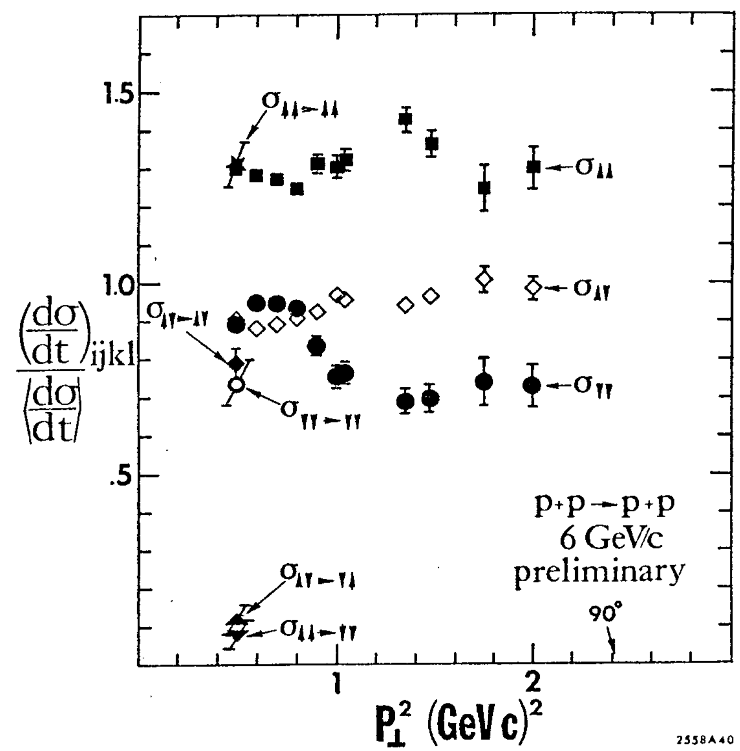

Figure 6

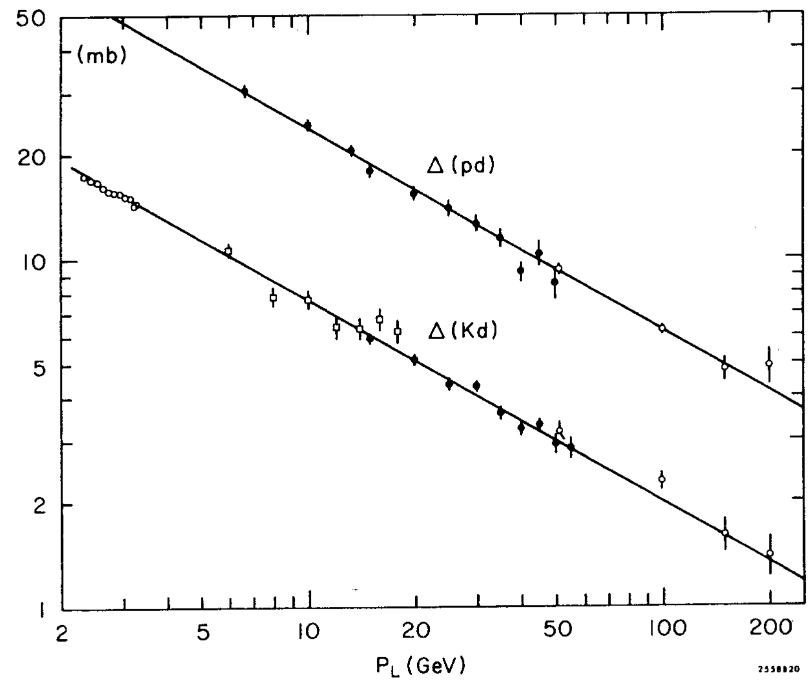

Figure 7

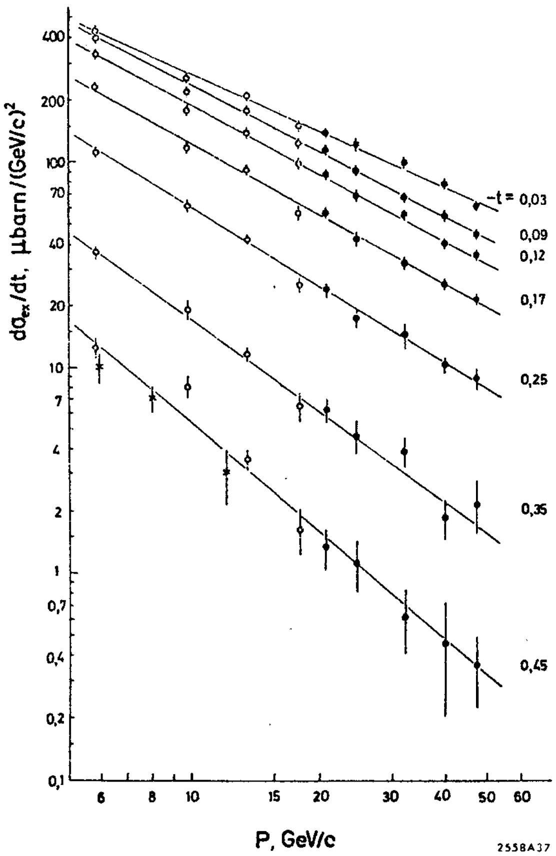

Figure 8

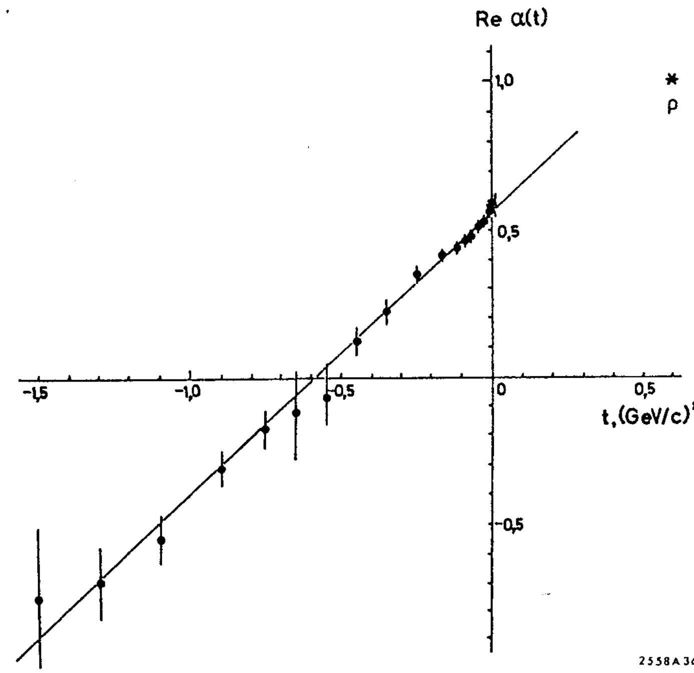

Figure 9

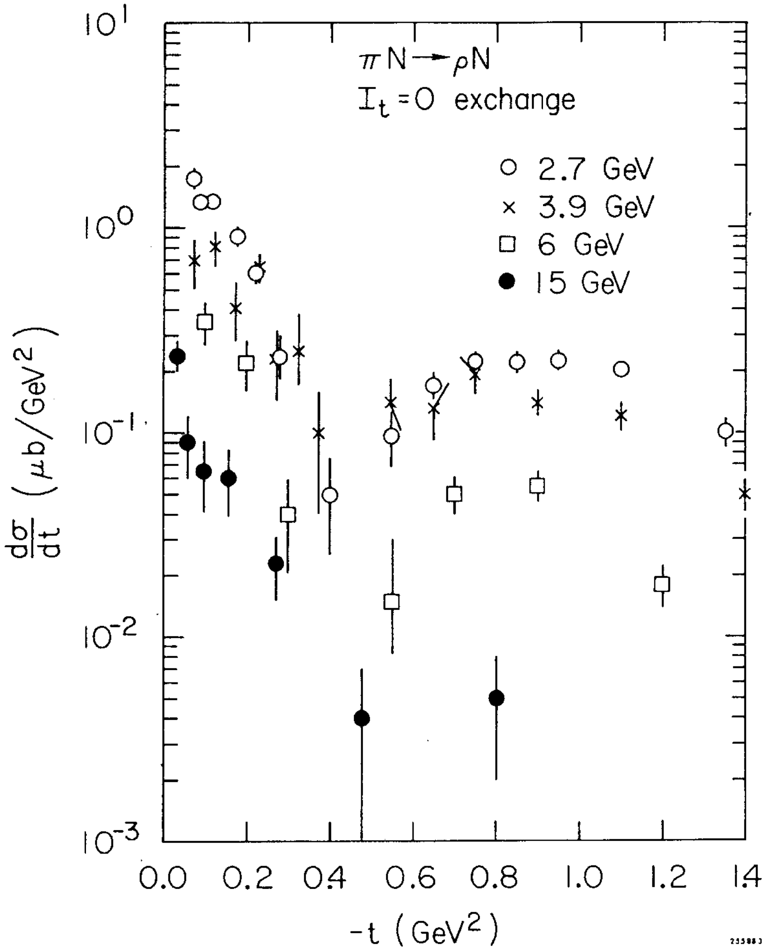

Figure 10

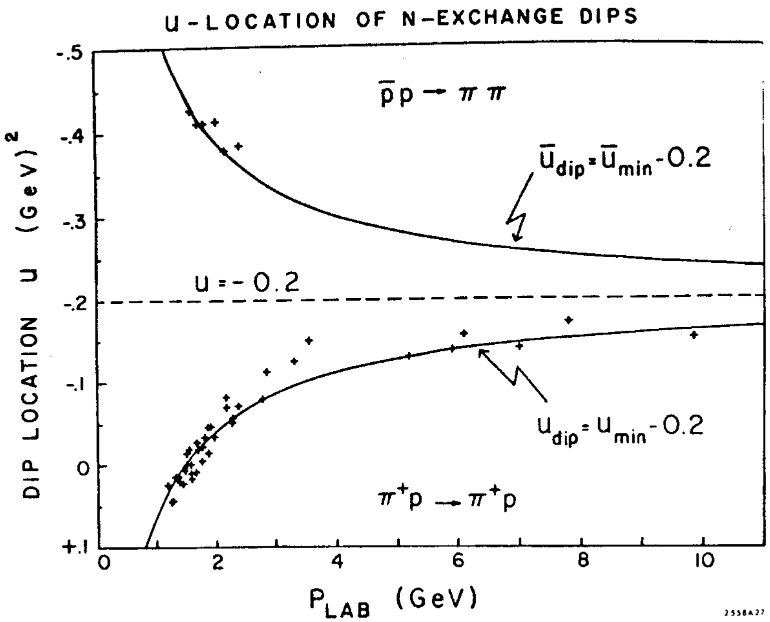

Figure 11

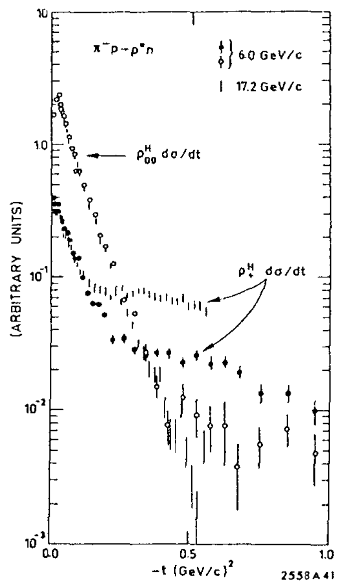

Figure 12

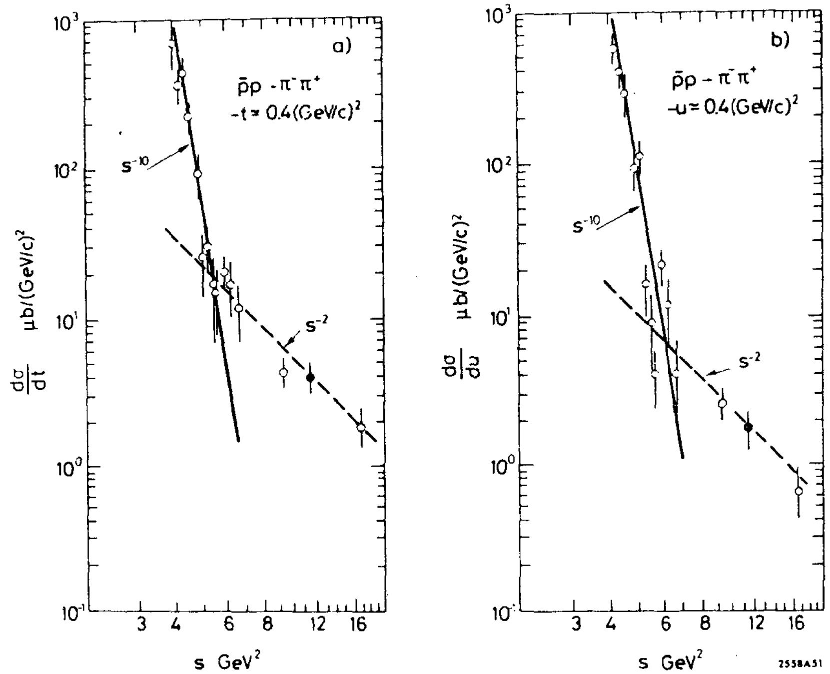

Figure 13

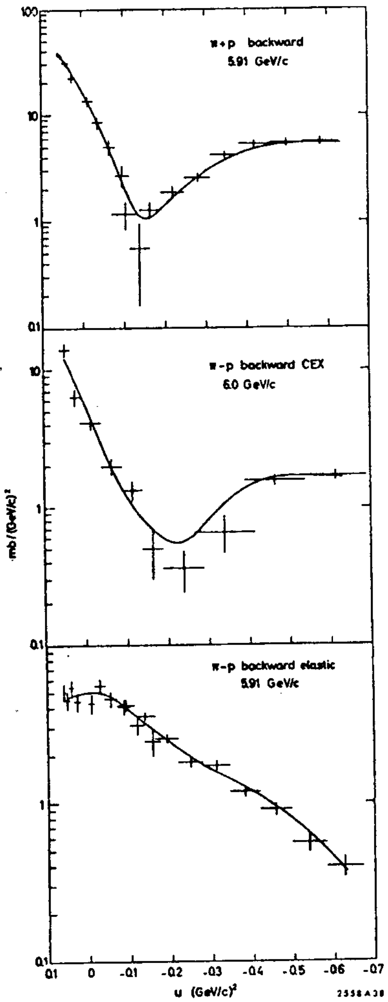

Figure 14

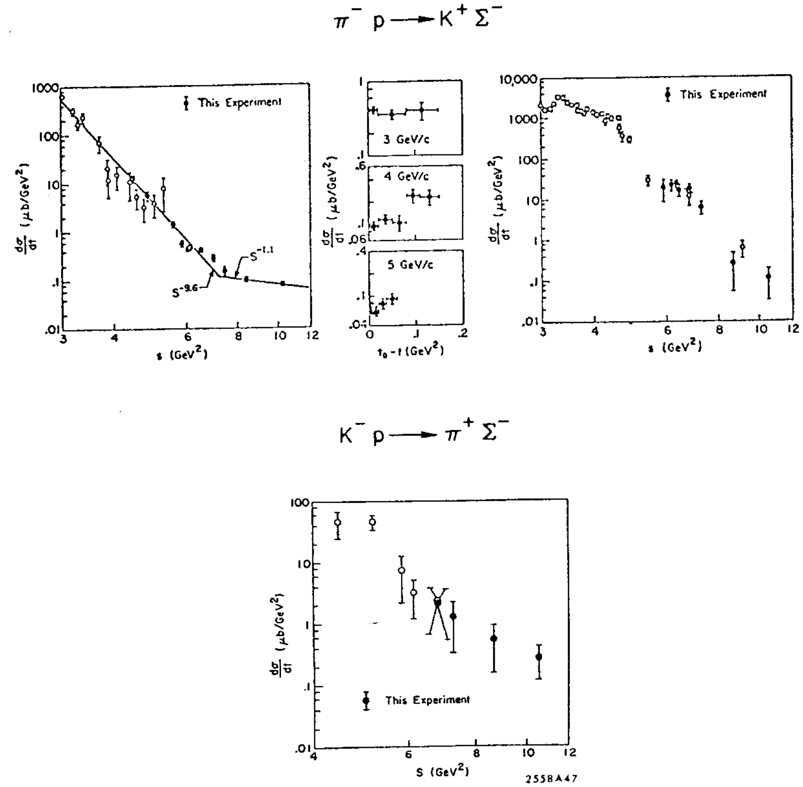

Figure 15

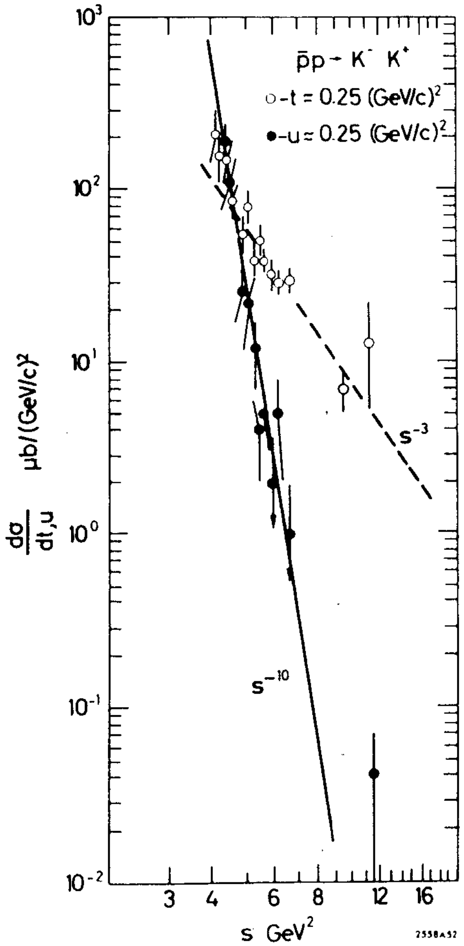

Figure 16

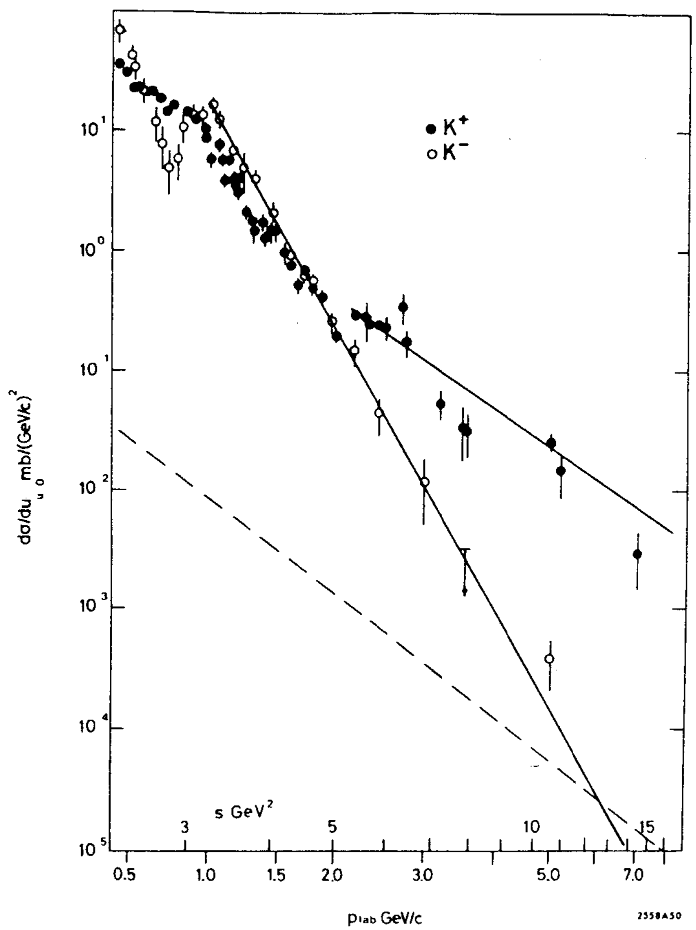

Figure 17

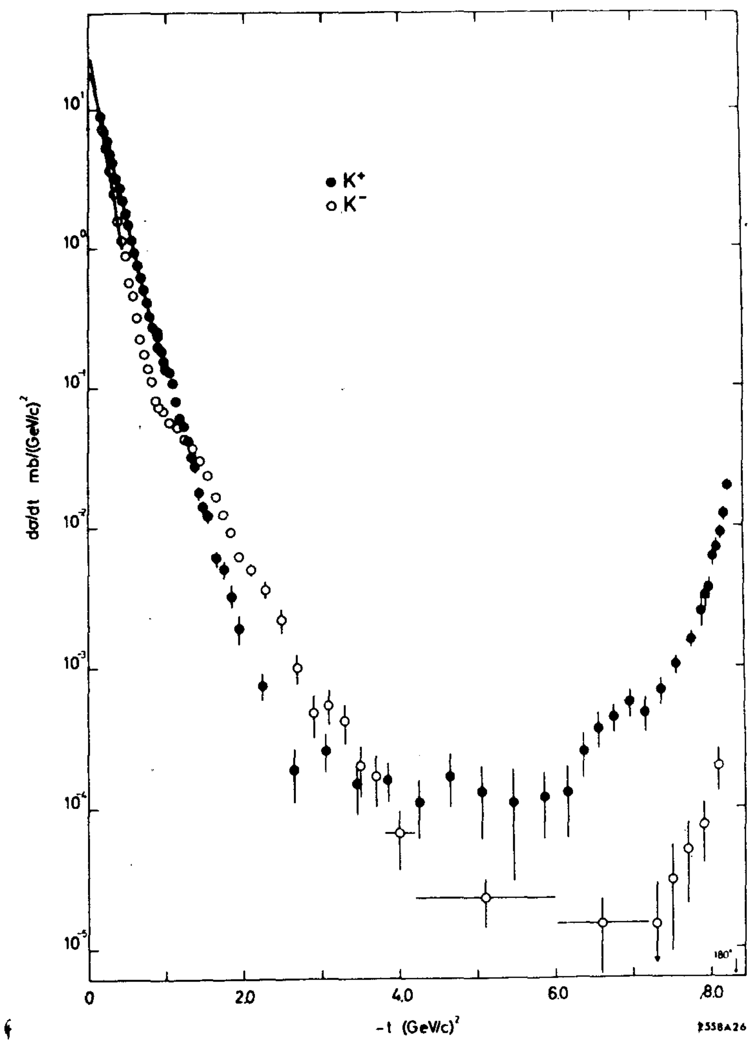

Figure 18

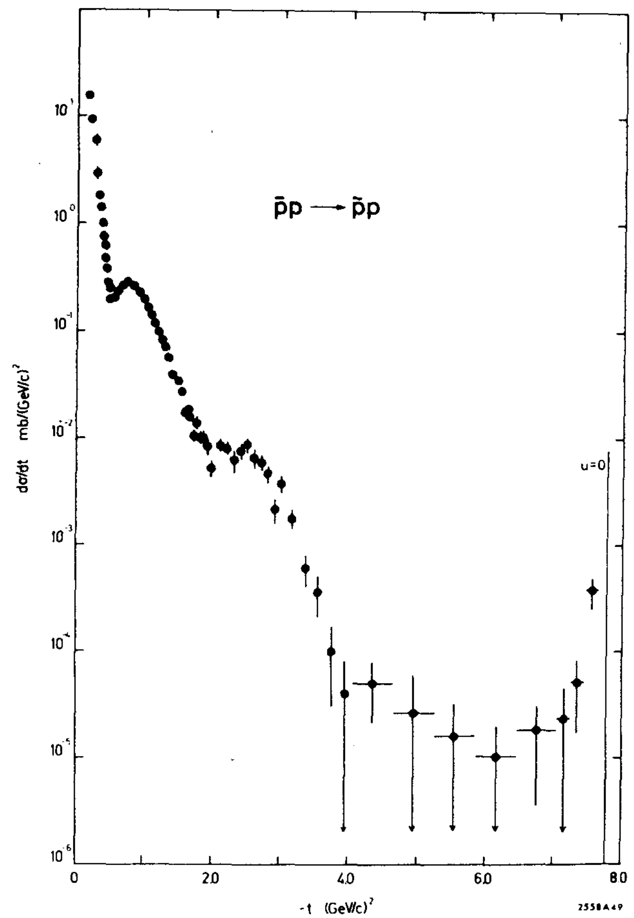

Figure 19

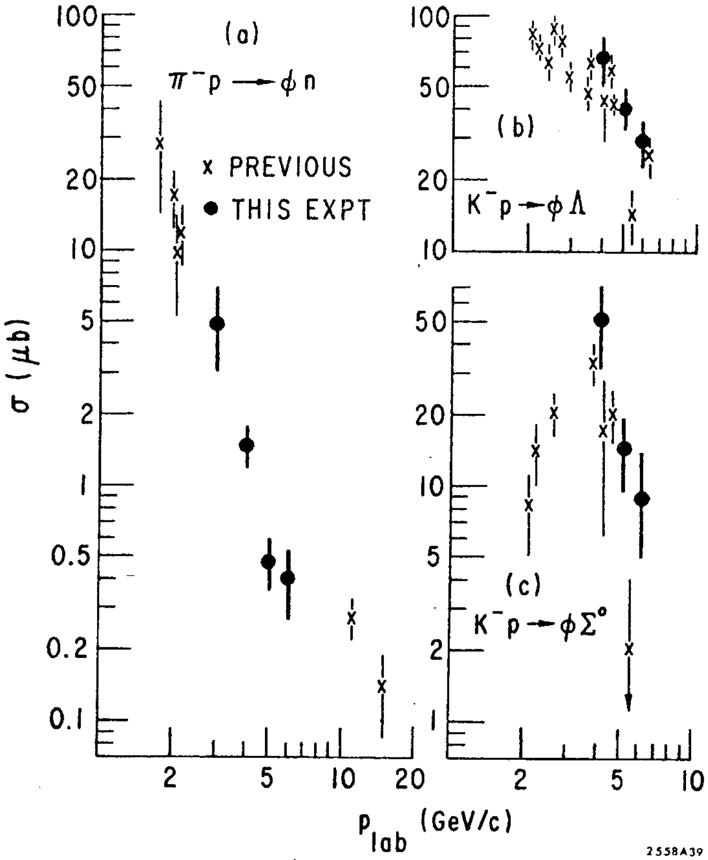

Figure 20

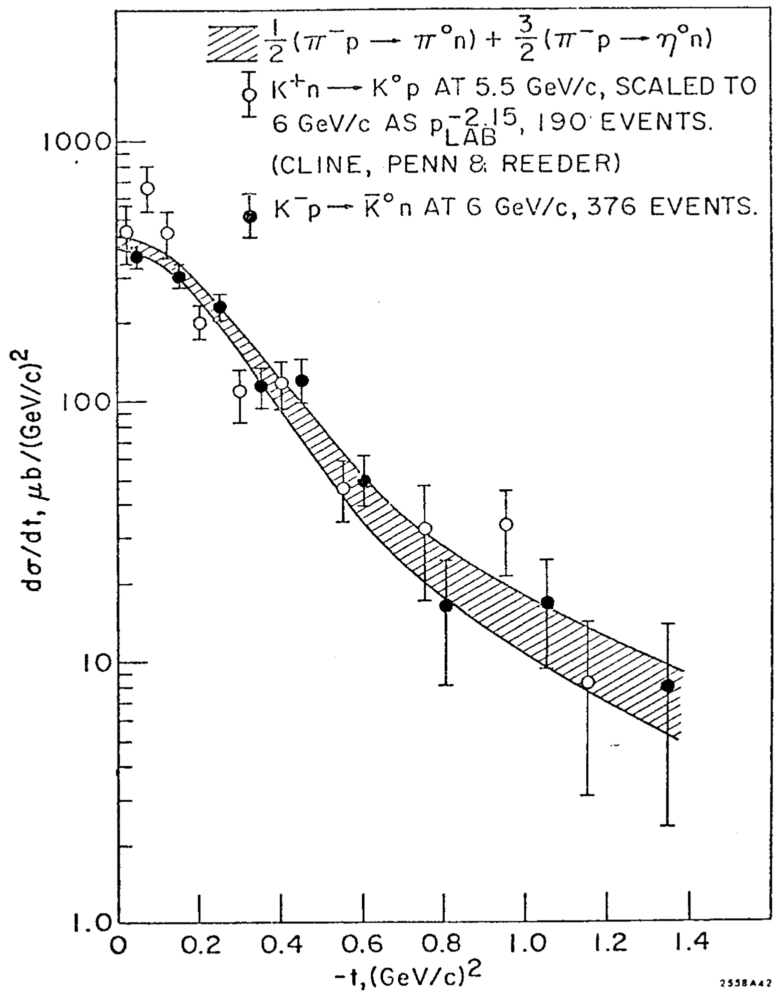

Figure 21

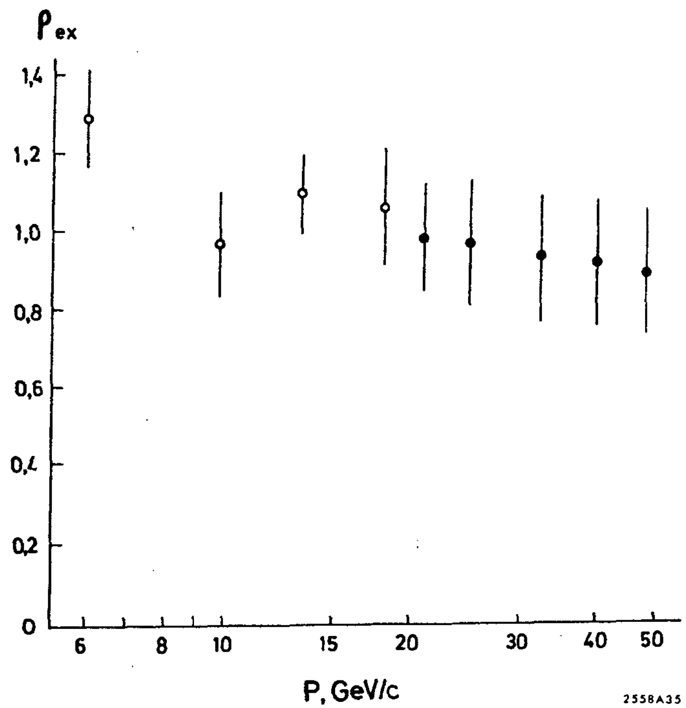

Figure 22

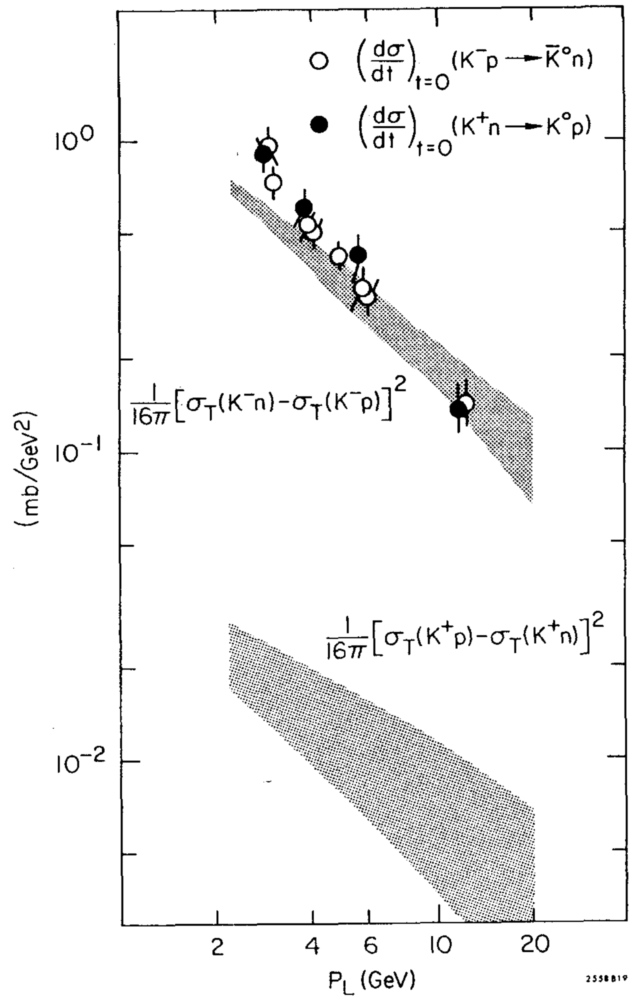

Figure 23

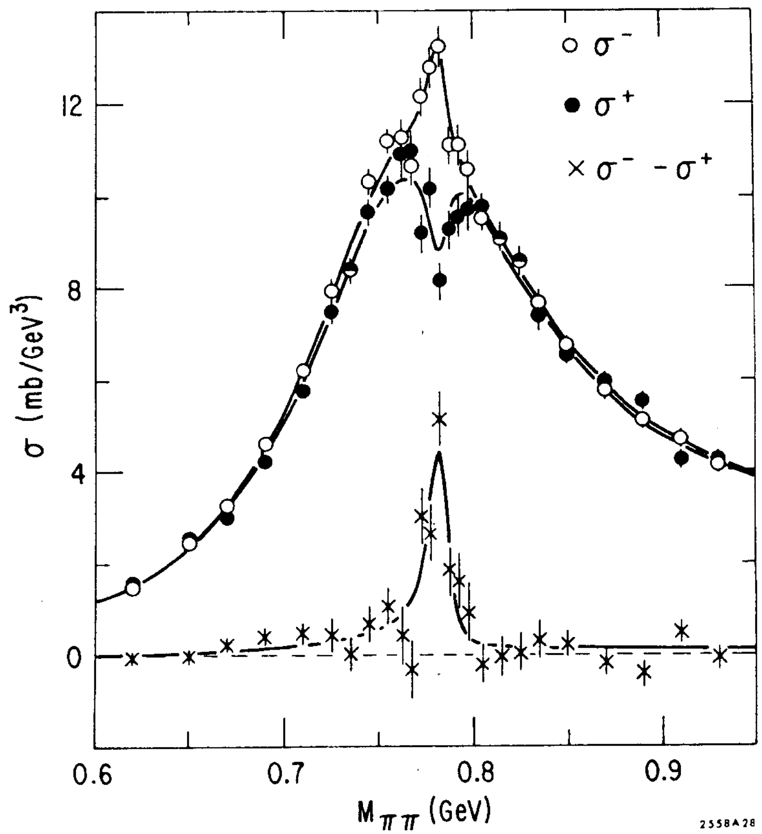

Figure 24

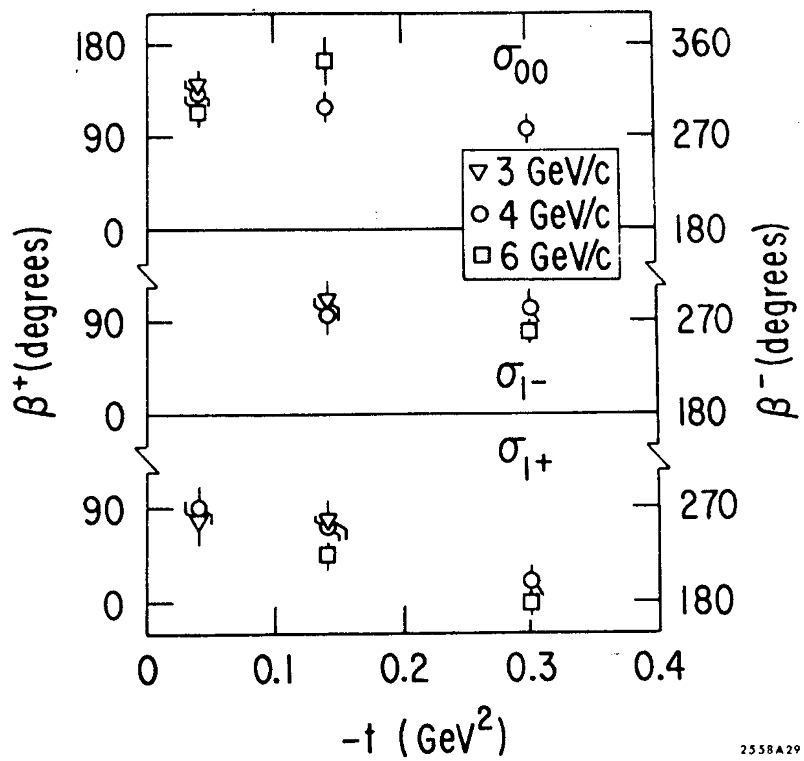

Figure 25

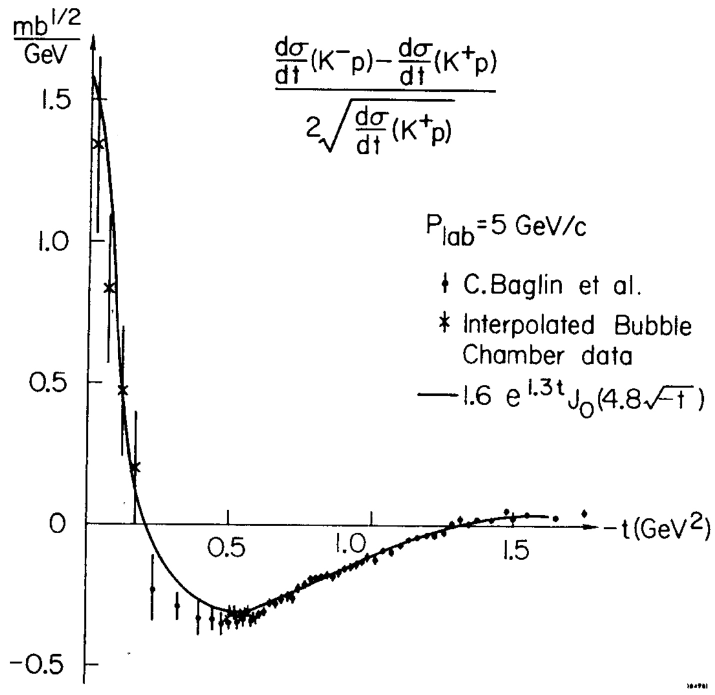

Figure 26

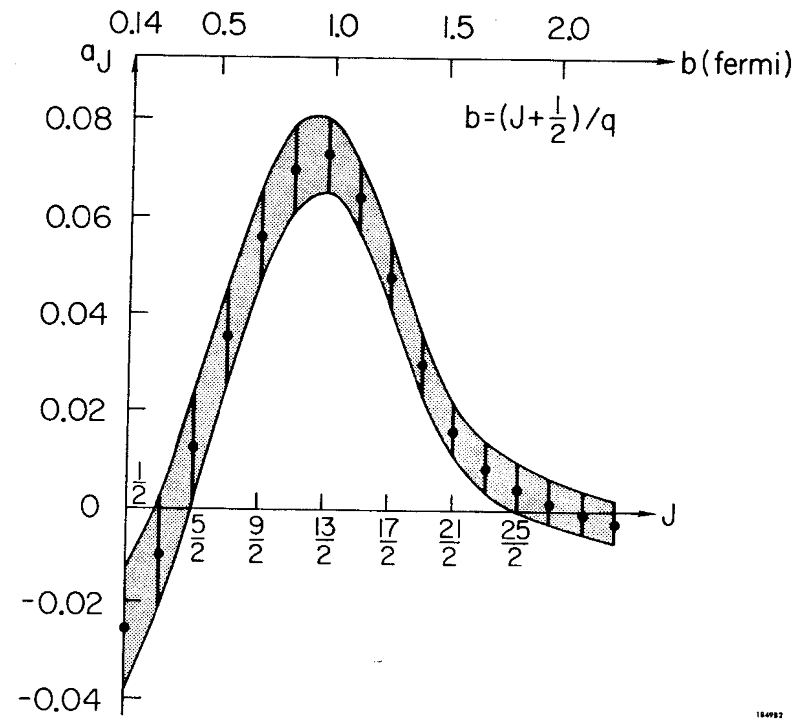

Figure 27

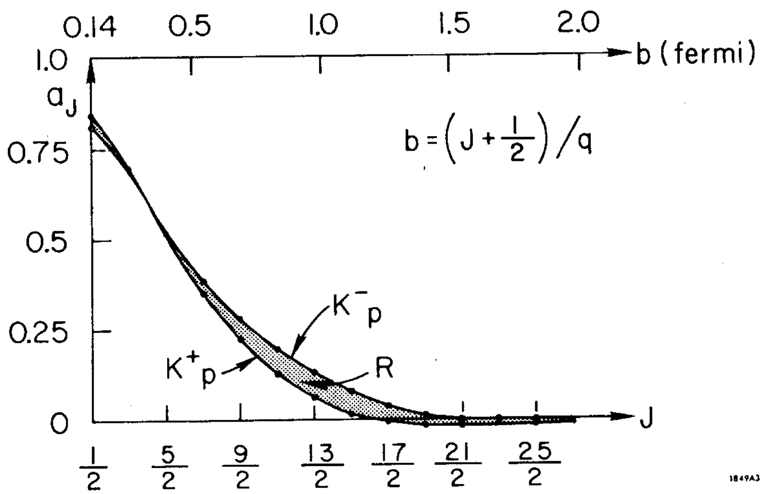

Figure 28

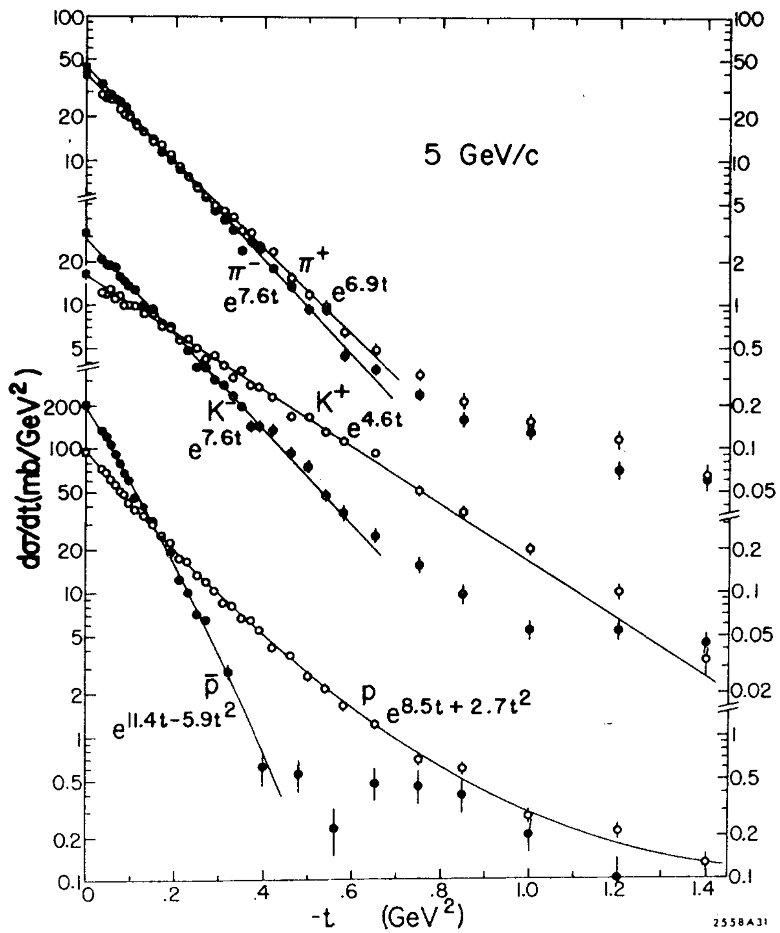

Figure 29

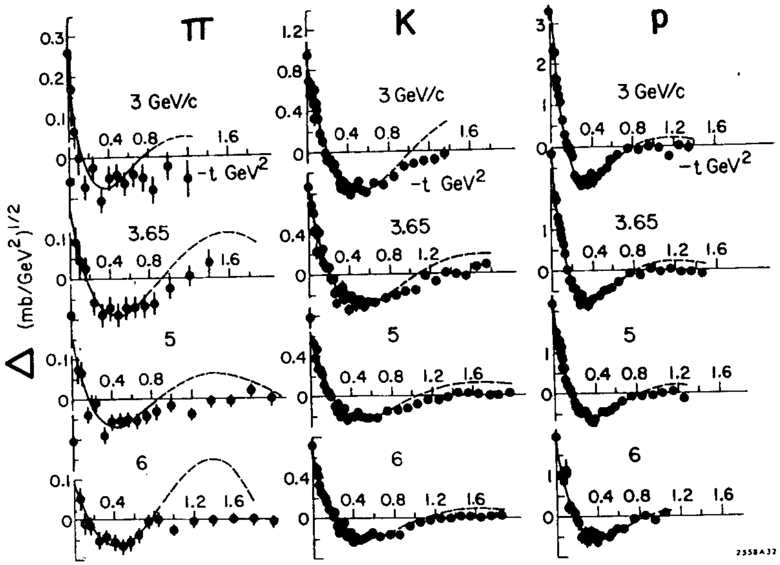

Figure 30

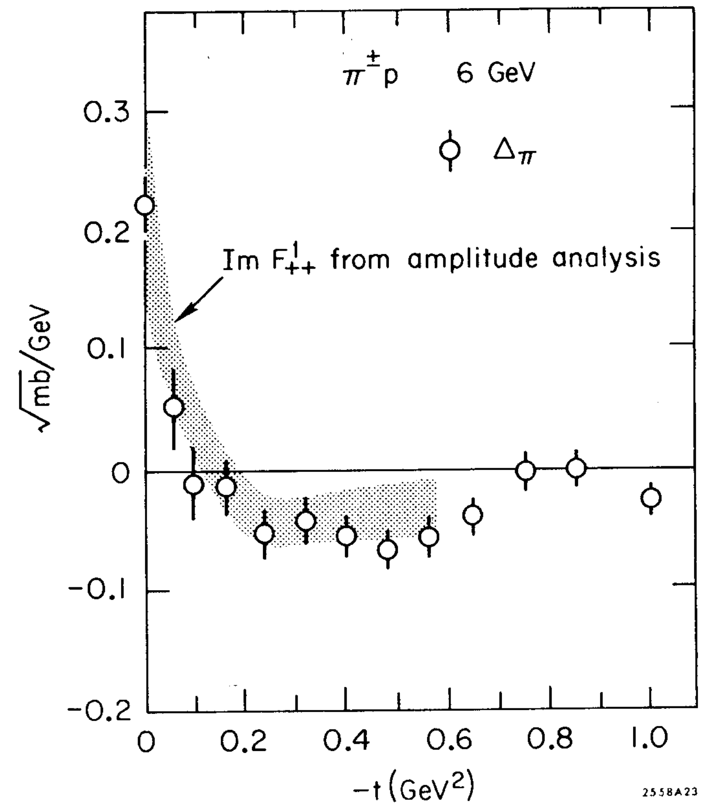

Figure 31

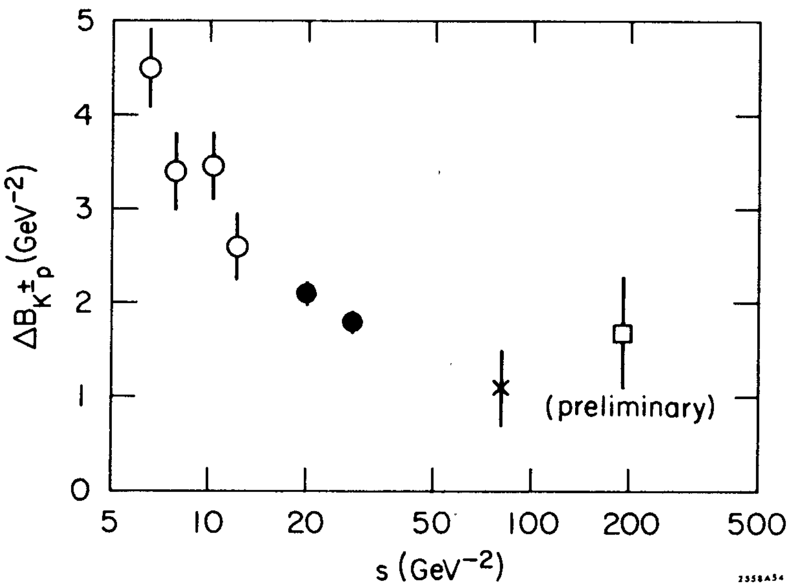

Figure 32

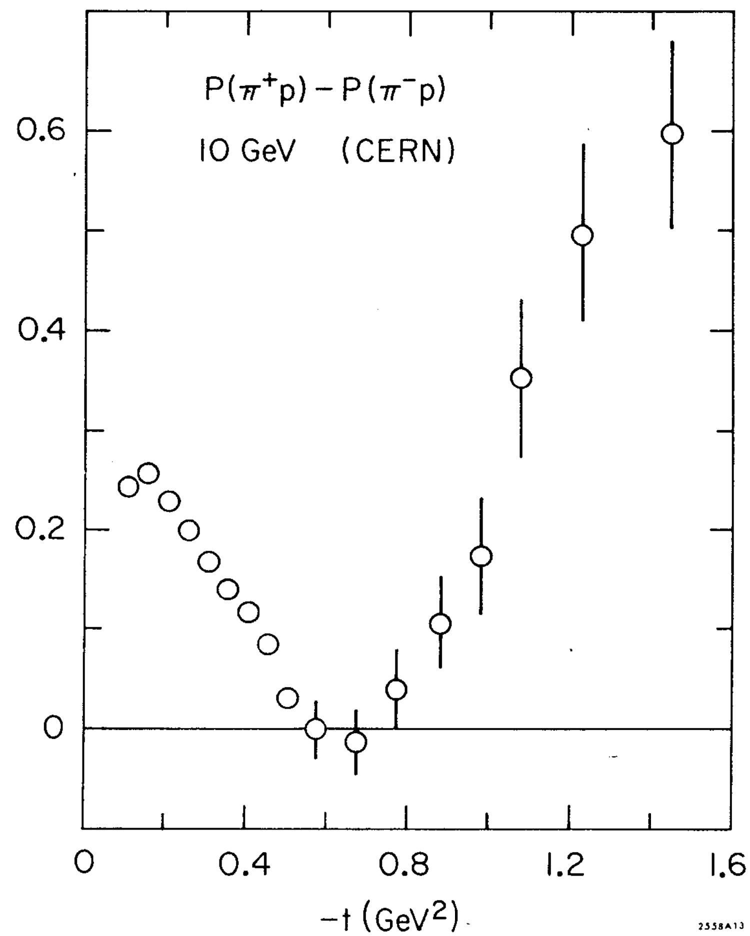

Figure 33

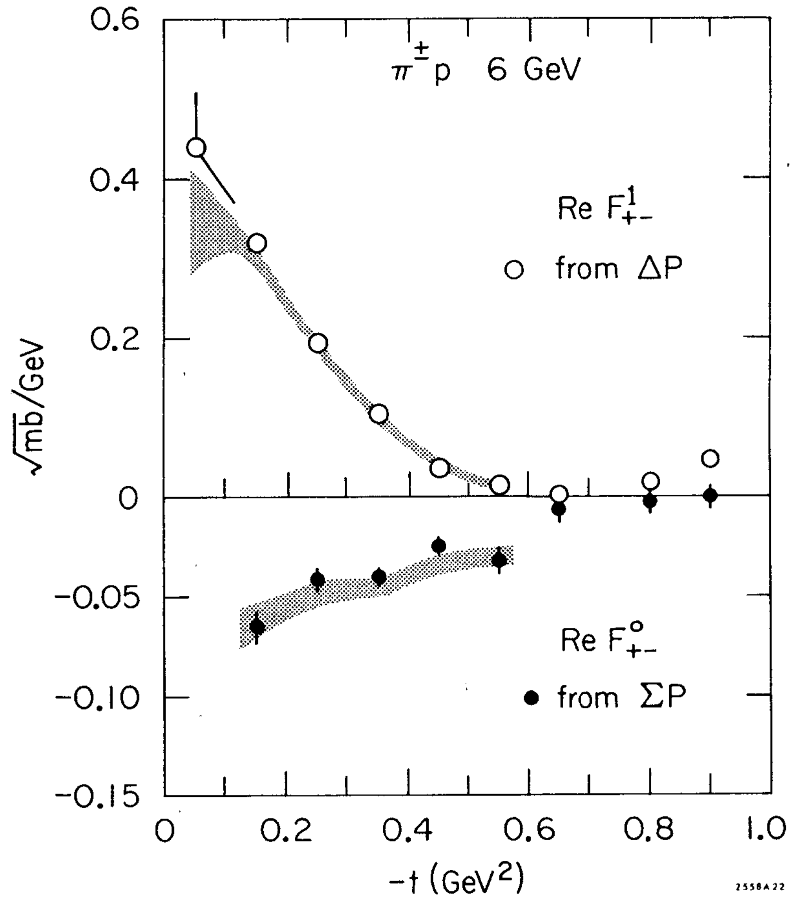

Figure 34

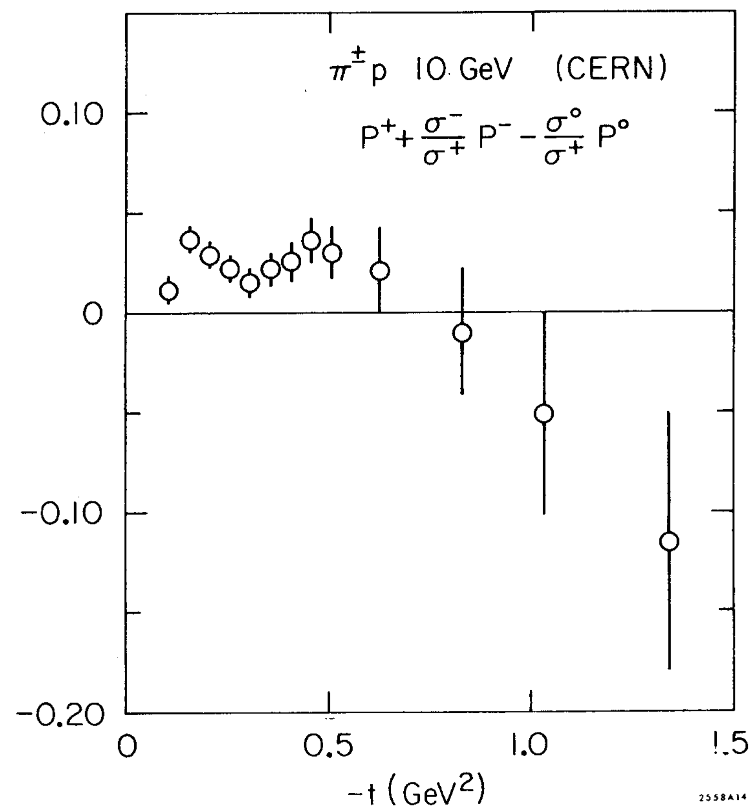

Figure 35

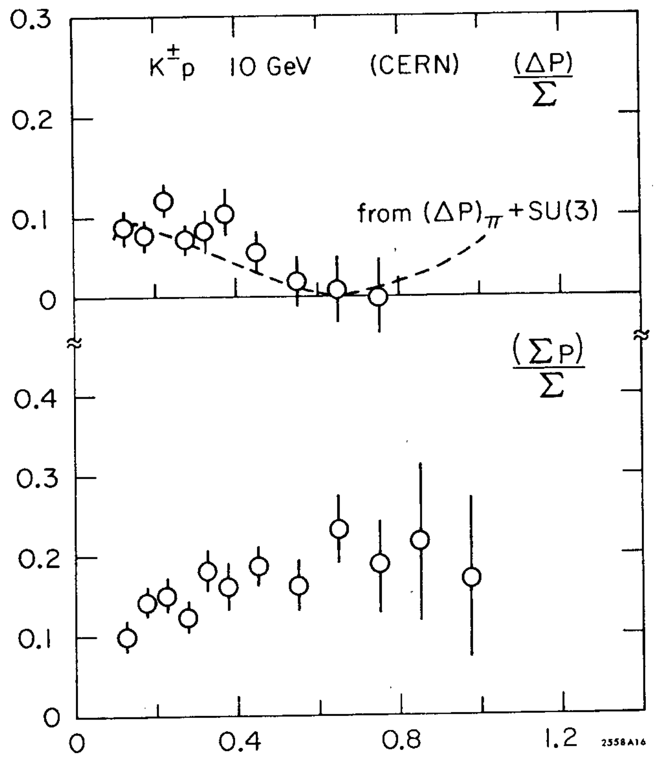

Figure 36

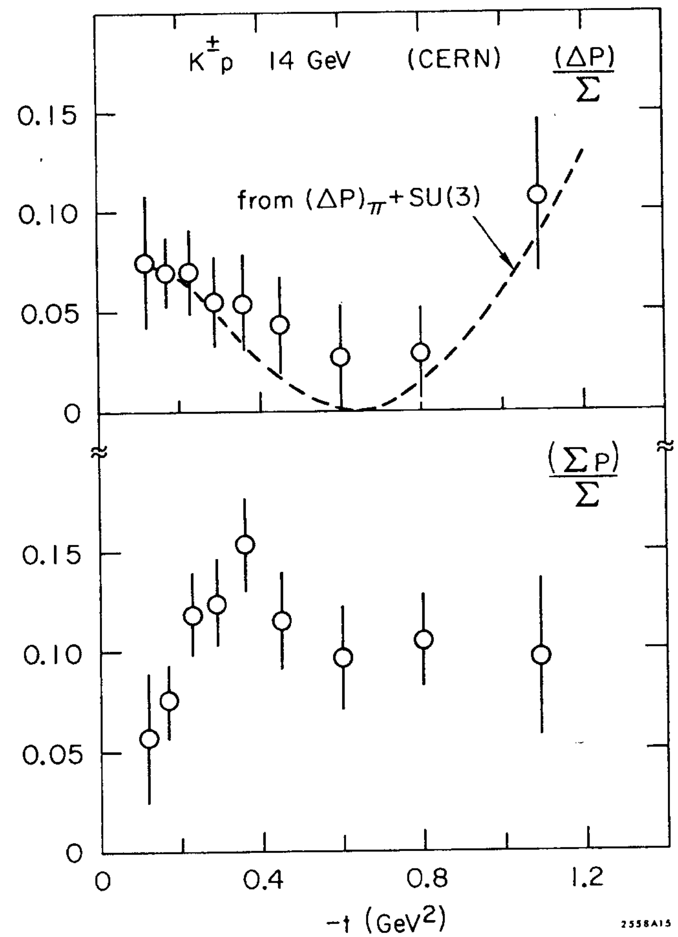

Figure 37

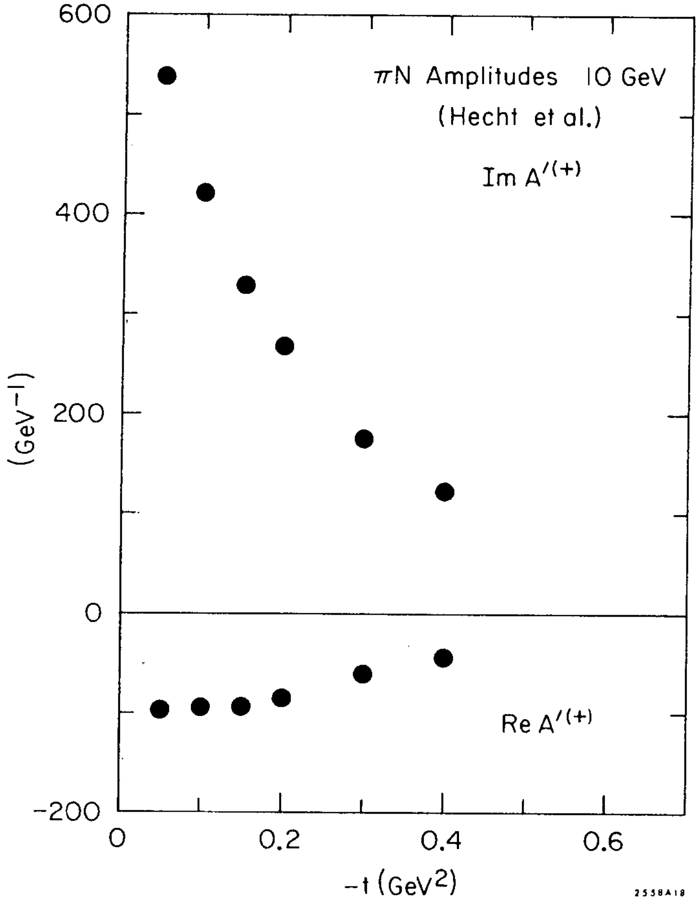

Figure 38

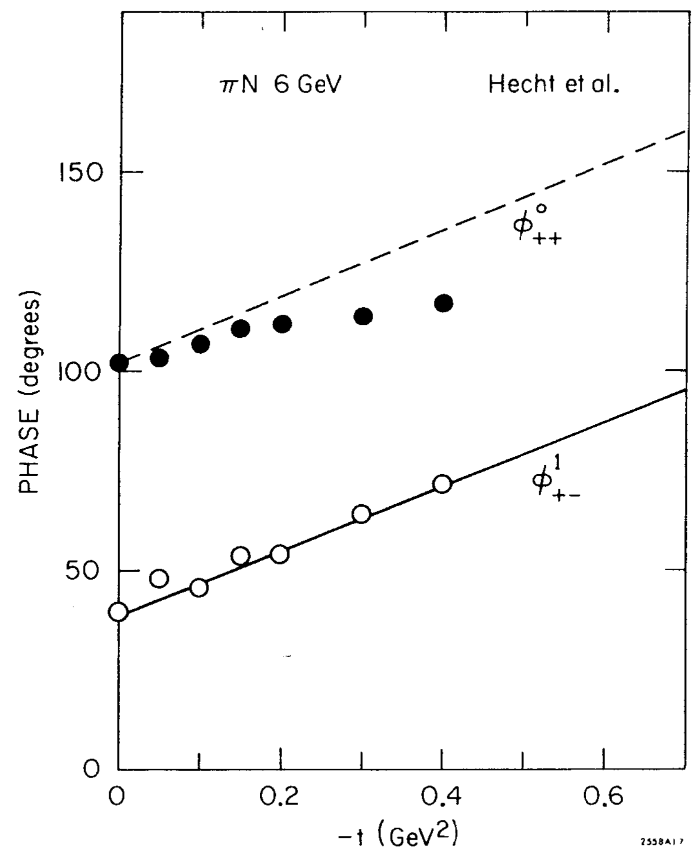

Figure 39

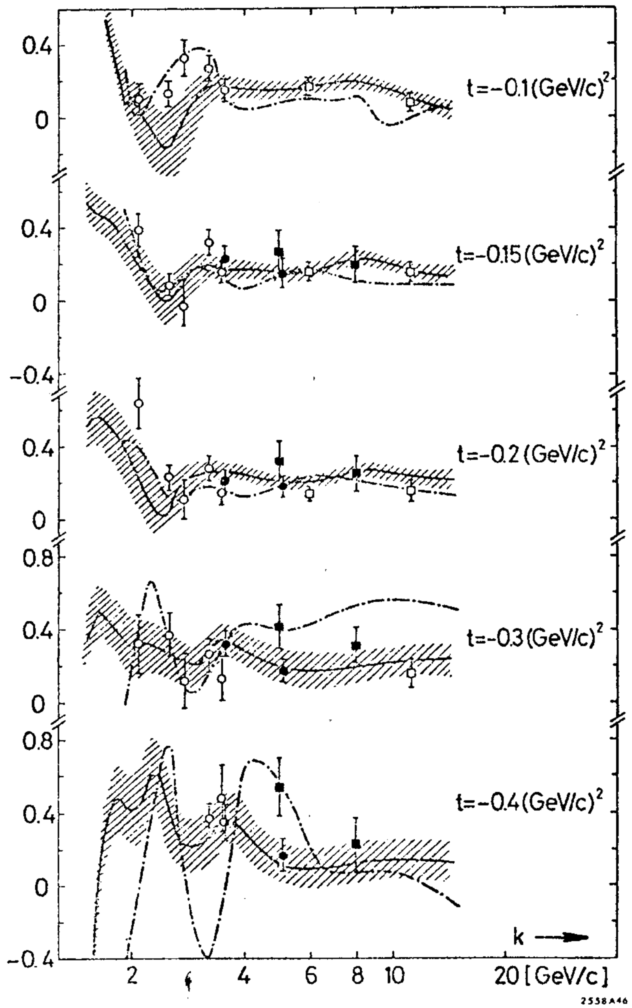

Figure 40

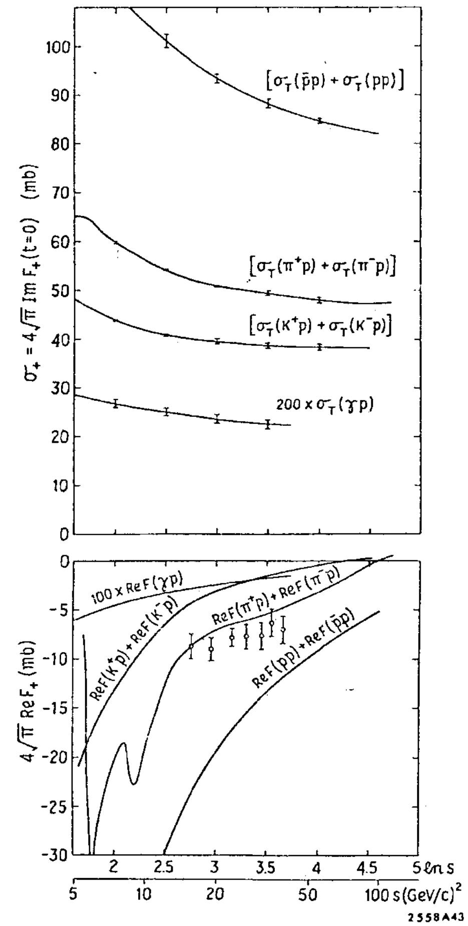

Figure 41

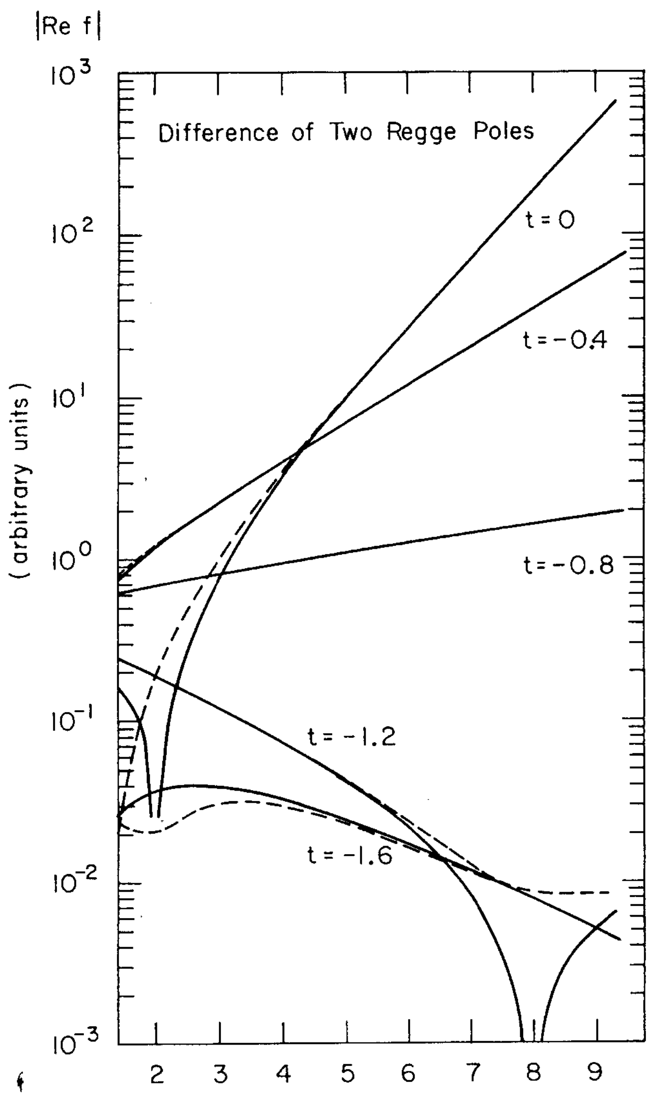

Figure 42a

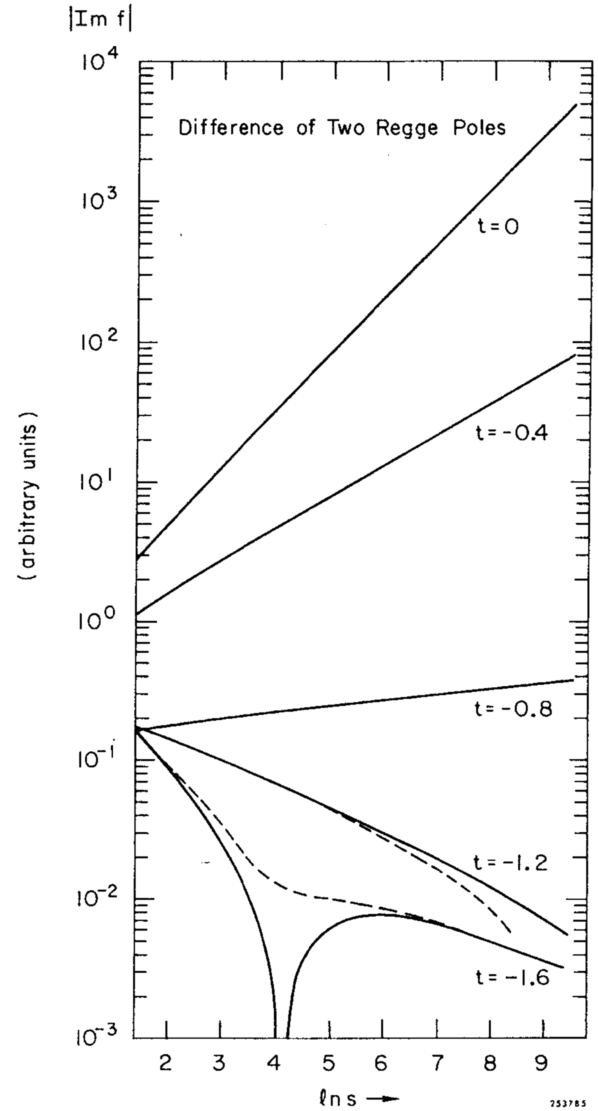

Figure 42b

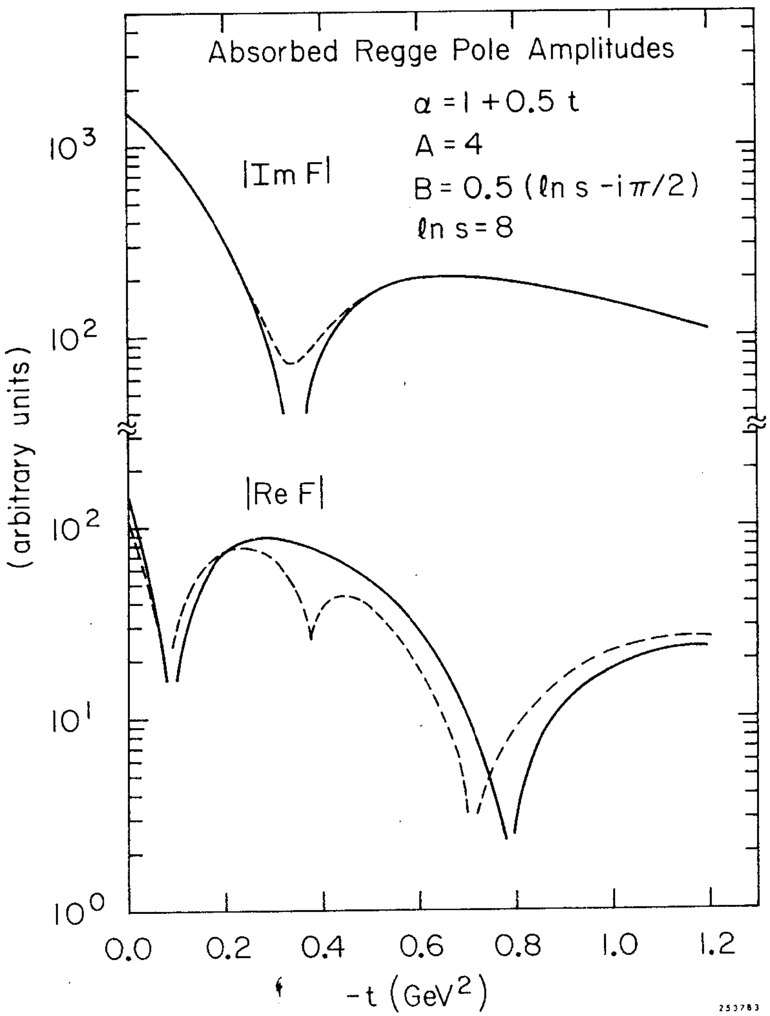

Figure 43

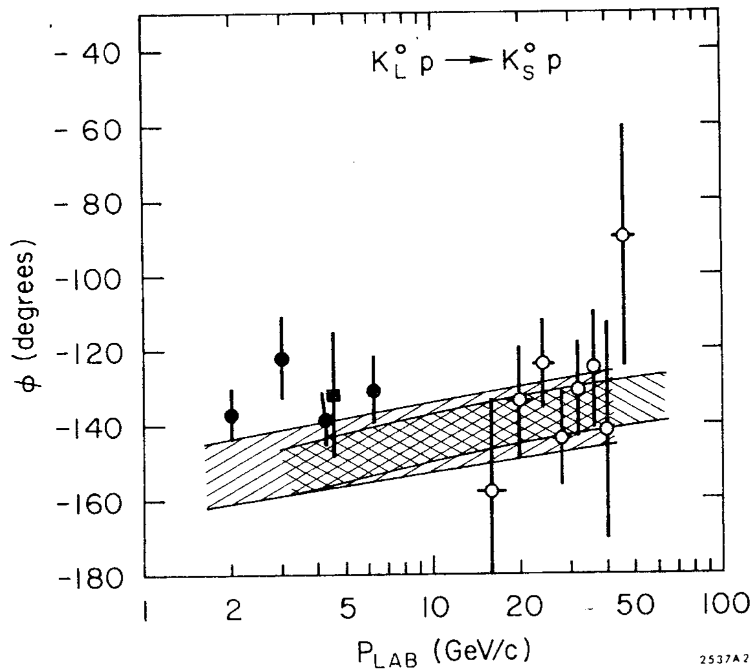

Figure 44

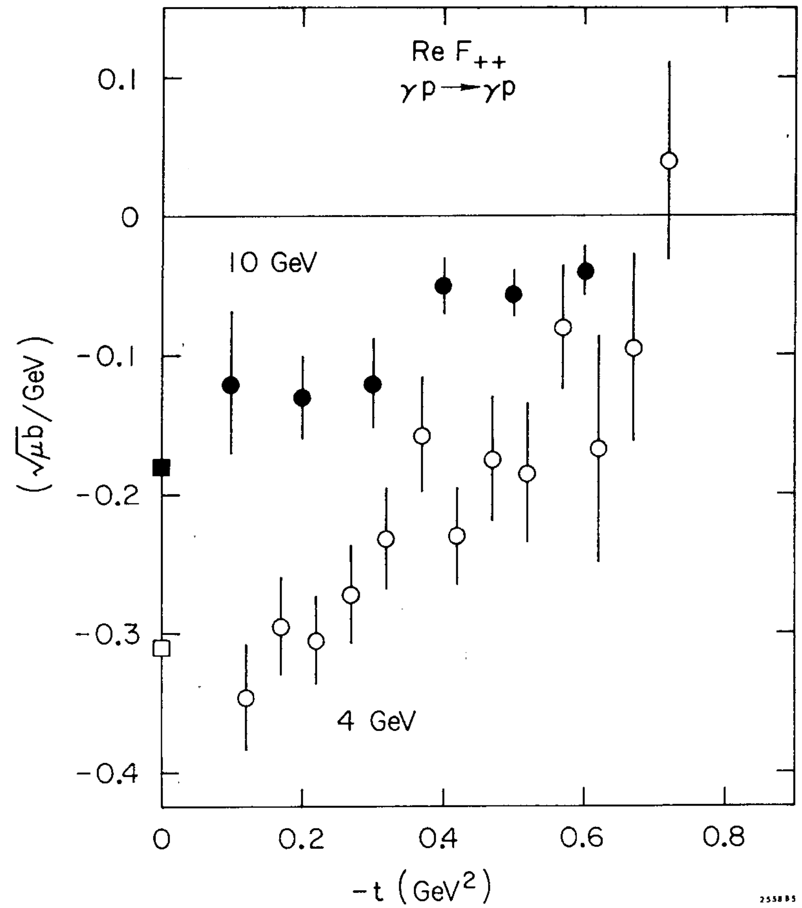

Figure 45

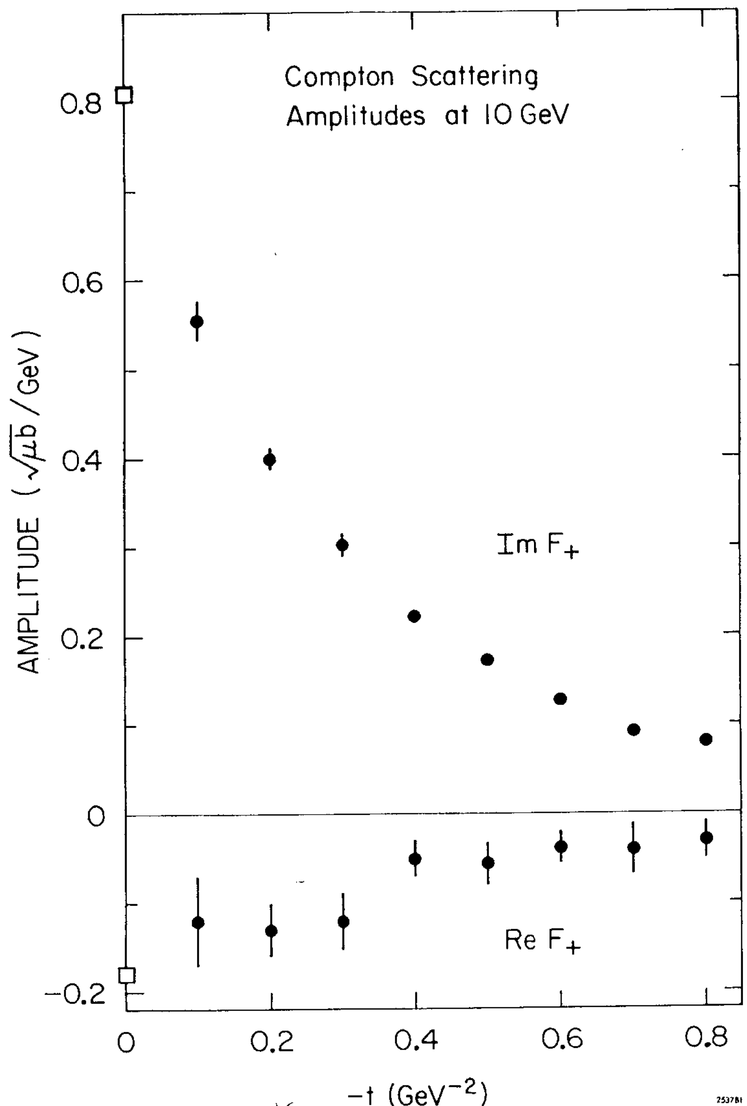

Figure 46

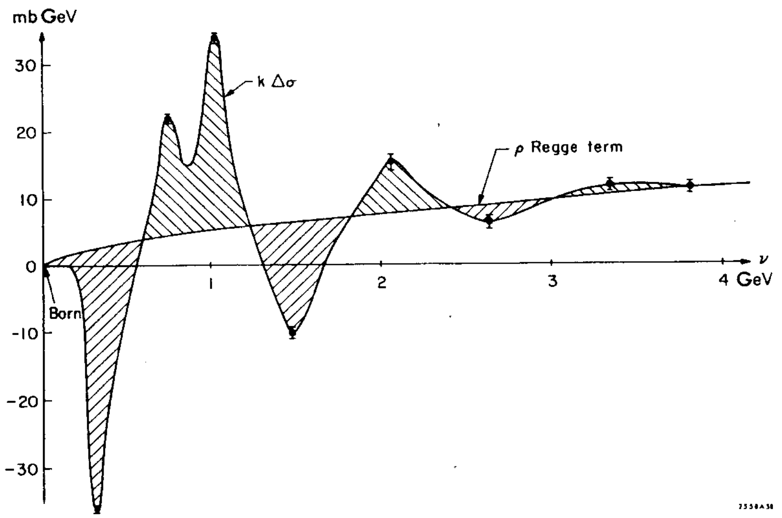

Figure 47

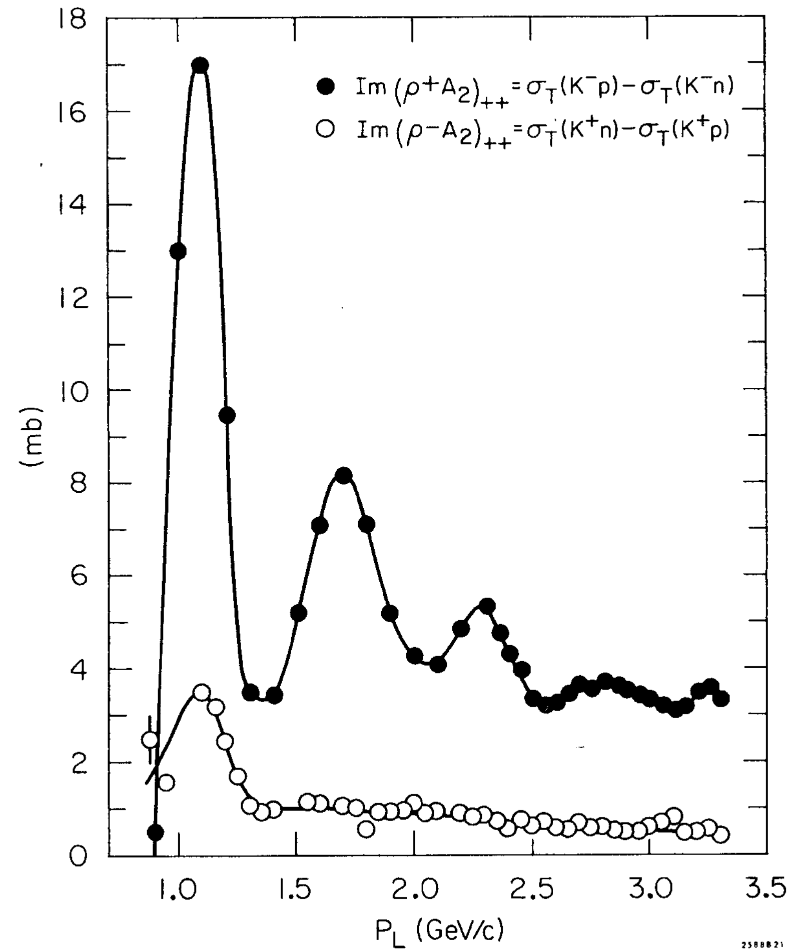

Figure 48

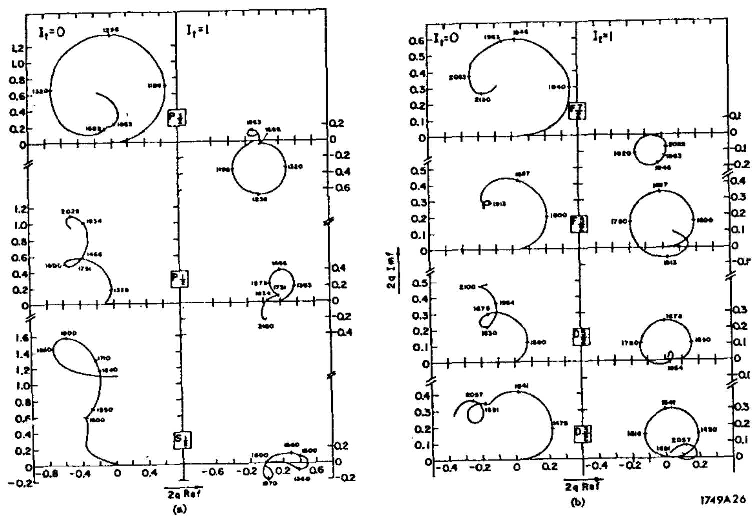

Figure 49

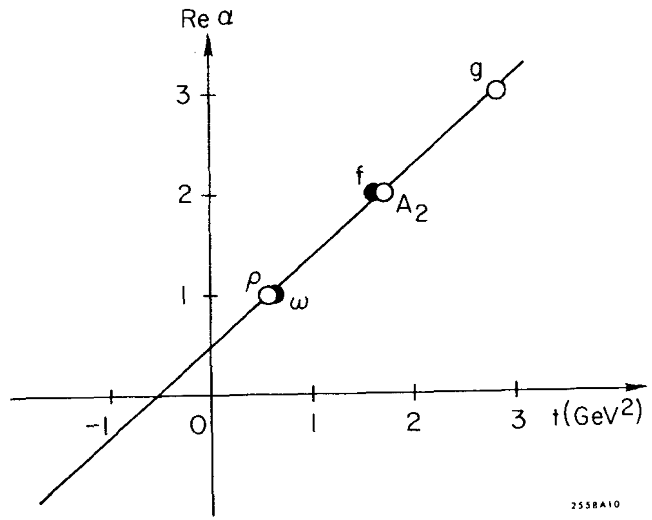

Figure 50

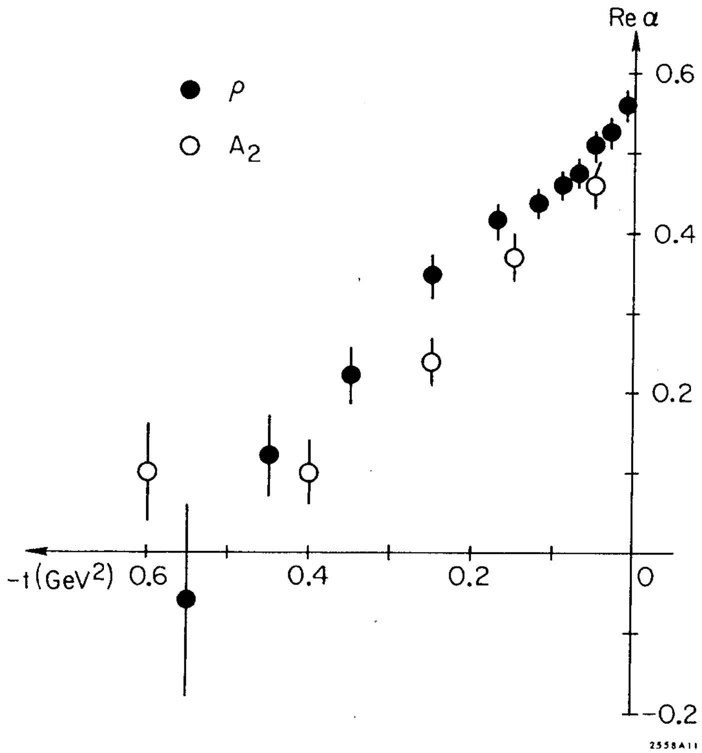

Figure 51

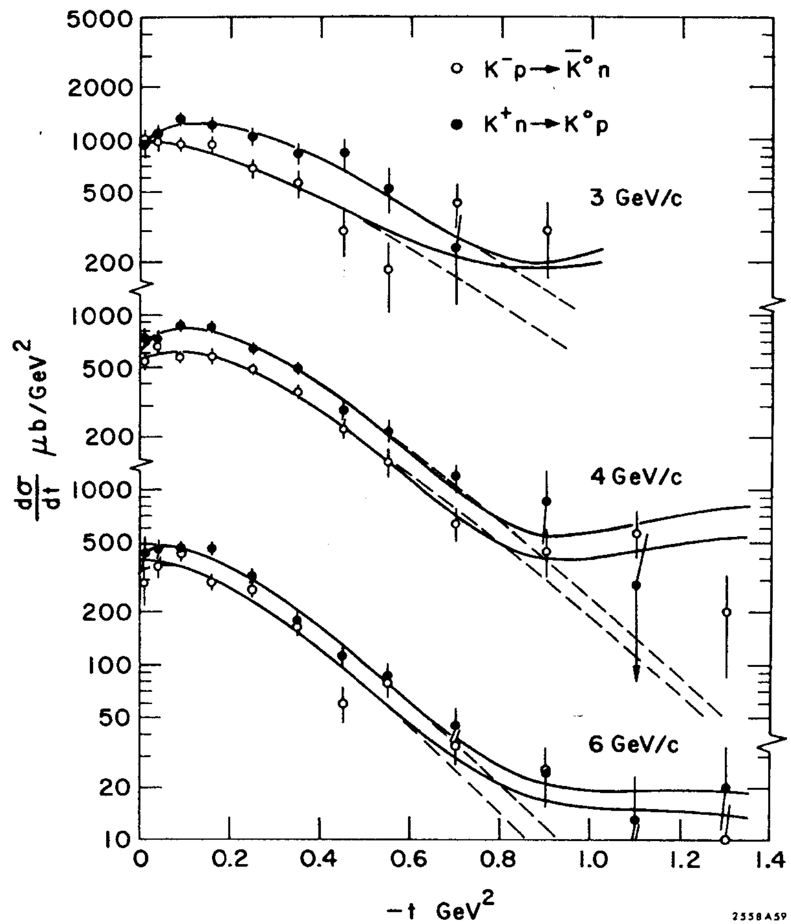

Figure 52

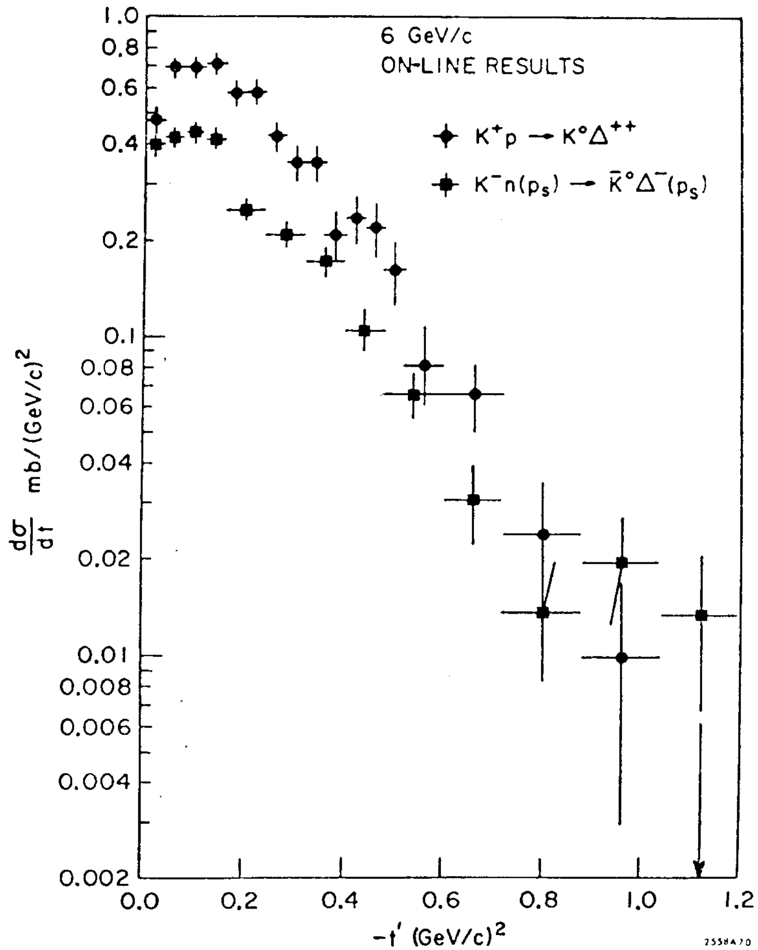

Figure 53

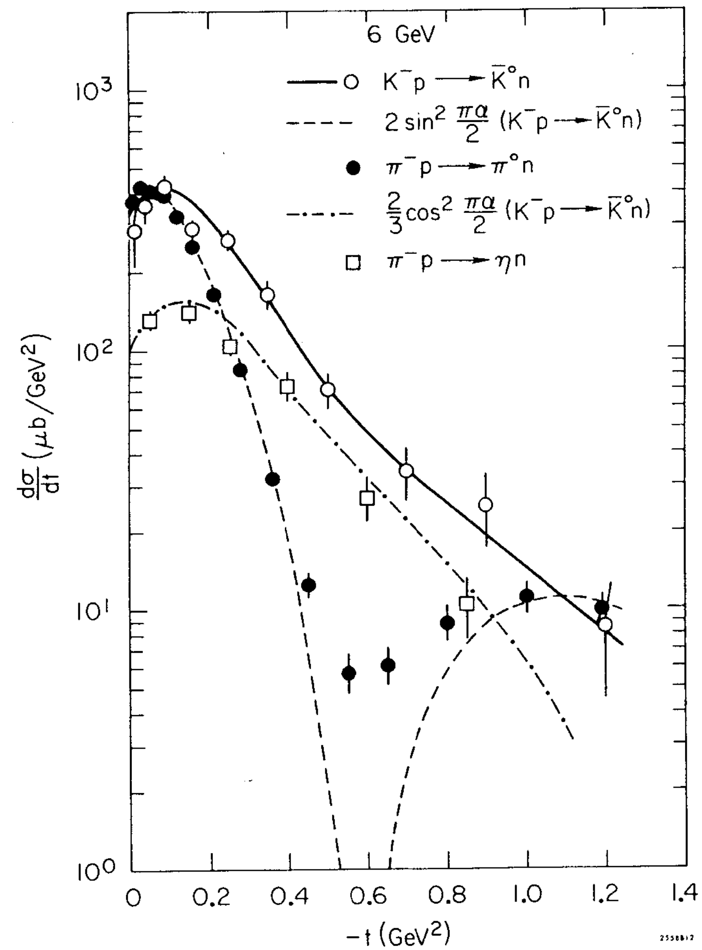

Figure 54

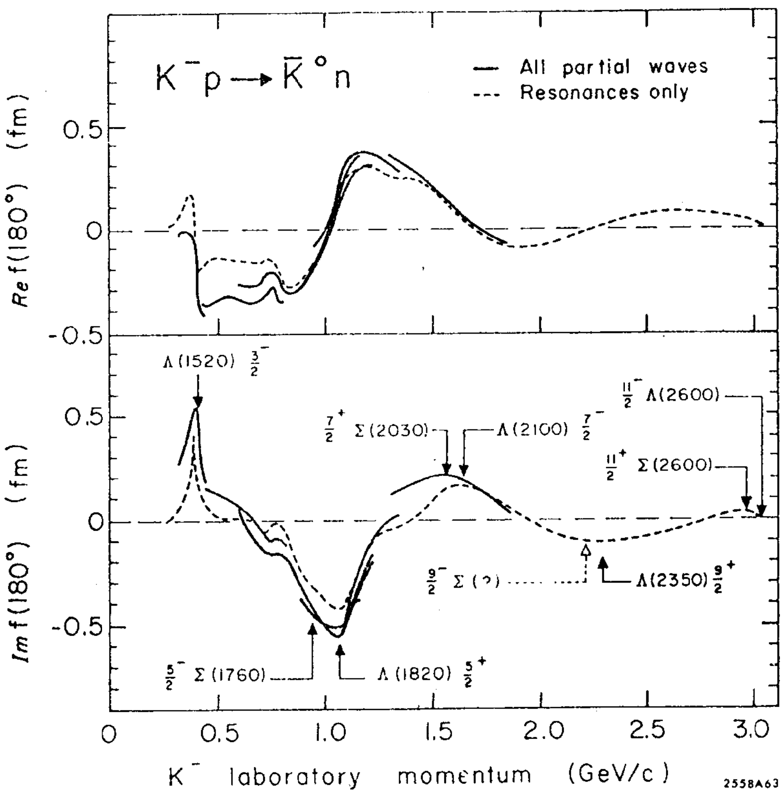

Figure 55

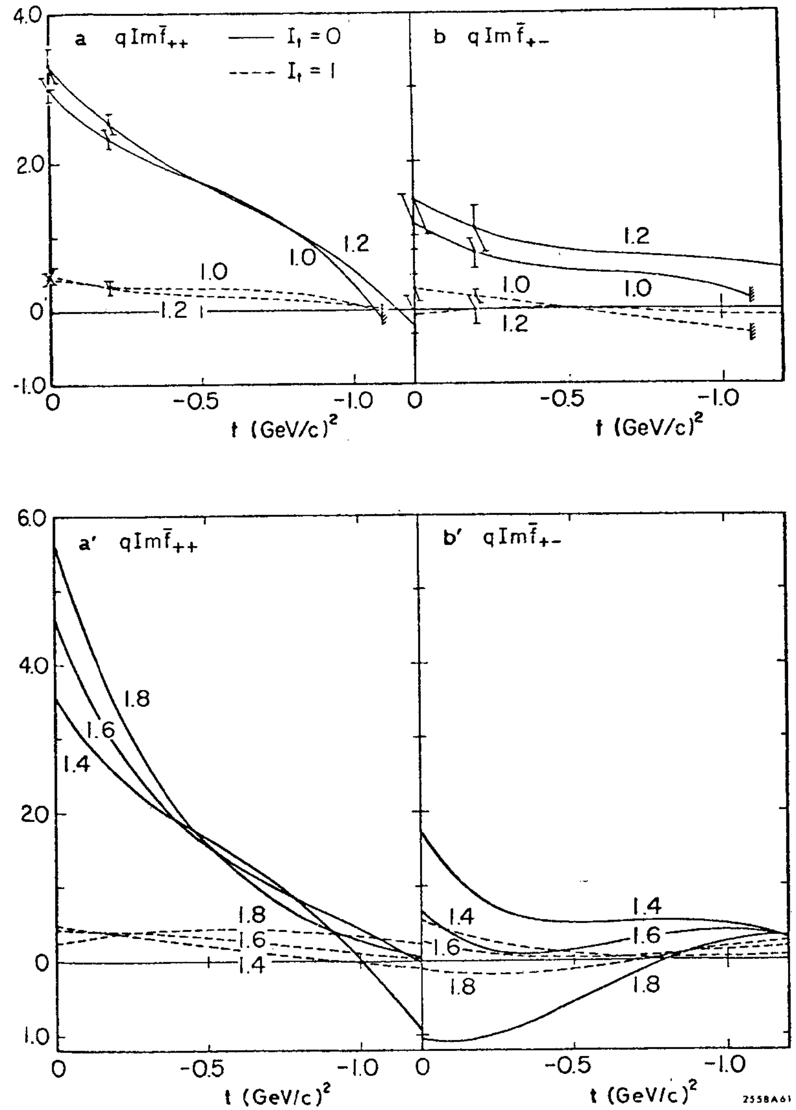

Figure 56

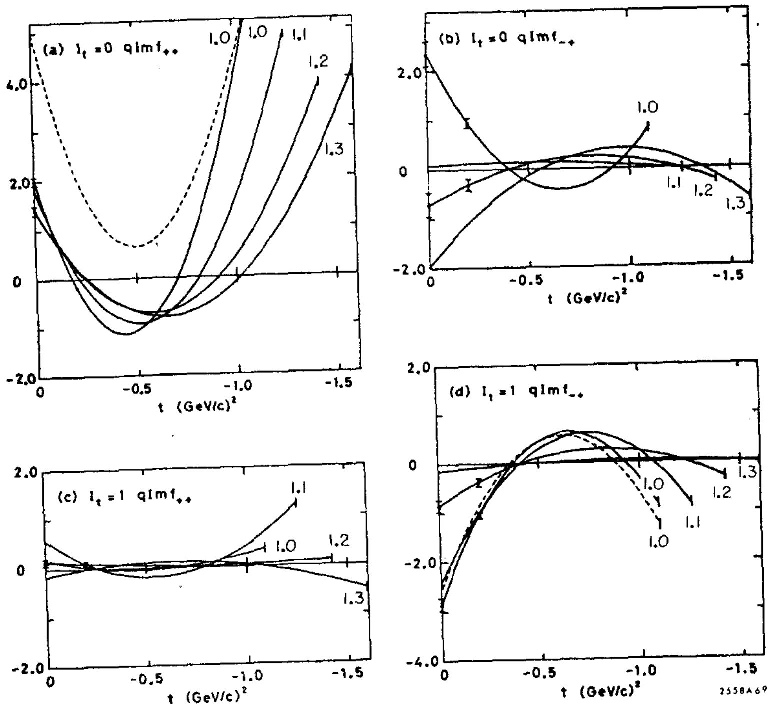

Figure 57

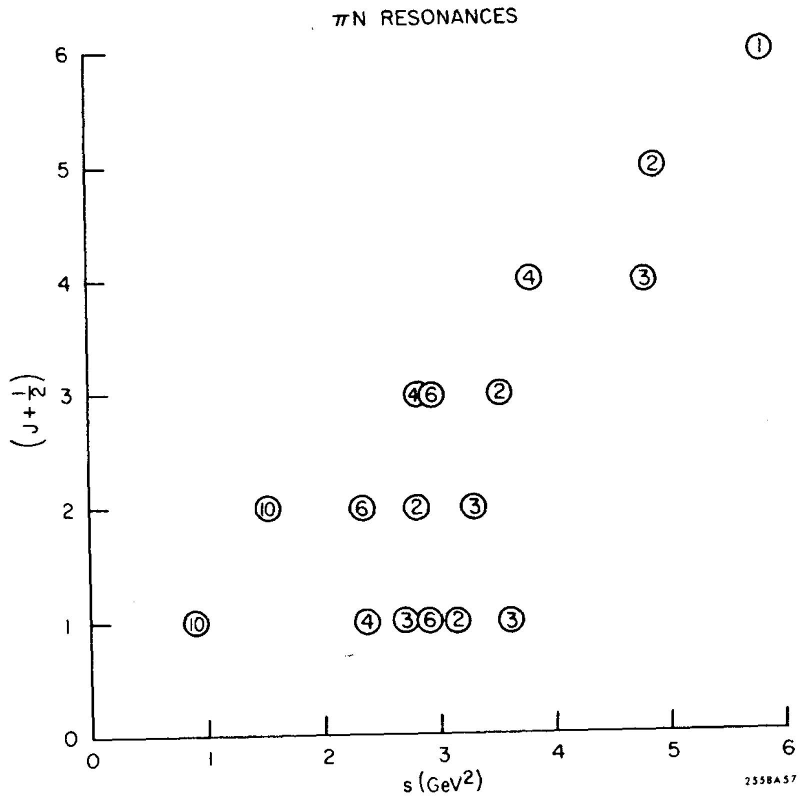

Figure 58

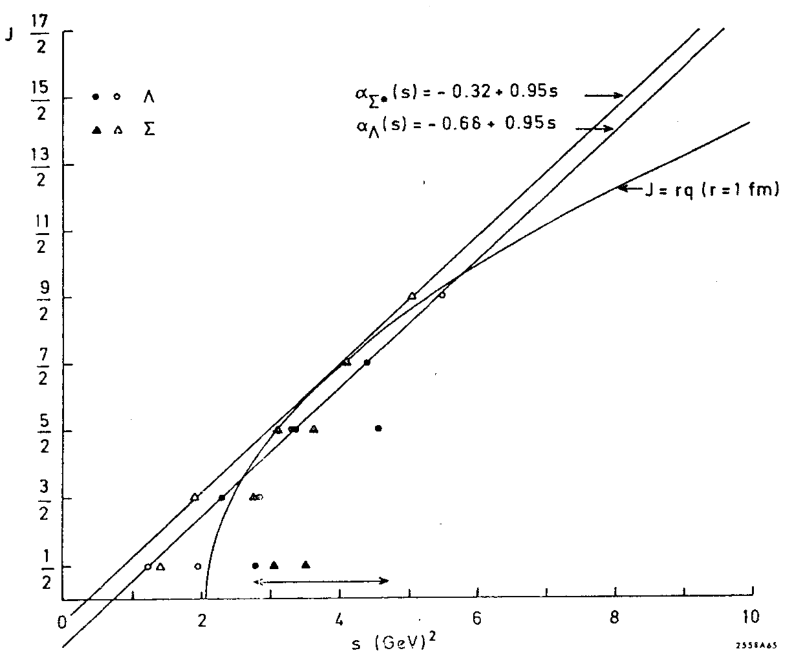

Figure 59

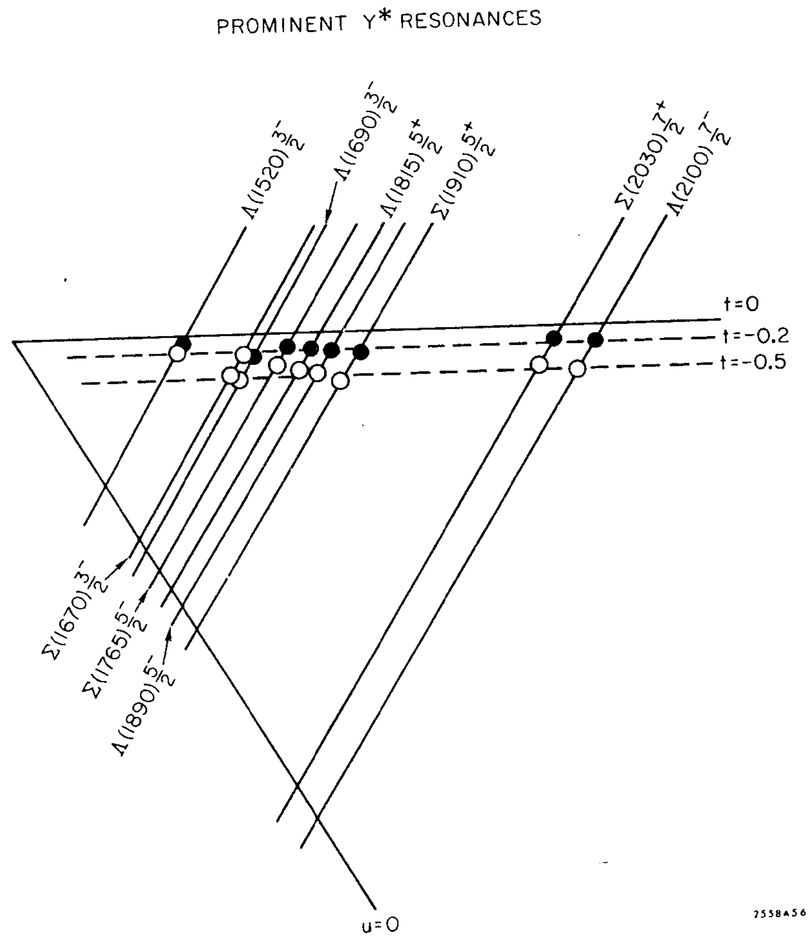

Figure 60

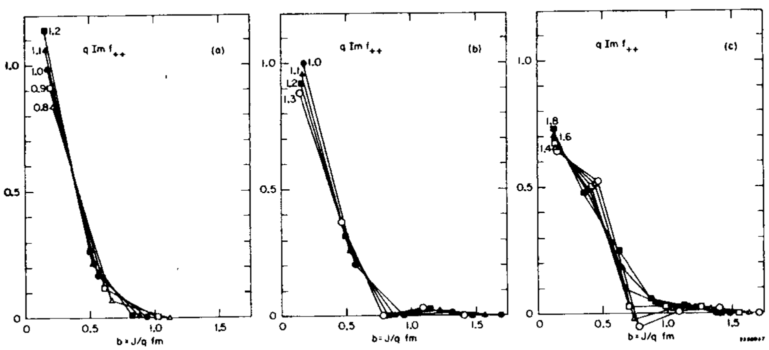

Figure 61

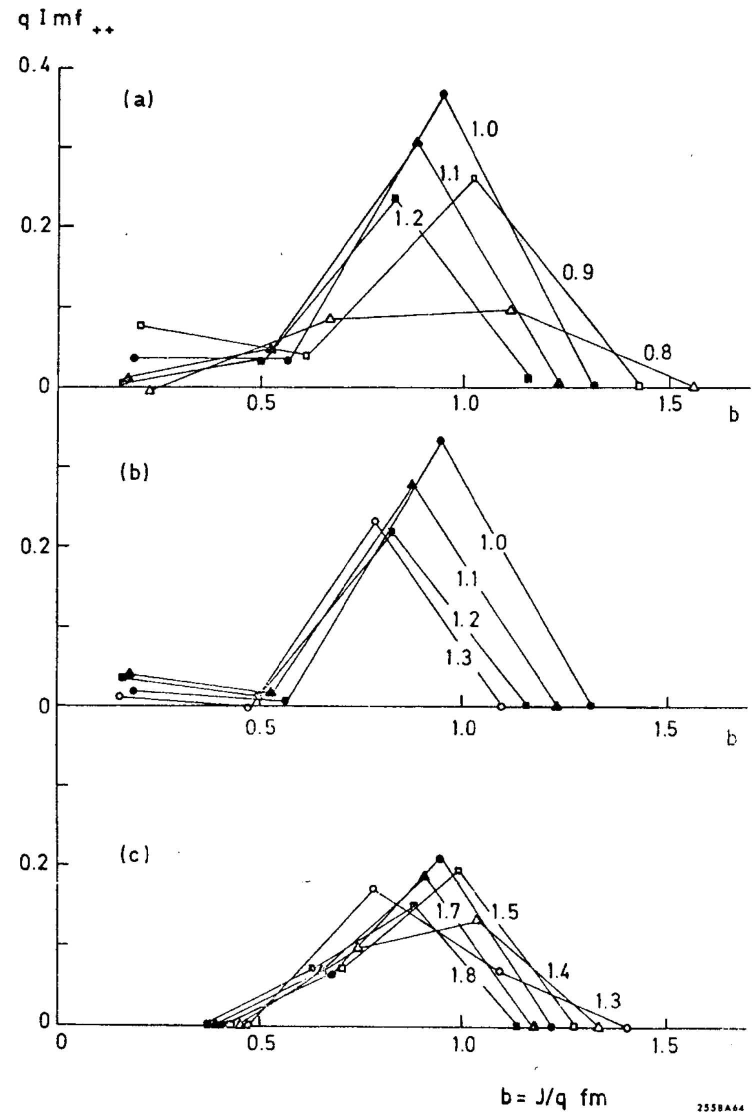

Figure 62

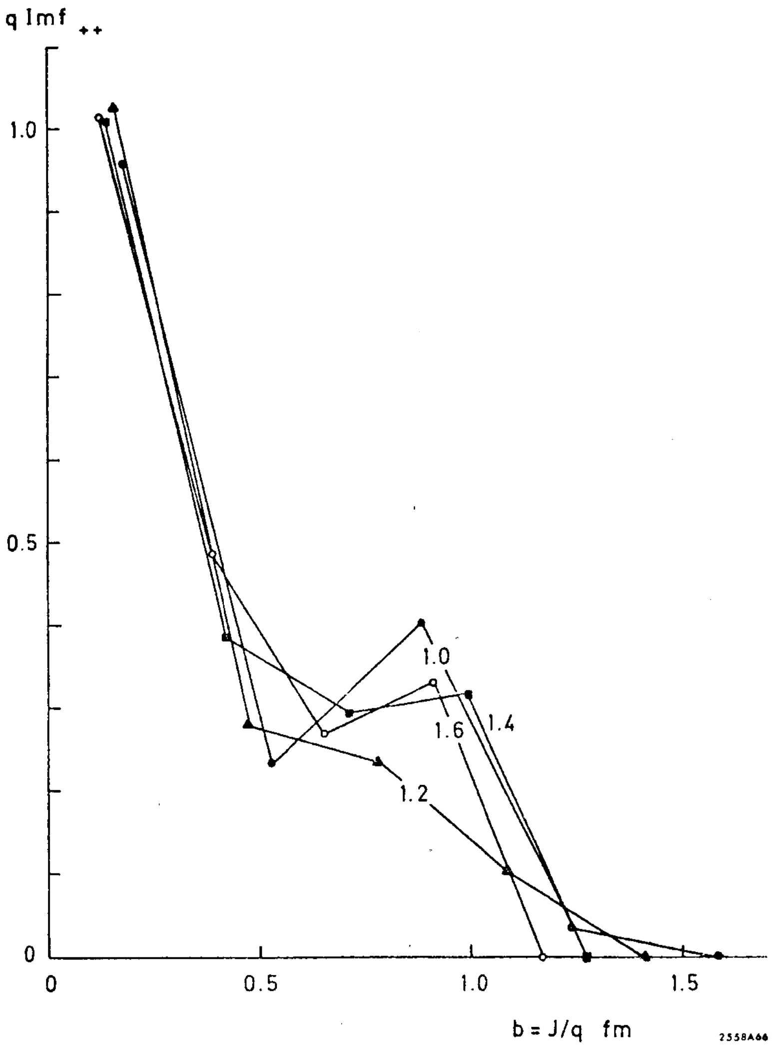

Figure 63

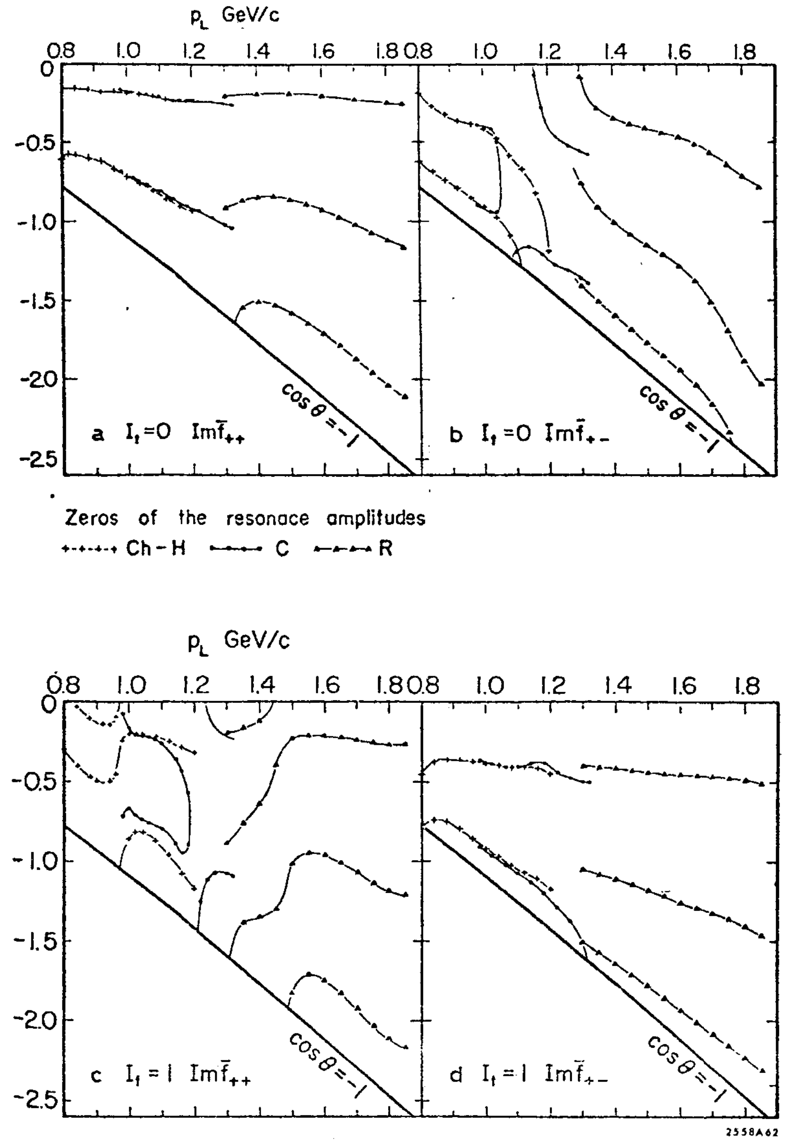

Figure 64

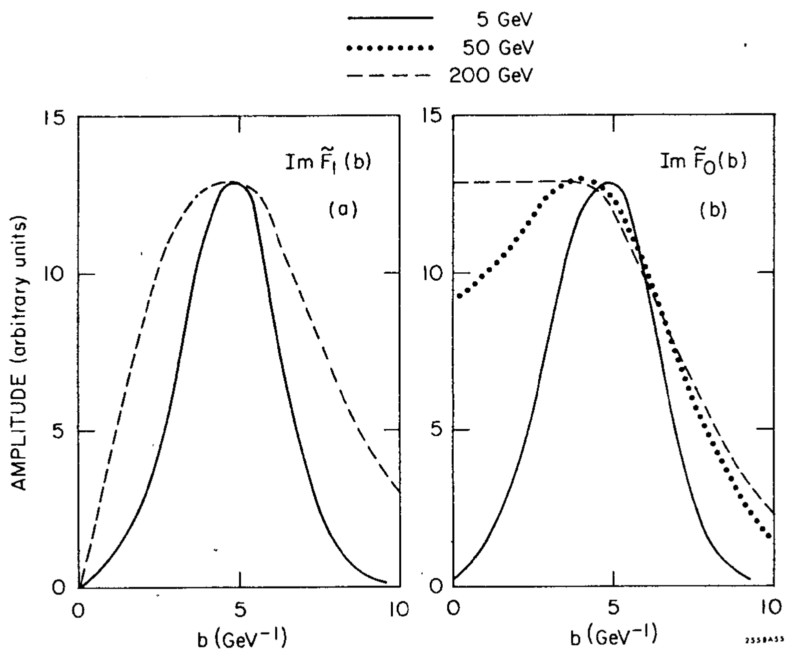

Figure 65

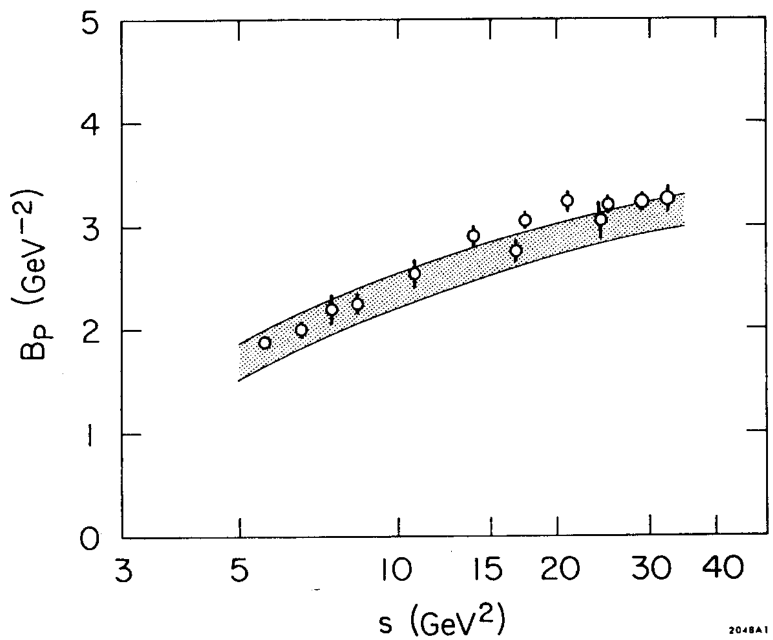

Figure 66

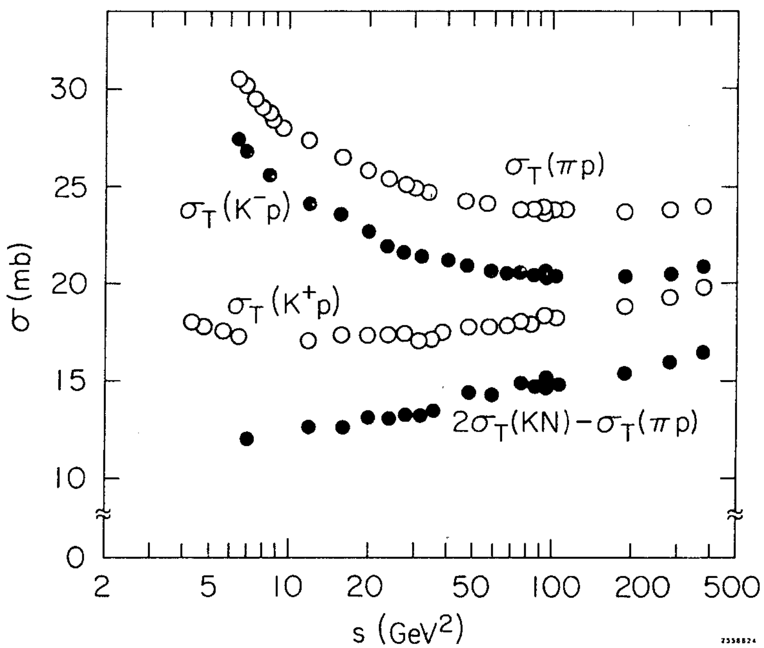

Figure 67

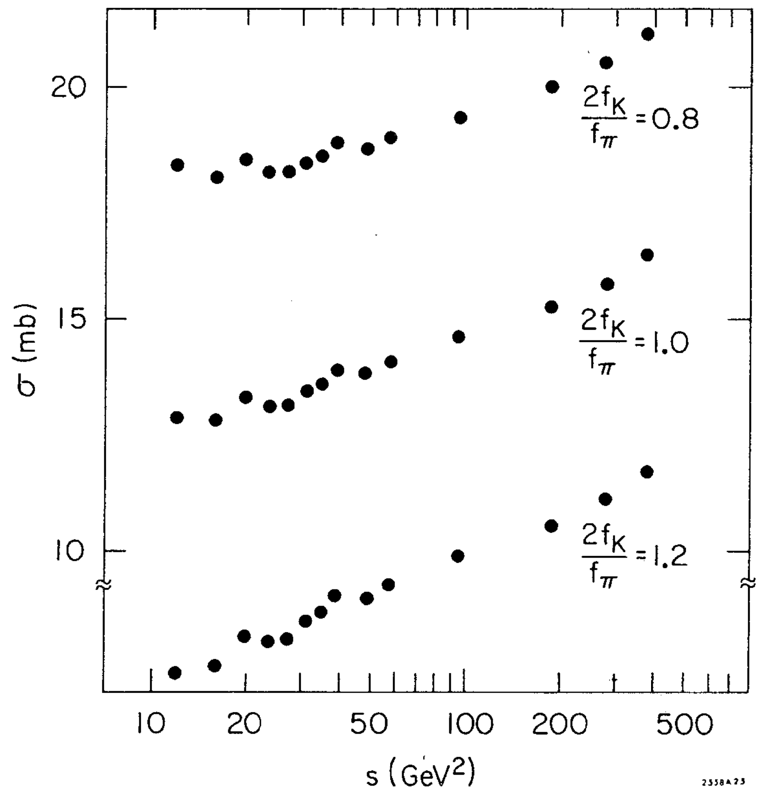

Figure 68

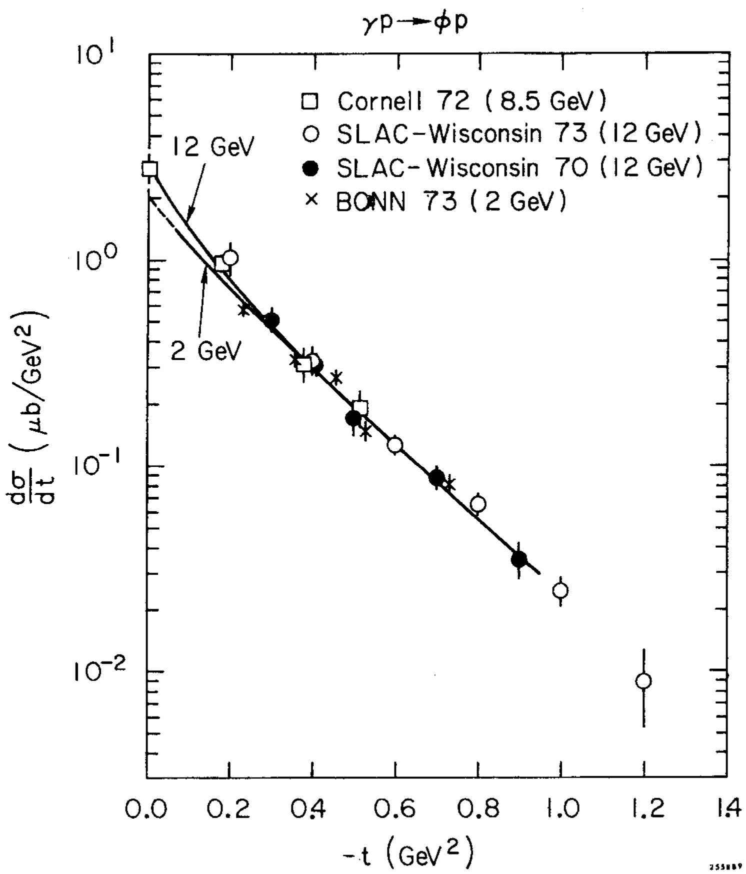

Figure 69

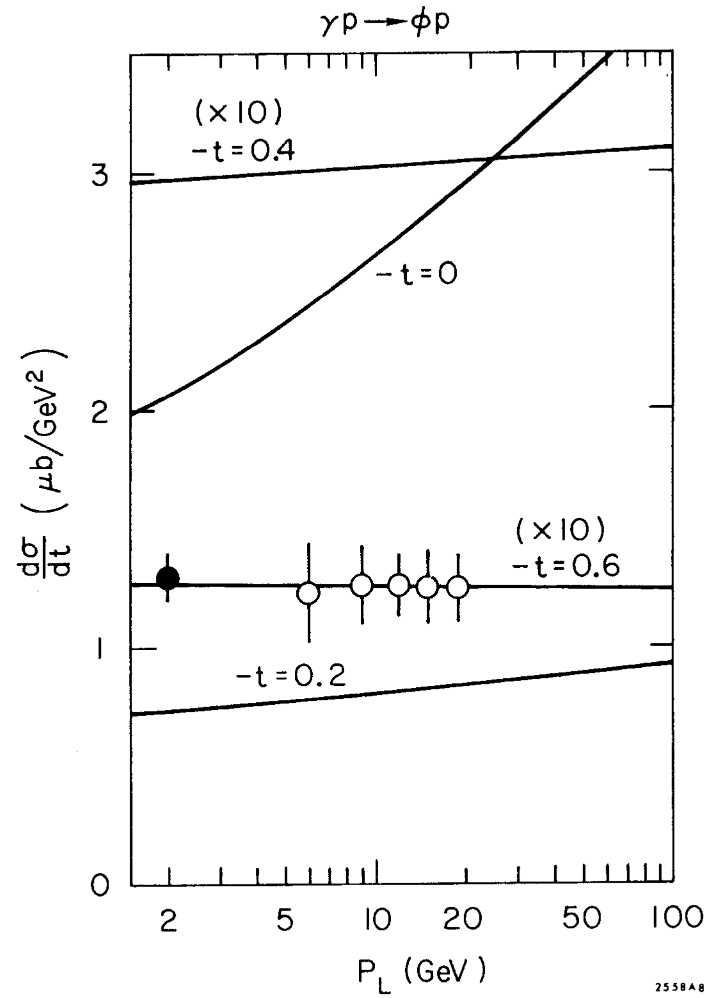

Figure 70

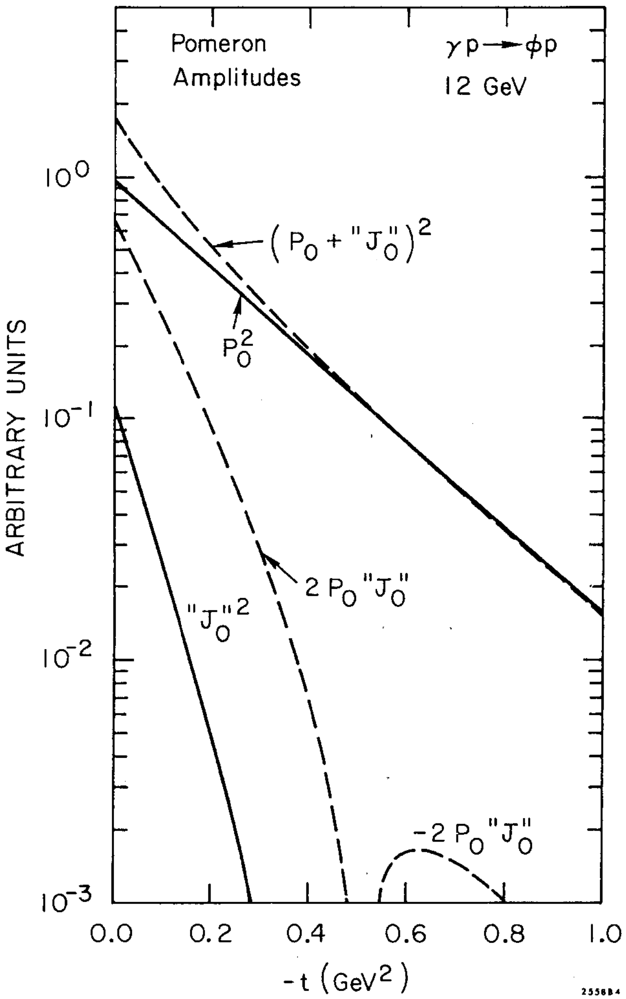

Pomeron
Amplitudes
$\gamma p \to \phi p$
12 GeV
$(P_0 + "J_0")^2$
P_0^2
$2 P_0 "J_0"$
$"J_0"^2$
$-2 P_0 "J_0"$
ARBITRARY UNITS
10^0
10^{-1}
10^{-2}
10^{-3}
0.0
0.2
0.4
0.6
0.8
1.0
$-t\ (GeV^2)$

Figure 71